Journal of Research of the National Bureau of Standards Vol. 48, No. 6, June 1952 Research Paper 2329

Effect of Strain-Temperature History on the Flow and Fracture of Ingot Iron at Low Temperatures[1]

Glenn W. Geil and Nesbit L. Carwile

The effect of the strain-temperature history of ingot iron on the true stress-strain relationship for tensile specimens extended at temperatures ranging from −196° to +100°C is reported. Specimens of ingot iron in various initial conditions were extended to a specified strain at a selected temperature and subsequently extended to fracture at a different temperature. The deviation of the true stress-strain values for the second stage of these tests from corresponding values for a single-stage test generally increase at a decreasing rate as the prestrain of the specimen increases.

The "rheotropic embrittlement" and work hardening (strain hardening plus strain aging) vary with the heat treatment and prestrain history of the ingot iron. The brittleness at or below −78°C of normalized or hot-rolled ingot iron is partially curable by prestraining in tension at room temperature. However, prestraining in tension of annealed ingot iron at room temperature decreases the ductility retained at −154° and −196°C. The predominance of strain aging at the higher temperatures and strain hardening at the lower temperatures causes the total work hardening of the specimen during deformation to maximum load to increase as the test temperature is either increased or decreased from about −120°C.

1. Introduction

In recent years several investigations [1 to 11][2] on the mechanical properties of metals at low temperatures have shown conclusively that the true stress-strain relationship of metals and alloys extended in tension depends on the strain-temperature history, as well as on the instantaneous values of strain, strain rate, and test temperature. In most of these investigations very little information was reported on the part played by strain aging during the prior history of the specimen, as strain aging was not pronounced in most of the metals studied. A previous investigation [10] at the Bureau showed that strain aging affected the true stress-strain relationship of ingot iron specimens extended in tension at slightly elevated temperatures and even at some subzero temperatures (−120° to +100° C). Within the temperature range, −196° to +100° C, of that investigation the strain hardening of ingot iron increased with a decrease in temperature, whereas the strain aging decreased with a decrease in temperature. Therefore, work hardening[3] of ingot iron may either increase or decrease with increase in testing temperature, depending upon the relative magnitude of the changes in strain hardening and strain aging with variation in temperature.

The rate of strain hardening of ingot iron is influenced by the mechanism of deformation. The spacing of the slip zones within the crystals and also the number of slip bands in a zone vary with the temperature of deformation of the metal. These factors are believed to be directly associated with the increase in the rate of strain hardening of the metal with decrease in testing temperature. Moreover, as previously reported [10], considerable deformation by twinning was observed in specimens of ingot iron slowly extended in tension at temperatures below about −120° C. The extent of the twinning during the tension test increased greatly as the temperature was lowered from about −120° to −196° C. The influence of this factor on the rate of strain hardening of the iron may be considerable.

The purpose of the present investigation was to obtain additional information on the influence of the strain-temperature history, and especially the effect of strain aging, on some of the tensile properties and the true stress-strain relationship for specimens of ingot iron subsequently tested in tension.

2. Material

The material used in this investigation was ingot iron in the conditions as annealed, hot-rolled, quenched and tempered, normalized, and cold-drawn. A detailed description of this material was reported in a previous paper [10]. The principal chemical constituents (in percent by weight) other than iron are as follows: Carbon, 0.02; manganese, 0.02; phosphorus, 0.005; sulfur, 0.018; silicon, 0.002; copper, 0.10; oxygen, 0.058; nitrogen, 0.002; and hydrogen, 0.0005. This iron was prepared from a single melt and was furnished by the manufacturer in the conditions as hot-rolled and as cold-drawn to 14- and 24-percent reductions of area. The heat treatments applied to the ingot iron in this laboratory are summarized in table 1.

Cylindrical tensile specimens with a 2-in. gage length were used. The reduced section was gradually tapered from each end; the diameter (0.438 in.) at the midsection of the gage length was about 0.003 in. less than at at each end. The specimens were finished to the final dimensions by grinding and polishing in the axial direction. The ends of the specimen were machined with ⅞ in. ×10 threads, and

[1] This investigation was sponsored (in part) by the Ordnance Department, U. S. Army, through the Ordnance Corps, Watertown Arsenal.

[2] Figures in brackets indicate the literature references at the end of this paper.

[3] As used in this paper the term "work hardening" relates to the increase in true stress with true strain and is the combined effect of strain hardening and strain aging. The term "strain hardening" refers to that portion of the hardening or strengthening of the metal during plastic deformation that is not time dependent and occurs concurrently with strain, whereas the term "strain aging" refers to that portion of the hardening or strengthening occurring during or subsequent to plastic deformation that is time dependent and occurs as a result of previous strain and not concurrent strain.

203779—52——1

the shoulder fillets were machined to a radius of 0.75 in.

TABLE 1. *Heat treatment of ingot iron* [1]

Designation	Diameter of rod	Temperature	Time	Remarks
	in.	*° F*	*hr*	
Annealed	0.875	1,750	1	Furance-cooled to 800° F in 20 hr, then air-cooled.
Normalized	.875	1,750	1	Air-cooled.
Quenched and tempered.	[2] .500	1,700	½	Quenched in iced brine.
		1,330	1	Furnace cooled to 100° F in 45 hr.

[1] All specimens were prepared from hot-rolled rods.
[2] Specimens machined to approximate ½ in. in diameter in reduced section and ¾ in. in diameter in shoulders prior to heat treatment.

3. Method of Investigation

The specimens were extended in tension in a pendulum hydraulic testing machine of 50,000-lb capacity. The specimens, except those tested at room temperature, were fully immersed in an appropriate liquid maintained at the desired temperature. The loading was so controlled that the rate of reduction of area of the specimen, beyond the region of initial yielding, was maintained at approximately 1 percent/minute. Measurements of the diameter of the specimen throughout the course of each test were made by means of a specially designed reduction of area gage [12]. Changes in diameter of a specimen were measured by this instrument with an accuracy of ± 0.0001 in. A detailed description of the testing equipment and the method of maintaining the desired temperature is given in previous papers [10, 12].

TABLE 2. *Two-stage test conditions*

Temperature of specimen			Load between stages
First stage	Second stage	Between stages	
°C	*°C*	*°C*	*lb*
100	−78	−78	200
Room	−78	−78	200
Do	−120	−120	200
Do	−154	−154	200
Do	−196	−196	200
−78	Room	−78	[2] 0
−78	−196	−196	200
−120	Room	−120	[2] 0
−154	do	−154	[2] 0
−196	do	−196	[2] 0
−196	−78	−78	200

[1] Two special tests also were made in which the load obtained at the end of the first stage was maintained between stages.
[2] Specimen was removed from the testing machine between stages.

In the present investigation, a specimen was extended at a selected temperature to a specified strain value and subsequently extended to fracture at a different temperature. In general, the specimen was kept in the testing machine between stages under a small load of approximately 200 lb to maintain the alinement of the specimen in the testing machine. However, when the second stage of a two-stage test was at room temperature, the specimen was removed from the testing machine between stages so that the adapters and adjacent portions of the head and base of the testing machine could be quickly brought to room temperature. Moreover, in two special tests the load attained at the end of the first stage was maintained on the specimen in the machine between stages. The specimens were kept cool between stages, as reported in table 2, in order to minimize strain aging during this period. Usually the second stage was begun approximately ½ hr after completion of the first stage.

4. Results and Discussion

True stress-strain data obtained in two-stage tension tests on ingot-iron specimens at selected temperatures ranging from −196° to +100° C are summarized in figures 1 and 2, and 4 to 9. True stress-strain curves obtained in the single-stage tension tests, reported in a previous paper [10], are included in these graphs as broken-line curves, and the upper end of these curves represents initial fracture. The true stress-strain values representing the completion of the first stage and the data obtained in the second stage of the two-stage tension tests are shown. The data obtained in the first stage of the test conforms to the curve representing the corresponding deformation in a single-stage test and these values are, in most cases, not plotted in these graphs. The true stress-strain values during the unloading and the initial part of the reloading also are not shown in some of the figures. The true-stress and true-strain values attained at the fracture area of the specimen at the initiation of fracture are designated in this paper as the fracture stresses and fracture strains, respectively, and, except for certain specifically designated cases, they are represented by the final true stress-strain values plotted in figures 1 and 2, and 4 to 9.

4.1. Annealed Ingot Iron

In order to determine the direct effect of a reduction of load in a tension test for a short time on the subsequent true stress-strain values, a special tension test was made at a single temperature (room temperature) on a specimen of annealed ingot iron. The deformation of this specimen was carried out in four stages and included an initial loading to a selected extension, an unloading to 200 lb for a period of 5 minutes, followed by a reloading to a second selected extension, then repeating the procedure until a total of four stages had been completed. As shown in figure 1, the true stress-strain values for this four-stage test generally coincided with those of a single-stage test made on a specimen of annealed ingot iron at room temperature, except for the true stresses at the initial strains of the second, third, and fourth stages; these true stresses were slightly higher than the corresponding stresses in a single-stage test. Apparently, the combined effect of the strain aging at room temperature during the 5-minute periods between stages and the unloading and reloading was sufficient to increase the true-stress values at the initial yielding in the last three stages but was not sufficient to affect appreciably the subsequent true-stress values. It is believed that, in general, short

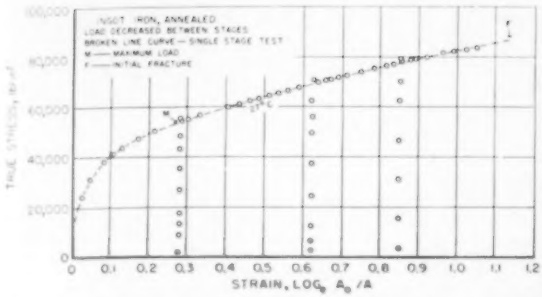

FIGURE 1. *True stress-strain values obtained with an annealed ingot-iron specimen that was extended in a four-stage tension test at room temperature.*

interruptions of this type in a tension test with ingot iron at room or lower temperatures, in which the temperature of the specimen is held constant during the test, have very little effect on the true stress-strain values, except those during the initial yielding in the next stage of the test.

Four specimens of annealed ingot iron were extended in tension at room temperature to specified strains (indicated as short vertical bars on the 27° C curve in fig. 2), and subsequently extended to fracture at −196° C. As shown in figure 2, these specimens exhibited very little ductility in the second-stage test, although a specimen of annealed ingot iron that was extended in a single-stage test at −196° C deformed to a strain of about 0.05 before initial fracture. In the two tests, in which the deformation of the specimen in the first stage of the test at room temperature was greater than the maximum load strain, the specimens fractured in the second-stage test without any appreciable plastic deformation, and the fractures occurred at the shoulder of the

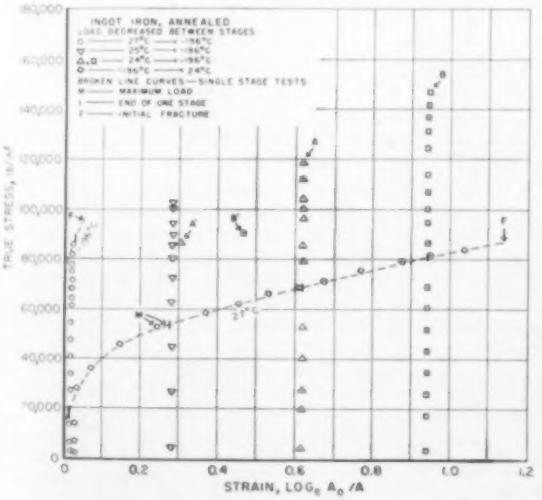

FIGURE 2. *True stress-strain values obtained with annealed ingot-iron specimens that were extended in two-stage tension tests at room temperature and −196° C.*

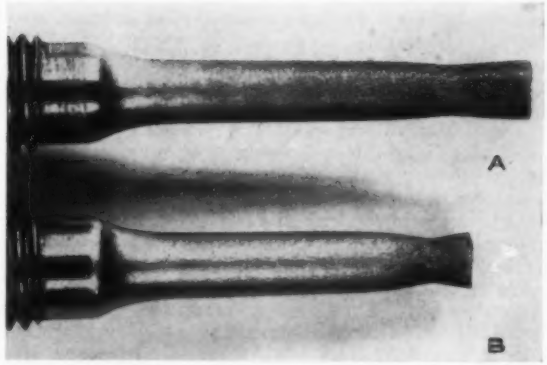

FIGURE 3. *Portions of two specimens of annealed ingot iron that were extended in tension at room temperature to strains beyond maximum load and subsequently fractured in tension at −196° C.*

A, True strain of 0.62 at room temperature; B, true strain of 0.94 at room temperature

necked section (fig. 3). The final true stress-strain values as determined by the final load and minimum cross-sectional-area measurements for these specimens are designated as points A and B in figure 2. As the fractures did not occur at the minimum cross section of the specimens, the stress values represented by points A and B are not fracture stresses; these data indicate only that the fracture stresses at −196° C for the position of the minimum section of the specimens of annealed ingot iron that were extended in tension at room temperature to these designated strain values were greater than the indicated stress values. The fracture stresses and fracture strains at −196° C of these specimens under the multiaxial stress conditions existing at the position of the actual fracture in the shoulder of the necked section are shown by the corresponding points A′ and B′ in figure 2. It may be noted that the fracture stresses at −196° C in the shoulder portion of the neck of the specimens are lowered to values below that of the tension specimen fractured at −196° C in uniaxial tension after extension at room temperature to maximum load. This may be attributed to the influence of biaxial compressive stresses at these positions.

As the ductility of specimens of annealed ingot iron in single stage tests at −196° C was small (strain of approximately 0.05), very little information could be obtained on the effect of prior strain at −196° C of specimens of annealed ingot iron on their tensile properties at room temperature. The data obtained on a specimen extended in the first stage of the test at −196° C to a strain of about 0.02 and then extended to fracture in the second-stage test at room temperature indicated that the total work hardening during the deformation at −196° C was approximately equivalent to the total work hardening of a specimen deformed the same amount at room temperature; the true stress-strain values obtained in the second stage of the test approximately coincided with the corresponding values ob-

tained in the single-stage test at room temperature (fig. 2). Thus the increase in the strain hardening at −196° C above that at room temperature was approximately equal to the strain aging at room temperature.

A specimen of annealed ingot iron was prestrained in tension at room temperature to maximum load and then extended to fracture at −154° C. This specimen retained considerably less ductility and hence had a lower fracture stress than a specimen extended to fracture in a single-stage test at −154° C, as shown in figure 4. The strain during the second stage of this test was very small in comparison with the strain beyond maximum load in the single-stage test at −154° C. The strain aging of the specimen during the deformation at room temperature apparently made the specimen quite brittle at the lower temperature.

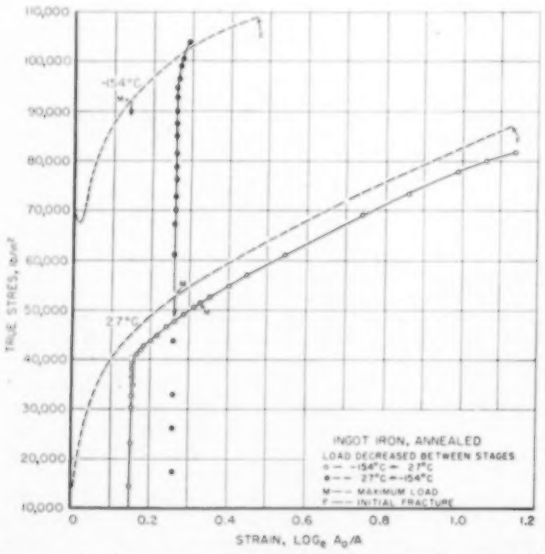

FIGURE 4. *True stress-strain values obtained with annealed ingot-iron specimens that were extended in two-stage tension tests at room temperature and −154° C.*

An annealed ingot-iron specimen was prestrained in tension at −154° C to maximum load and then extended to fracture at room temperature. The true stress-strain curve for the second stage of this test (fig. 4) is considerably below the corresponding part of the curve for a single-stage test with a specimen at room temperature, and thus the total work hardening of the specimen during the first stage of the test at −154° C was less than that of a specimen deformed to the same strain at room temperature. Strain aging in specimens of ingot iron during deformation in tension at −154° C is very slight [10]. Moreover, strain hardening increases with a lowering of the test temperature from room temperature to −154° C. The data in figure 4, therefore, indicate that the strain aging of the iron at room temperature was much greater than was the increase in strain hardening with decrease from room temperature to −154° C.

In order to determine the specific influence of the degree of the prestraining of annealed ingot-iron specimens at one temperature on their deformation characteristics at another temperature, two series of two-stage tests were made. One series of specimens was prestrained in tension at room temperature to different strains and subsequently extended to fracture at −78° C. The true stress-strain data for these tests are summarized in figure 5. The true stress-strain curves for the second stage of these tests are above the corresponding portion of the curve for a single-stage test at −78° C. Another series of specimens was prestrained in tension at −78° C to different strains and subsequently extended to fracture at room temperature. The true stress-strain curves (fig. 5) for the second stage of each

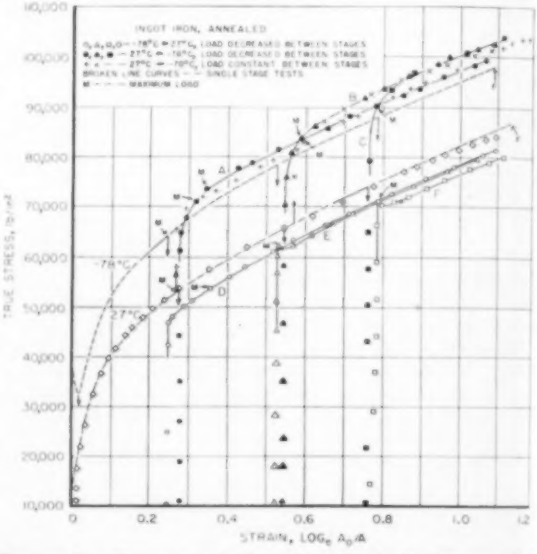

FIGURE 5. *True stress-strain values obtained with annealed ingot-iron specimens that were extended in two-stage tension tests at room temperature and −78° C.*

of these tests, except for the specimen prestrained only to the lower yield, are below the corresponding portion of the curve for a single-stage test at room temperature. The curve for the second-stage test of the specimen prestrained to the lower yield coincided with the curve for the single-stage test at room temperature. The combined effect of the strain hardening and strain aging during the prestraining at −78° C in this test was equivalent to the combined effect of the strain hardening and strain aging during the deformation to the same strain at room temperature. In general, the deviation of the true stress-strain curve for the second stage of a two-stage test from the curve for a single-stage test at the same temperature (fig. 5) increases at a decreasing rate as the amount of prestraining in the first stage increases. The above data indicate that

the strain aging of a specimen of annealed ingot iron at any strain during deformation in tension at a constant temperature varies with the strain; the strain aging at any strain depends greatly upon the amount of the prior strain aging of the specimen.

In order to determine the effect of maintaining a relatively high stress on the specimen between test stages, two special tests were made in which the load attained at the end of the first stage was maintained on the specimen until the beginning of the second stage. The true stress-strain values obtained in these tests (fig. 5) show no significant deviation from the true stress-strain curves of corresponding two-stage tests in which the load was reduced to about 200 lb between stages. The retained ductility at −78° C of the specimen prestrained at room temperature to a strain of about 0.26 with no reduction of the load between stages was slightly greater than that of the specimen prestrained at room temperature to approximately the same amount, with the load reduced to 200 lb between stages. This small difference in ductility, however, is not believed to be significant. In general, the strains to fracture of the specimens in the two-stage tests summarized in figure 5 were approximately the same at both temperatures and also were about the same as those for the single-stage tests at these temperatures.

Ripling and Baldwin in reporting on the phenomenon they called the "rheotropic embrittlement" of steel [11] concluded that a large part of the deficiency in ductility of annealed steels at low temperatures is rheotropic and can be removed by prestraining under more ductile conditions at a higher temperature. The data obtained in the present investigation on annealed ingot iron, however, indicate that the low-temperature embrittlement of this material is not rheotropic in the manner proposed by Ripling and Baldwin; prestraining of the annealed ingot iron at room temperature reduced, rather than increased, the ductility retained either at −154° or −196° C. The embrittlement due to strain aging during the prestraining of the specimens at room temperature, is believed to be the main cause for the loss in the retained ductility at −154° or −196° C. Another factor that probably has considerable influence on the retained ductility is a decrease in the degree of deformation twinning occurring at the low temperature following a prestraining at room temperature. This latter factor is being studied in some detail and will be discussed in a separate report.

4.2. Normalized Ingot Iron

The true stress-strain data for two normalized ingot-iron specimens that were extended in tension in two-stage tests at room temperature and −78° C are presented in figure 6. The effect of the prestraining in the first stage of the tension test on the total work hardening of these specimens was similar to that already described for two-stage tests with annealed ingot iron at these temperatures. The ductility, however, was affected quite differently. As

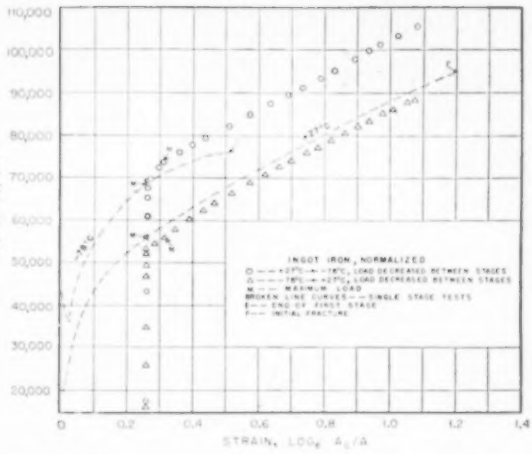

FIGURE 6. *True stress-strain values obtained with normalized ingot-iron specimens that were extended in two-stage tension tests at room temperature and −78° C.*

illustrated in figures 25 and 26 of the previous paper [10], the ductility of normalized ingot iron, and to a lesser degree that of hot-rolled ingot iron, extended to fracture in single-stage tests was much lower at −78° C than at room temperature. The strain to fracture of ingot iron in the annealed, quenched, and tempered, or cold-drawn conditions, however, was nearly the same at room temperature and at −78° C. The decrease in the ductility at −78° C of the ingot iron in the normalized or hot-rolled condition may be associated with a greater amount of carbon and nitrogen initially retained in solid solution in these conditions than in the other conditions. The data for the two-stage tests of the normalized ingot iron (fig. 6) show that the iron in this condition apparently is subject to rheotropic embrittlement in the manner proposed by Ripling and Baldwin; prestraining the specimen at room temperature to just beyond the maximum load increased greatly the ductility retained at −78° C, as indicated by the fracture strain of approximately 1.1 for this two-stage test and the fracture strain of approximately 0.5 for the single stage test at −78° C. Prestraining a specimen at −78° C to the maximum load decreased the ductility retained at room temperature. Apparently, the rheotropic embrittlement of the specimen during the prestraining at −78° C was not completely removed by the subsequent deformation at room temperature.

4.3. Quenched and Tempered Ingot Iron

The data obtained in two-stage tension tests with specimens of quenched and tempered ingot iron are summarized in figure 7. These results indicate that the effect of prestraining specimens at room temperature and −78° C is approximately the same as that described previously for specimens of the annealed ingot iron; the difference in magnitude of strain aging at −78° C and room temperature was greater than the difference in strain hardening at these tempera-

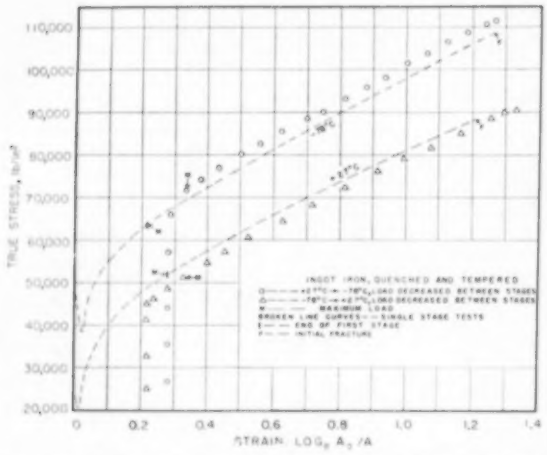

FIGURE 7. *True stress-strain values obtained with quenched and tempered ingot-iron specimens that were extended in two-stage tension tests at room temperature and −78° C.*

tures, and the predominating effect of the strain aging resulted in greater total work hardening during the prestraining at room temperature than at −78° C. The ductility retained by the specimens in the second stage of the tests was not affected appreciably by the difference in the prior strain histories.

4.4. Hot-Rolled Ingot Iron

As the ductility of the hot-rolled ingot iron was considerable, even at low temperatures (fracture strain of approximately 0.3 at −196° C), specimens were prestrained in tension at temperatures ranging from −196° to +100° C and then extended to fracture at different temperatures. The true stress-strain data for these tests and the curves obtained in single-stage tests at these temperatures are summarized in figure 8. Prestraining specimens approximately to maximum load at −196°, −120°, or −78° C had little specific effect on the ductility retained in the second stage of the tests at room temperature. The deformation under ductile conditions at room temperature apparently removed any rheotropic embrittlement that may have occurred during the prestraining at low temperature. As the work hardening of a specimen of ingot iron during deformation at −196° C is mainly strain hardening, and as strain hardening increases with decrease in temperature from −78° to −196° C, the data showing equal work hardening of the hot-rolled ingot-iron specimens during the prestraining at −78° and −196° C (fig. 8) indicate that strain aging occurred to a considerable extent during the prestrain of the specimen at −78° C. The work hardening during the prestraining in tension at −120° C of a specimen approximately to maximum load was the least for this series of tests and resulted in the greatest lowering of the points representing the true stress-strain values for the second stage of the tests from the curve for the single-stage test at room temperature. The strain aging of hot-rolled ingot iron during deformation was very much less at −120° C than at −78° C. However, as shown in figure 12 of a previous investigation [10], strain aging occurs to an appreciable extent in specimens of hot-rolled ingot iron deformed in tension at −120° C and at −138° C.

Although the total work hardening (mainly strain hardening) of a specimen during prestraining approximately to maximum load at −196° C was about equal to the total work hardening (strain hardening plus strain aging) of a specimen deformed to the same strain at −78° C, the resulting rheotropic properties of these two specimens were different. The points representing the true stress-strain values for the second-stage test at −78° C of the specimen prestrained at −196° C gradually rise above the corresponding portion of the curve for the specimen extended in the single-stage test at −78° C (fig. 8). These data indicate that the strain aging during the deformation from maximum load to fracture of the former specimen was much greater than that of the latter specimen. As the fracture strains of the above specimens were about equal, the deformation during the second-stage test at −78° C apparently removed most of the low-temperature embrittlement that had occurred during the prestraining at −196° C.

The specimen of hot-rolled ingot iron that was prestrained in tension at room temperature to a small strain of approximately 0.03, broke in the threads during the second-stage test at −196° C without any appreciable plastic deformation of the specimen.

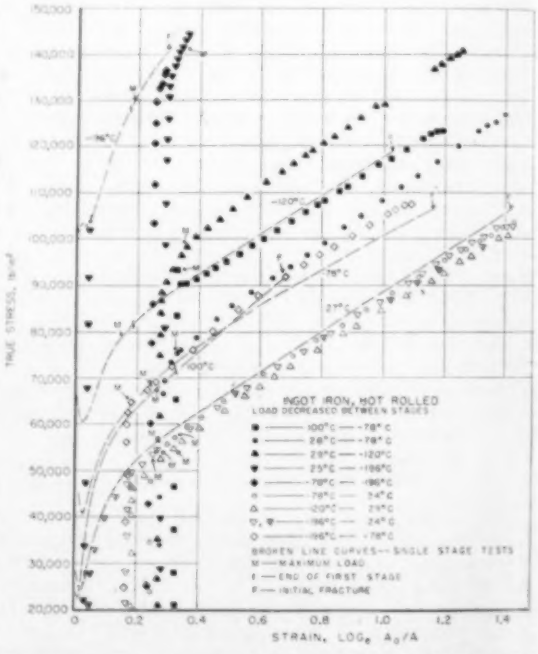
TRUE STRESS, lb/in²
STRAIN, $\log_e A_o/A$
INGOT IRON, HOT ROLLED
LOAD DECREASED BETWEEN STAGES
BROKEN LINE CURVES — SINGLE STAGE TESTS
M — MAXIMUM LOAD
I — END OF FIRST STAGE
F — INITIAL FRACTURE

FIGURE 8. *True stress-strain values obtained with hot-rolled ingot-iron specimens that were extended in two-stage tension tests at different temperatures.*

The final value plotted in figure 8 for this test does not represent the fracture stress and fracture strain at −196° C of the prestrained metal. As the yield stress of this specimen at −196° C was at least equal to or greater than that represented by the final plotted value, and as this point lies approximately on the true stress-strain curve for the single-stage tension test on hot-rolled ingot iron at −196° C, the prestraining of the specimen at room temperature, apparently did not decrease the stress necessary for continued deformation of the metal at −196° C.

Specimens of hot-rolled ingot iron that were prestrained in tension at room temperature approximately to maximum load and then extended to fracture at −78°, −120°, and −196° C, exhibited strain-aging effects similar to those described above for the specimens prestrained at low temperatures. However, a difference was observed in the effect of the prestraining at room temperature on the ductility retained at lower temperatures, and this should be pointed out. Prestraining at room temperature approximately to the maximum load improved the ductility retained by the specimen at the lower temperature and the fracture strains of the specimens in the two-stage tests were greater than those of the specimens fractured in the single-stage tests at the same low temperatures (fig. 8). Thus, the rheotropic embrittlement of the hot-rolled ingot iron during the second stage of these tests was reduced by the prestraining under the more ductile conditions at room temperature.

A specimen of hot-rolled ingot iron was prestrained in tension at 100° C to a strain slightly beyond the maximum load and then extended to fracture at −78° C. The strain aging of this specimen during the deformation at 100° C was much greater than that of specimens deformed at room temperature, and is indicated by the position of the true stress-strain values in figure 8 for the second stage of the test; the elevation of these points above the curve for the single-stage test at −78° C is much greater than that for the specimen prestrained at room temperature. The fracture strain of the specimen prestrained at 100° C was about equal to that of the specimen extended to fracture in a single-stage test at −78° C. However, it was considerably less than that of the specimen prestrained at room temperature and extended to fracture at −78° C. The embrittlement of the specimen by the great amount of strain aging during the deformation at 100° C apparently was about equal to the rheotropic embrittlement during the deformation of a specimen to the same strain in the single-stage test at −78° C.

The true stress-strain data for hot-rolled ingot iron specimens (fig. 8) indicate that the strain hardening is the predominating factor affecting the variation of the total work hardening with temperature at temperatures below −120° C, whereas the strain aging is the predominating factor affecting the total work hardening at temperatures above −120° C.

As described earlier, the ductility of specimens of normalized ingot iron was much less at −78° C and at lower temperatures than at room temperature, and prestraining of a specimen at room temperature greatly improved the ductility retained at −78° C. The ductility of the annealed ingot iron specimens was less at −154° C and −196° C than at room temperature. However, prestraining specimens of annealed ingot iron at room temperature reduced the ductility retained at −154° C and −196° C. Moreover, the ductility of specimens of ingot iron in the condition either as annealed, or as quenched and tempered, was about the same at −78° C as at room temperature and prestraining specimens at room temperature had little, if any, effect on the ductility retained at −78° C. The effect of prestraining of ingot iron at room temperature on the rheotropic embrittlement of the specimens at lower temperatures apparently depends greatly upon the initial condition of the iron.

4.5. Cold-Drawn Ingot Iron

The true stress-strain data obtained in two-stage tension tests with specimens of cold-drawn ingot iron are summarized in figure 9. These samples of the originally hot-rolled ingot iron had been cold-drawn by the manufacturer to 14- and 24-percent reduction of area, and were aged at room temperature for several months. The total work hardening during the prestraining in tension at room temperature to a strain of approximately 0.25 of a specimen of ingot iron cold-drawn to 14 percent reduction of area was slightly greater than that of a specimen deformed to the same strain at −78° C. The total work harden-

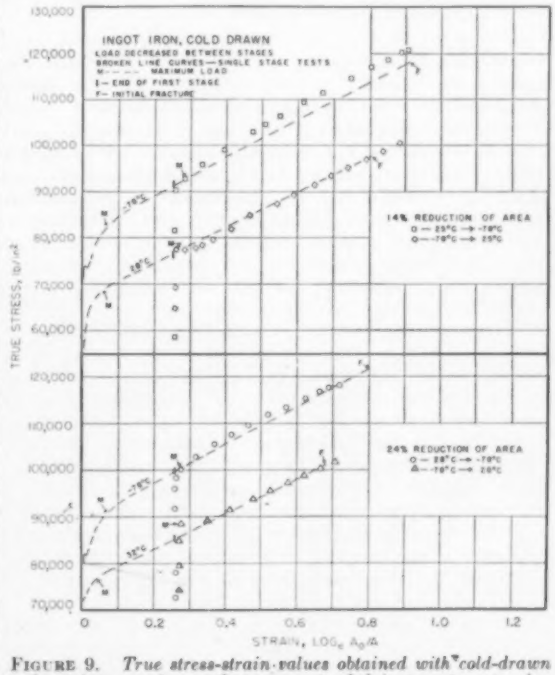

FIGURE 9. *True stress-strain values obtained with cold-drawn ingot-iron specimens that were extended in two-stage tension tests at room temperature and −78° C.*

ing during the prestraining in tension to a strain of approximately 0.25 at room temperature and at −78° C of specimens of ingot iron cold-drawn to 24-percent reduction of area was approximately the same as indicated by the coincidence of the true stress-strain values for the second stage of these tests with the true stress-strain curves for the single-stage tests. The degree of strain aging during the deformation in tension of these specimens of the cold-drawn iron was much less than that of the hot-rolled ingot-iron specimens due to the prior strain aging that had occurred during the cold-drawing and storage of the iron.

5. Summary

A study was made to determine the effect of the strain-temperature history of ingot iron on the true stress-strain relationship for specimens extended in tension at temperatures ranging from −196° to +100° C. Specimens of annealed, normalized, quenched and tempered, hot-rolled and cold-drawn ingot iron were extended in tension to specified true-strain values at a selected temperature and subsequently extended to fracture at a different temperature. The true stress-strain values obtained in these two-stage tests were compared with those obtained in single-stage tension tests at the same temperatures. The deviation of the true stress-strain curves for the second stage of these tension tests with ingot iron from the true stress-strain curve for a single-stage test at the same temperature generally increases at a decreasing rate as the prestrain of the specimen is increased.

The amount of strain aging and the rheotropic brittleness of specimens of ingot iron vary with the heat treatment and prestrain history of the specimens. The rheotropic brittleness at −78° C or at lower temperatures of normalized or hot-rolled ingot iron is sensitive to and in part curable by prestrain under ductile conditions at higher temperatures; the ductility retained by the specimens in subsequent extension in tension at low temperature is increased. However, prestraining specimens of annealed ingot iron in tension under ductile conditions at room temperature decreases the ductility retained in subsequent extension in tension at −154° or −196° C.

The work hardening of ingot iron during deformation in tension at temperatures below −120° C is mainly strain hardening, and increases with lowering of the testing temperature. As the temperature is increased above −120° C, the influence of the strain aging during the deformation in increasing the total work-hardening rate becomes the predominating factor, and the rate of work hardening increases with increase in testing temperature. The data obtained on the tension specimens of hot-rolled ingot iron indicate that the part of the total work hardening due solely to the strain aging during the deformation to maximum load is considerable at temperatures as low as −78° C. Even at −78° C the work hardening due to the strain aging is approximately equal to the increase in strain hardening that occurs as the testing temperature is lowered from −78° to −196° C. At +100° C, the magnitude of the strain aging is at least equal to or greater than the strain hardening.

The data presented in this paper, together with those reported previously [10], show that the strain aging of ingot iron is a very important factor affecting the true stress-strain relationship at temperatures as low as −120° C. Strain aging apparently occurs to some extent at temperatures as low as −154° C. These data are contrary to the generally prevailing belief that the strain aging of ingot iron is insignificant at sub-zero temperatures.

The authors are indebted to C. R. Johnson and J. D. Grimsley for assistance in this investigation.

6. References

[1] D. J. McAdam, Jr., G. W. Geil, and R. W. Mebs, Effect of combined stresses and low temperatures on the mechanical properties of some non-ferrous metals, Trans. Am. Soc. Metals. **37,** 497 (1946).

[2] D. J. McAdam, Jr., G. W. Geil, and R. W. Mebs, Influence of plastic deformation, combined stresses, and low temperatures on the breaking stress of ferritic steels. Trans. Am. Inst. Mining Met. Engrs. **172,** 323 (1947).

[3] D. J. McAdam, Jr., G. W. Geil, and F. J. Cromwell, Influence of low temperatures on the mechanical properties of 18:8 chromium-nickel steel, J. Research NBS **40,** 375 (1948) RP1882.

[4] J. E. Dorn, A. Goldberg, and T. E. Tietz, The effect of thermal-mechanical history on the strain hardening of metals, Trans. Am. Inst. Mining Met. Engrs. **185,** 325 (1949).

[5] T. E. Tietz and J. E. Dorn, The effect of strain histories on the work hardening of metals, Trans. Am. Soc. Met. **41A,** 163 (1949).

[6] T. E. Tietz, R. A. Anderson, and J. E. Dorn, Effect of prestraining temperatures on the recovery of cold worked aluminum, Trans. Am. Inst. Mining Met. Engrs. **185,** 921 (1949).

[7] W. D. Jenkins and T. G. Digges, Influence of strain rate and temperature on the creep of cold-drawn ingot iron, J. Research NBS **43,** 117 (1949).

[8] E. J. Ripling and G. Sachs, The effect of strain-temperature history on the flow and fracture characteristics of an annealed steel, Trans. Am. Inst. Mining Met. Engrs. **185,** 78 (1949).

[9] W. E. Jenkins and T. G. Digges, Creep of high-purity copper, J. Research NBS **45,** 153 (1950) RP2121.

[10] G. W. Geil and N. L. Carwile, Tensile properties of ingot iron at low temperatures, J. Research NBS **45,** 129 (1950) RP2119.

[11] E. J. Ripling and W. M. Baldwin, Jr., Rheotropic embrittlement of steel, Trans. Am. Soc. Metals **43,** 778 (1951).

[12] G. W. Geil and N. L. Carwile, A reduction-of-area gage for use at low temperatures, J. Research NBS **43,** 527 (1949) RP2044.

WASHINGTON, February 5, 1952.

Journal of Research of the National Bureau of Standards Vol. 48, No. 6, June 1952 Research Paper 2330

Gradient Methods in the Solution of Systems of Linear Equations[1]

Marvin L. Stein

The results of various experiments with iterative methods for solving systems of linear algebraic equations are discussed. Modifications of the optimum gradient method are compared, and the rather interesting self-acceleration properties of a class of methods here named "almost optimum" gradient methods are pointed out.

1. Introduction

The method of steepest descent, or the optimum gradient method, has been known to mathematicians since the time of Cauchy [1].[2] Others who have discussed this method include Curry [2], Forsythe and Motzkin [3], Householder [4], Kantorovitch [5], and Temple [6]. Its infrequent application in computational work is no doubt due to the slowness with which it converges. This slowness of convergence is unfortunately generally true of gradient methods. However, with the advent of large-scale computing machinery it has become feasible to seriously consider them in practical numerical analysis.

In a forthcoming paper, Hestenes and Stein [7] discuss a large class of gradient procedures for solving systems of linear equations. These procedures contain the optimum gradient method as a special case. The present note is mainly a report on some numerical experiments with them that were carried out on the IBM Card-Programmed Electronic Calculator at the Institute for Numerical Analysis of the National Bureau of Standards. Some attention is also given to an experiment in which the problem of solving a system of linear equations was changed to an equivalent eigenvalue problem and then solved by a modification of one of the gradient methods discussed by Hestenes and Karush [8]. The most striking result of the experiments indicates that there is a large class of gradient methods that is *self-accelerating*, that is, which irregularly shows a large increase in the rate of convergence without the introduction of any modification in the computational routine. This behavior is in sharp contrast to that of the method of steepest descent, which in the light of the present results can no longer be considered as optimum from an over-all point of view unless modified by some special accelerating routine [9].

2. Summary of the Theory

Let A denote an m-rowed and n-columned matrix, and let b and x be m-rowed and n-rowed column vectors, respectively. The vector $r(x)=b-Ax$ is then an m-rowed column vector. In the following a star (*) affixed to the symbol for any vector or matrix will indicate its conjugate transpose. Hence, if H is a positive $m\times m$ Hermitian matrix, we have $H^*=H$, $r^*Hr>0$, provided $r\neq 0$. Clearly, the nonnegative real-valued function

$$f(x)=r^*Hr \tag{1}$$

vanishes if and only if

$$Ax=b. \tag{2}$$

Therefore, the problem of minimizing (1) is equivalent to the problem of solving the system (2), provided a solution exists. If no solution exists, a vector x which minimizes $f(x)$ yields a best fit of b by Ax in a least-squares sense with the metric determined by H.

Hestenes and Stein [7] have analyzed the following algorithm for constructing the minimum of (1). Consider iterations of the type

$$x_{i+1}=x_i+\alpha_i\xi_i \quad (i=0,1,2,\ldots), \tag{3}$$

where x_0 is chosen initially and where, after x_i has been determined, the gradient vector ξ_i is defined by the rule $\xi_i=A^*Hr(x_i)$. If $\xi_i=0$, the problem is solved. If $\xi_i\neq 0$, the scalar α_i is taken to be of the form $\alpha_i=\beta_i\gamma_i$, where

$$\gamma_i=\frac{\xi_i^*\xi_i}{\xi_i^*A^*HA\xi_i}$$

and β_i is any complex number. The sequence (3) has been shown to converge to the minimum of $f(x)$ provided the coefficients β_i satisfy the conditions

$$\frac{1}{\beta_i}+\frac{1}{\bar{\beta}_i}\geq 1+\delta, \qquad |\beta_i|\geq\delta,$$

where δ is arbitrary on the range $0<\delta<1$.

Setting $\beta_i\equiv 1$ gives the optimum gradient method, which has the following geometrical interpretation. Starting at x_0, one proceeds along the normal to that member of the family of concentric ellipsoids

$$f(x)=\text{constant}, \tag{4}$$

which passes through x_0 until a point tangent to another ellipsoid of the family is reached. One then goes along the normal to this second ellipsoid until one is again at a point of tangency to a member of (4),

[1] The preparation of this paper was sponsored (in part) by the Office of Naval Research.

[2] Figures in brackets indicate the literature references at the end of this paper.

203779—52——2

and so on until the common center is reached. Clearly, it would be highly desirable to land on an axis of the family. However, as simple two-dimensional examples illustrate, one usually overshoots the major axis by proceeding all the way to a point of tangency. Hence, it was conjectured by M. R. Hestenes that of the allowed values of β_i some of those chosen from the range $\beta_i<1$ would yield better convergence than $\beta_i=1$. This conjecture is the motivation for the experimental work whose results will be tabulated and discussed below.

3. Experimental Data

The algorithm described in the preceding section was carried out for the problem $Ax=b$ with

$$A=\begin{pmatrix} .06667 & .02634 & -.04640 & -.07368 & -.02131 & -.00431 \\ .02634 & .26841 & -.02243 & .15952 & -.05923 & -.12797 \\ -.04640 & -.02243 & .10932 & .05150 & -.04100 & .08558 \\ -.07368 & .15952 & .05150 & .25152 & -.01141 & -.07169 \\ -.02131 & -.05923 & -.04100 & -.01141 & .14403 & .01105 \\ -.00431 & -.12797 & .08558 & -.07169 & .01105 & .19450 \end{pmatrix} \tag{5}$$

and

$$b=\begin{pmatrix} -.008809 \\ -.014279 \\ -.000243 \\ .004576 \\ .008043 \\ -.004895 \end{pmatrix}. \tag{6}$$

Runs were made with fixed values of β_i ranging between $\beta_i=.1$ and $\beta_i=1.9$. Since the matrix A and the vector b were obtained from an original matrix B and vector c as

$$A=B^*B, \qquad b=B^*c, \tag{7}$$

A is positive and symmetric. Hence, a convenient metric is

$$H=A^{-1}. \tag{8}$$

In the metric (8) the gradient becomes $\xi_i=r(x_i)$. Thus the other significant quantities defined in section 2 assume the form

$$\gamma_i=\frac{r^*(x_i)\,r(x_i)}{r^*(x_i)\,Ar(x_i)}$$

$$f(x_i)=c^*c-(x_i^*b+b^*x_i)+x_i^*Ax_i$$

$$=c^*c-x_i^*(b+r(x_i)).$$

Table 1 lists runs of $f(x_i)$ and $f(x_i)/f(x_{i-1})$ for various fixed values of β_i. In each case the initial $x=x_0$ was zero. The values of $f(x_i)$ are given here to the same number of places as in the original calculation, while the ratios $f(x_i)/f(x_{i-1})$ have been cut down from a six-place table. Table 2 gives the values of α_i corresponding to the runs listed in table 1. These numbers were originally computed to 10 places. The results listed in tables 1 and 2 are based for the most part on single runs of the Card-Programmed Calculator. The main check used in the machine computations was the monotonicity of $f(x)$. However, the run $\beta_i=.9$ has been exactly duplicated on two separate occasions The results of the run $\beta_i=1$ check closely with results obtained by A. I. Forsythe in an entirely independent manner.

TABLE 1

i \ β	$f(x_i)$	$\frac{f(x_i)}{f(x_{i-1})}$	$f(x_i)$	$\frac{f(x_i)}{f(x_{i-1})}$	$f(x_i)$	$\frac{f(x_i)}{f(x_{i-1})}$	$f(x_i)$	$\frac{f(x_i)}{f(x_{i-1})}$
	0.1		0.3		0.6		0.8	
0	333840	------	333840	------	333840	------	333840	------
1	293093	0. 8779	224451	0. 6723	153663	0. 4603	127922	0. 3832
2	257410	. 8782	152582	. 6798	98661	. 6421	93810	. 7333
3	226497	. 8799	111480	. 7306	77941	. 7900	73423	. 7827
4	199981	. 8829	87335	. 7834	67416	. 8650	65477	. 8918
5	177424	. 8872	72579	. 8310	61492	. 9121	58631	. 8954
6	158324	. 8923	63339	. 8727	57677	. 9379	55826	. 9521
7	142190	. 8981	57304	. 9047	55073	. 9548	51049	. 9144
8	128561	. 9041	52467	. 9156	52979	. 9620	49055	. 9609
9	117033	. 9103	44607	. 8502	51324	. 9688	23614	. 4814
10	107265	. 9165	39040	. 8752	49694	. 9682	22633	. 9584
11	98962	. 9226	38532	. 9870	48416	. 9743	19411	. 8576
12	91885	. 9285	36121	. 9374	46747	. 9655	18091	. 9320
13	85836	. 9342	35705	. 9885	45718	. 9780	16729	. 9247
14	80647	. 9395	34881	. 9769	41494	. 9076	16068	. 9605
15	76184	. 9447	34138	. 9787	40042	. 9650	14243	. 8864
16	72336	. 9495	33281	. 9749	39063	. 9755	13389	. 9400
17	68999	. 9539	32693	. 9823	38192	. 9777	13008	. 9715
18	66094	. 9579	31085	. 9508	37193	. 9738	12727	. 9784
19	63546	. 9614	30737	. 9888	36444	. 9799	12414	. 9754
20	61295	. 9646	29969	. 9750	35033	. 9613	12152	. 9789
21	59273	. 9670	29460	. 9830	34325	. 9798	11807	. 9716
22	57423	. 9688	27849	. 9453	18343	. 5344	11544	. 9777
23	55677	. 9696	27540	. 9889	16437	. 8961	10972	. 9504
24	53951	. 9690	27027	. 9814	16011	. 9741	10595	. 9656
25	52120	. 9661	26105	. 9659	15288	. 9548	3694	. 3486
26	49948	. 9583	25789	. 9879	14955	. 9782	2468	. 6681
27	46891	. 9388	21529	. 8348	13055	. 8729	2389	. 9680
28	42130	. 8985	21171	. 9834	12441	. 9530	1956	. 8187
29	36978	. 8777	20929	. 9886	12216	. 9819	1767	. 9033
30	31700	. 8573	20649	. 9866	11111	. 9095	1723	. 9751
	0. 85		0.9		0.95		1.0	
0	333840	------	333840	------	333840	------	333840	------
1	124168	0. 3719	121487	0. 3639	119877	0. 3591	119341	0. 3575
2	91763	. 7390	89569	. 7373	87412	. 7292	85444	. 7160
3	71835	. 7828	70668	. 7890	70104	. 8020	70047	. 8198
4	64192	. 8936	63092	. 8928	62460	. 8910	62360	. 8902
5	57521	. 8961	57047	. 9042	57261	. 9168	57853	. 9277
6	54774	. 9522	54256	. 9511	54401	. 9500	54959	. 9500
7	49772	. 9087	50251	. 9262	51556	. 9477	52692	. 9587
8	47378	. 9519	47793	. 9511	49435	. 9589	50807	. 9642
9	27275	. 5757	38645	. 8086	46729	. 9453	49095	. 9663
10	25034	. 9178	33695	. 8719	44495	. 9522	47519	. 9679
11	23465	. 9373	31606	. 9380	40884	. 9188	46036	. 9688
12	22561	. 9615	30107	. 9526	38017	. 9299	44634	. 9695
13	21653	. 9597	27239	. 9047	28607	. 7525	43304	. 9702
14	21039	. 9716	25370	. 9314	22911	. 8009	42036	. 9707
15	20108	. 9557	24619	. 9704	20890	. 9118	40825	. 9712
16	19456	. 9676	24072	. 9778	19416	. 9294	39667	. 9716
17	16602	. 8533	23518	. 9770	18906	. 9737	38557	. 9720
18	14946	. 9002	23014	. 9786	18497	. 9784	37489	. 9723
19	14384	. 9624	22453	. 9756	18089	. 9779	36462	. 9726
20	13963	. 9707	21954	. 9778	17701	. 9785	35473	. 9729

TABLE I.—Continued

i \ β	$f(x_i)$	$\frac{f(x_i)}{f(x_{i-1})}$	$f(x_i)$	$\frac{f(x_i)}{f(x_{i-1})}$	$f(x_i)$	$\frac{f(x_i)}{f(x_{i-1})}$	$f(x_i)$	$\frac{f(x_i)}{f(x_{i-1})}$
	0.85		0.9		0.95		1.0	
21	12095	.8662	21356	.9728	17306	.9777	34518	.9731
22	10917	.9026	20842	.9759	16935	.9786	33597	.9733
23	10509	.9626	20115	.9651	16551	.9773	32706	.9735
24	10201	.9707	19515	.9702	16190	.9782	31843	.9736
25	8748	.8576	18227	.9340	15818	.9770	31008	.9738
26	7837	.8959	17230	.9453	15469	.9779	30197	.9738
27	7570	.9659	598	.0347	15103	.9763	29413	.9740
28	7366	.9730	280	.4682	14761	.9773	28648	.9740
29	6762	.9180	273	.9750	14396	.9753	27910	.9742
30	6352	.9394	264	.9670	14059	.9766	27191	.9742
	1.1		1.3		1.6		1.9	
0	333840		333840		333840		333840	
1	121486	.3639	138645	.4153	196562	.5888	293091	.8779
2	82591	.6798	84466	.6092	124599	.6339	256477	.8751
3	70272	.8508	69395	.8216	85428	.6856	219046	.8540
4	62921	.8954	62726	.9039	68391	.8006	188063	.8585
5	58869	.9356	58755	.9367	60665	.8870	162609	.8646
6	55940	.9502	56019	.9534	56682	.9343	141685	.8713
7	53827	.9622	53906	.9623	54199	.9562	124461	.8784
8	52009	.9662	52138	.9672	52332	.9655	110243	.8858
9	50457	.9701	50571	.9699	50740	.9696	98480	.8933
10	49000	.9711	49131	.9715	49290	.9714	88712	.9008
11	47669	.9728	47784	.9726	47936	.9725	80574	.9083
12	46391	.9732	46512	.9734	46660	.9734	73768	.9155
13	45190	.9741	45301	.9740	45440	.9738	68046	.9224
14	44031	.9743	44144	.9745	44277	.9744	63212	.9290
15	42929	.9750	43035	.9749	43165	.9749	59100	.9349
16	41866	.9752	41970	.9752	42097	.9752	55587	.9405
17	40851	.9757	40948	.9756	41068	.9755	52560	.9455
18	39865	.9759	39961	.9759	40077	.9759	49934	.9500
19	38917	.9762	39009	.9762	39123	.9762	47640	.9540
20	38001	.9765	38091	.9765	38200	.9764	45618	.9575
21	37114	.9766	37203	.9767	37307	.9766	43820	.9606
22	36257	.9769	36341	.9768	36444	.9769	42212	.9633
23	35426	.9771	35506	.9770	35607	.9770	40757	.9655
24	34619	.9772	34700	.9773	34795	.9772	39433	.9675
25	33835	.9773	33912	.9773	34007	.9773	38219	.9692
26	33073	.9775	33149	.9775	33239	.9774	37097	.9706
27	32333	.9776	32407	.9776	32496	.9776	36053	.9718
28	31613	.9777	31684	.9777	31770	.9776	35075	.9729
29	30913	.9778	30982	.9778	31066	.9778	34155	.9738
30	30230	.9779	30298	.9779	30380	.9779	33283	.9744

TABLE 2.

i \ β	0.1	0.3	0.6	0.8	0.85	0.9	0.95	1.0	1.1	1.3	1.6	1.9
1	0. 553	1. 660	3. 320	4. 427	4. 703	4. 980	5. 257	5. 533	6. 087	7. 193	8. 853	10. 513
2	. 595	2. 094	3. 576	2. 827	2. 691	2. 602	2. 558	2. 551	2. 625	2. 983	3. 751	4. 613
3	. 635	2. 377	3. 491	4. 642	5. 158	5. 543	5. 657	5. 442	4. 437	3. 242	3. 335	3. 844
4	. 670	2. 764	3. 585	2. 676	2. 532	2. 486	2. 525	2. 641	3. 057	3. 514	3. 335	3. 827
5	. 702	3. 319	3. 587	6. 157	7. 173	7. 484	6. 865	5. 781	4. 217	3. 635	3. 398	3. 826
6	. 732	4. 064	3. 766	2. 391	2. 315	2. 362	2. 508	2. 756	3. 369	3. 740	3. 522	3. 827
7	. 762	5. 168	3. 714	12. 626	16. 049	13. 847	9. 251	6. 267	4. 197	3. 822	3. 684	3. 829
8	. 792	7. 863	4. 012	2. 027	2. 030	2. 141	2. 412	2. 829	3. 620	3. 883	3. 824	3. 832
9	. 825	22. 205	3. 688	125. 896	108. 543	50. 509	12. 958	6. 466	4. 166	3. 921	3. 903	3. 834
10	. 862	21. 294	4. 390	2. 248	3. 025	1. 886	2. 248	2. 849	3. 766	3. 944	3. 939	3. 837
11	. 902	1. 519	3. 336	25. 889	4. 738	17. 968	22. 431	6. 513	4. 112	3. 956	3. 955	3. 841
12	. 947	11. 598	5. 688	1. 825	2. 912	2. 128	2. 085	2. 853	3. 847	3. 963	3. 963	3. 845
13	. 996	1. 198	2. 492	15. 493	6. 140	29. 005	79. 571	6. 530	4. 066	3. 968	3. 967	3. 849
14	1. 052	4. 095	19. 081	2. 087	2. 634	2. 525	1. 958	2. 856	3. 895	3. 971	3. 970	3. 855
15	1. 113	3. 761	1. 447	27. 349	9. 972	5. 586	27. 906	6. 542	4. 036	3. 973	3. 973	3. 860
16	1. 182	4. 595	4. 218	3. 301	2. 206	3. 407	2. 685	2. 858	3. 926	3. 975	3. 975	3. 866
17	1. 260	2. 977	3. 611	4. 480	41. 576	5. 009	4. 786	6. 550	4. 016	3. 977	3. 976	3. 873
18	1. 349	9. 809	4. 832	3. 474	1. 799	3. 207	3. 565	2. 859	3. 947	3. 978	3. 978	3. 880
19	1. 454	1. 233	2. 990	4. 986	9. 919	5. 628	4. 596	6. 557	4. 005	3. 979	3. 979	3. 887
20	1. 581	4. 668	8. 239	3. 103	2. 218	2. 954	3. 488	2. 860	3. 961	3. 981	3. 980	3. 895
21	1. 742	2. 893	1. 919	6. 463	41. 303	6. 818	4. 747	6. 563	3. 998	3. 982	3. 981	3. 903
22	1. 958	11. 156	116. 743	2. 567	1. 799	2. 657	3. 398	2. 861	3. 970	3. 983	3. 982	3. 911
23	2. 264	1. 131	1. 259	13. 274	10. 109	9. 627	4. 942	6. 568	3. 994	3. 984	3. 983	3. 918
24	2. 735	3. 300	1. 595	1. 962	2. 207	2. 332	3. 295	2. 862	3. 976	3. 984	3. 984	3. 926
25	3. 534	6. 757	9. 841	198. 581	44. 570	20. 471	5. 200	6. 571	3. 992	3. 985	3. 985	3. 933
26	5. 083	1. 714	1. 759	1. 628	1. 793	2. 015	3. 179	2. 863	3. 981	3. 986	3. 986	3. 940
27	8. 606	35. 356	30. 924	2. 204	8. 887	326. 505	5. 550	6. 574	3. 991	3. 986	3. 986	3. 946
28	15. 945	0. 755	1. 344	42. 957	2. 314	1. 817	3. 049	2. 863	3. 984	3. 987	3. 987	3. 952
29	20. 844	0. 993	2. 467	1. 695	24. 873	3. 018	6. 038	6. 576	3. 990	3. 988	3. 988	3. 957
30	25. 971	2. 110	22. 538	5. 189	1. 884	6. 291	2. 907	2. 864	3. 986	3. 988	3. 988	3. 962

4. Conversion to an Eigenvalue Problem

By introducing the variable x_{n+1}, an equation $Bx=c$ can be expressed in the homogeneous form $Cy=0$, where

$$C=(B \quad c), \qquad y=\begin{pmatrix} x \\ x_{n+1} \end{pmatrix}.$$

Multiplying through by C^* gives the system of order one higher $Dy=0$, where

$$D=\begin{pmatrix} B^*B & B^*c \\ c^*B & c^*c \end{pmatrix}$$

is a symmetric matrix whose least eigenvalue is zero. The nontrivial eigenvector corresponding to this zero eigenvalue yields a solution of the original system of linear equations.

As is well known, the least eigenvector of the symmetric matrix D can be found by minimizing the Rayleigh quotient

$$\mu(y)=\frac{y^*Dy}{y^*y}, \qquad y\neq 0.$$

Hestenes and Karush [8] have examined in detail the convergence of various methods for accomplishing the minimization of μ. The following algorithm for constructing a sequence $\{y_i\}$ that minimizes μ is a modification of their "optimum α" procedure. We define the gradient as $\xi_i=\xi(y_i)=Dy_i-\mu(y_i)y_i$. Let

$$\gamma_i=\frac{1}{\mu(\xi_i)}, \qquad \mu(\xi_i)\neq 0,$$

and let $\alpha_i=\beta\gamma_i$, where β is a positive number less than or equal to one. Then, given y_i, we determine y_{i+1} by the formula $y_{i+1}=y_i-\alpha_i\xi_i$.

This algorithm was actually carried out with the matrix

$$D=\begin{pmatrix} A & b \\ b^* & c^*c \end{pmatrix},$$

where A is given by (5), b is given by (6) with all components multiplied by 10 and $c^*c=.333840$. In view of (7) $Dy=0$ is actually a problem of the type just described. Runs were made with various values of β ranging between .7 and 1. For purposes of comparison, the same starting point (origin) as

in the computations recorded in section 3 was used and a record of

$$f(x)=\frac{y^*Dy}{|y_{n+1}|^2}$$

was kept. In table 3[3] we present the results of the run $\beta=.9$. The runs for other values of β showed substantially the same unstable behavior, while that for $\beta=1$ (optimum) showed a very stable behavior and as a result converged quite slowly. The numbers $f(x_i)$ and α_i, appearing in table 3, were originally computed to 10 places. The ratios $f(x_i)/f(x_{i-1})$ were computed from the original values of $f(x_i)$ and then cut down to the present size.

TABLE 3.

i	$f(x_i)$	$f(x_i)/f(x_{i-1})$	$0.9\gamma_i$
0	333840	------	------
1	121482	0. 3639	0. 4980
2	86700	. 7137	. 2575
3	70323	. 8111	. 7076
4	57533	. 8181	. 3951
5	60698	1. 0550	. 5478
6	53564	0. 8825	. 3968
7	53869	1. 0057	. 5494
8	49788	0. 9242	. 3479
9	46902	. 9420	. 5237
10	45704	. 9744	. 3046
11	41266	. 9029	. 5577
12	41045	. 9947	. 2761
13	36337	. 8853	. 6639
14	36011	. 9910	. 2482
15	31318	. 8697	. 9109
16	30291	. 9672	. 2189
17	24919	. 8226	1. 7145
18	22095	. 8867	0. 1909
19	7468	. 3380	5. 9172
20	6963	. 9324	0. 2758
21	5985	. 8595	. 6081
22	5541	. 9258	. 2493
23	4642	. 8378	. 8282
24	4206	. 9060	. 2201
25	3171	. 7540	1. 5481
26	2644	. 8339	0. 1912
27	264	. 0998	6. 6970
28	151	. 5733	0. 1766
29	117	. 7708	1. 4380
30	91	. 7806	0. 1908
31	11	. 1274	6. 4755
32	8	. 6933	0. 1890

5. Conclusion

The error function $f(x)$ goes monotonically to zero in each of the gradient methods. Hence the number $P_n=100f(x_n)/f(x_0)$ tells us what percentage of the distance from the starting point to zero remains to be covered at the nth step. Table 4 gives P_{30} for various values of β_i. We note

[3] The author thanks R. M. Hayes for furnishing him with most of the data appearing in table 3.

TABLE 4.

β	0. 1	0. 3	0. 6	0. 8	0. 85	0. 9
P_{30}	9. 49	6. 18	3. 33	0. 52	1. 90	0. 08
β	0. 95	1. 0	1. 1	1. 3	1. 6	1. 9
P_{30}	4. 21	8. 14	9. 05	9. 07	9. 10	9. 97

after 30 steps that, with the exception of the case $\beta_i\equiv\beta=.1$, all the gradient methods for values $\beta<1$ are converging faster than the optimum method, while all the gradient methods for values $\beta>1$ are converging at a slightly slower rate than the optimum method. For the eigenvalue method we have $P_{32}=.002$. The increased rate of convergence for this case is offset on the Card-Programmed Calculator by the greater length of time needed for each step. However, on a high-speed machine this factor would be negligible. An explanation of the speedier convergence of the eigenvalue procedure lies in the fact that the transformation of the problem to the homogeneous form has shrunk the ratio of the largest and the smallest nonzero eigenvalues. This improvement of "condition" is something that one could not generally expect to occur [10].

The ratios $f(x_i)/f(x_{i-1})$ compare the rate of convergence at each step with that of a geometric progression having the same ratio. A study of these numbers and of the corrections α_i brings into sharp focus the contrast between the instability of the gradient methods employing $\beta<1$ and the stability of those employing $\beta\geq 1$. In the method of steepest descent it is just this stability that permits acceleration. However, this acceleration must be achieved through a modification of the computational routine. On the other hand, the instability of the methods using $\beta<1$ leads to occasional accelerations without the introduction of any changes whatsoever in the computing routine.

From the point of view of using the "almost optimum" gradient method on a large scale computer, its self-acceleration property has more than theoretical interest. As is well known, the high-speed memory capacity of the computers now in existence is rather limited. Hence, the necessity of storing a special acceleration routine might prove to be a severe handicap indeed.

It is worth while to compare the values of α_i with the reciprocal eigenvalues of the matrices A and D. For A these reciprocal eigenvalues have been found to be approximately 2.0, 3.9, 5.7, 12.1, 63, and 372, while for D the finite reciprocal eigenvalues range between approximately 8.35 and 0.189.[4] We will pay particular attention to the points at which acceleration took place. One sees that preceding an acceleration there was a "smoothing run" during which the α_i's were in the range of the small reciprocal eigenvalues. On the iteration immediately before an acceleration, α_i was almost equal to the smallest reciprocal eigenvalue, while on the iteration

[4] These values were furnished by R. M. Hayes.

during which acceleration took place α_i was between the highest and next to highest reciprocal eigenvalues. It was just this technique of choosing α_i that the present author helped develop in previous experiments with a "fixed α" gradient method, which were conducted under the direction of M. R. Hestenes. In this method the operator chooses the value of α just before each iteration, and by judicious choices he can successfully accelerate the method to a considerable extent. However, this requires too many judgments of the operator to be practical for a fast machine or an inexperienced operator. Hence, it is quite hopeful to note the existence of methods suitable for high-speed machines that can duplicate the fixed α acceleration procedures without any intervention by the operator once the process has started.

6. References

[1] A. Cauchy, Méthode générale pour la résolution des systèmes d'équations simultanées, Compt. rend. L'Académie Sciences **25**, 536 (1847).

[2] H. B. Curry, The method of steepest descent for nonlinear minimization problems, Quart. Applied Math. **2**, 258 (1944).

[3] G. E. Forsythe and T. S. Motzkin, Asymptotic properties of the optimum gradient method, Bul. Am. Math. Soc. **57**, 183 (1951).

[4] A. S. Householder, Notes on numerical methods (1949–51) (typescript available at Oak Ridge National Laboratory).

[5] L. V. Kantorovitch, On an effective method of solving extremal problems for quadratic functionals, Compt. rend. (Doklady) de l'Académie des Sciences de l'URSS **48**, 455 (1945).

[6] G. Temple, The general theory of relaxation methods applied to linear systems, Proc. Roy. Soc. (London) **169** [A] 476 (1938–39).

[7] M. R. Hestenes and M. L. Stein, The solution of linear equations by minimization, in manuscript at the National Bureau of Standards, Los Angeles, Calif.

[8] M. R. Hestenes and W. Karush, A method of gradients for the calculation of the characteristic roots and vectors of a real symmetric matrix, J. Research NBS **47**, 45 (1951) RP2227.

[9] The problem of accelerating the optimum gradient method has recently been considered by G. E. Forsythe and T. S. Motzkin in a paper entitled, Acceleration of the optimum gradient method, presented to the American Mathematical Society (Stanford meeting) (April 28, 1951).

[10] For a discussion of the effect of this type of transformation on the condition of a matrix, see G. E. Forsythe and T. S. Motzkin, An extension of Gauss's transformation for improving the condition of systems of linear equations, typescript available at National Bureau of Standards, Los Angeles, Calif.

Los Angeles, August 13, 1951.

Journal of Research of the National Bureau of Standards Vol. 48, No. 12, June 1952 Research Paper 2311

An Alkaline Solution of Potassium Chromate as a Transmittancy Standard in the Ultraviolet

Geraldine W. Haupt

The need for a means of testing the reliability of the photometric scale of spectrophotometers in the ultraviolet region (where glasses are unsuitable) has led to the study of an aqueous solution of potassium chromate having the composition 0.0400 g/liter of K_2CrO_4 in 0.05 N KOH. Based on extensive measurements, using photographic, photoelectric, and visual spectrophotometry, standard values of spectral transmittancy have been determined for 1.000 and 2.000 cm of solution at 25° C from 220 to 500 mμ. These values have been tabulated along with derived values of absorbancy, molar absorbancy index a_M, and $\log_{10} a_M$. The latter values have been compared graphically with those of other observers. Changes in spectral transmittancy with changes in temperature have been determined. The work has also included a study of the effects due to the container bottle and to age of solutions over periods up to 8 years, and a comparison of results obtained with the solution prepared either from K_2CrO_4 or from $K_2Cr_2O_7$ as one of the reagents.

1. Introduction

A means of testing the reliability of the photometric scale of spectrophotometers in the ultraviolet region has been in demand for a number of years. With the introduction of commercial photoelectric spectrophotometers for the ultraviolet in 1940, the demand increased considerably.

Although glass filter standards of spectral transmittance [1, 2] [1] have proved to be a very satisfactory and valuable means of testing the reliability of the photometric scale of spectrophotometers in the visible region, they are in general unsatisfactory in the ultraviolet. Not only do all but a few special glasses absorb completely below 290 mμ, but, in addition, the ultraviolet spectral transmittances of many glasses change on exposure to strong ultraviolet radiant flux [2, 3, 4]. In these respects solutions in cells with quartz end plates are found to be superior to glasses for use in the ultraviolet. In addition, solutions are reproducible and can be prepared in the laboratory from specifications with relatively small time and cost. Various solutions have been studied or recommended [2] [3] for this purpose. Preeminent among these is an aqueous solution of potassium chromate, K_2CrO_4 (0.04 g/liter) in 0.05 N KOH. This has alternate regions of high transmission and absorption in the ultraviolet, and this one solution in 1- and 2-cm thicknesses covers the transmittancy scale from about 0.90 to about 0.01 (0.046 to 2.0 in absorbancy). Several investigators have previously worked with this solution, and from the information available in 1940 this appeared to be one of the best for the purpose. It was accordingly selected for calibration.[4]

To make the solution most useful as a calibration standard of spectral transmittancy in the ultraviolet, information should be available regarding its permanence, or stability, under specified conditions (including the effects of the container bottles on the spectral transmittancy) and regarding any change in its spectral transmittancy with temperature over the range of room temperatures to be expected. Such data have accordingly been obtained.

This investigation was started in 1940 and discontinued in 1943 because of the war. It was resumed in 1948, and preliminary data have been published [8, 9, 10]. The present paper describes the work leading up to the determination of these preliminary values, based solely on the measurements made in 1940–43, and describes the recent work on new solutions with a new instrument, on the basis of which the final values were derived as herein published.

2. Preparation of Solutions

All the potassium chromate solutions studied were prepared in the Bureau's Chemistry Division by W. Stanley Clabaugh. The solutions are of two general types (A) those prepared by dissolving the salt in dilute solution of KOH, and (B) those prepared by dissolving the salt in distilled water.

The type (A), or alkaline, solutions were prepared as follows:

(A_1): A solution of K_2CrO_4 stock material, reagent grade, 0.0400 g/liter, in 0.05 N KOH (solution of potassium hydroxide prepared by dissolving 3.3 g of potassium hydroxide sticks (85% KOH) of reagent

[1] Figures in brackets indicate the literature references at the end of this paper.

[2] For example, Brode [5, p. 209] lists potassium chromate, azobenzene, and potassium nitrate as solutions that can be accurately prepared as standards for the calibration of spectrophotometers.

[3] Photoelectric Spectrophotometry Group of England has recently conducted a collaborative test on the use of $K_2Cr_2O_7$ [6].

[4] Solutions can, of course, also be used in the visible region. In fact, the aqueous solutions of copper sulfate and cobalt ammonium sulfate used in the Davis-Gibson filters [7, 8, 9, 10] have been recommended for that purpose.

These solutions have their limitations for use as calibration standards both in the shortwave end of the visible region and in the ultraviolet region. In the visible, neither of them has sufficient absorption in the violet to be of much value for the purpose. In the ultraviolet, the copper sulfate solution varies rather rapidly from high transparency at wavelengths above 330 mμ to high absorption at wavelengths below 270 mμ and thus has no general utility over the whole region. The cobalt ammonium sulfate solution used in the Davis-Gibson filters [7] has too high transparency between 230 and 400 mμ to be of much value as a spectrophotometric standard. Solutions prepared at 10 times this concentration were found (unpublished data) to be unstable with time throughout the ultraviolet and were thus considered undesirable for use as spectrophotometric calibration standards.

quality in sufficient distilled water to make 1 liter).

(A_2): A solution of K_2CrO_4 of the same concentration and alkalinity as (A_1) but prepared from 0.0303 g of $K_2Cr_2O_7$[3], which, when converted gave 0.0400 g of K_2CrO_4/liter. This follows from the reaction $K_2Cr_2O_7+2KOH=2K_2CrO_4+H_2O$.

The purpose of dissolving the potassium chromate in dilute solutions of KOH was to prevent any dichromate from forming. In A_2 a potassium chromate solution was prepared by means of a different material, potassium dichromate. This solution was prepared to determine whether the spectrophotometric data from A_1 and A_2 would be identical. Since they were found to be identical, there is a distinct advantage in using potassium dichromate as one of the reagents rather than potassium chromate, because in stock material potassium dichromate exists in a purer state. A special sample of potassium chromate that had been recrystallized four times was used in the preparation of one of the B, or neutral, solutions with the view to studying the effect of the purity of the potassium chromate.

The solutions prepared in 1940, 1942, and again in 1949 were stored in liter bottles of the ordinary storeroom glass type with glass stoppers. For further study of the effect of storage, half of the 1940 alkaline solution prepared from K_2CrO_4 and half of the 1940 neutral solutions were stored in similar bottles lined with ceresin. The tips of the rubber stoppers used were also covered with ceresin. Also half of the alkaline solutions prepared by methods A_1 and A_2 in 1949 were stored in alkali-resistant glass (Corning glass 728).

None of the solutions was exposed to light except when actually in use to fill the cells for their measurement. No solution was ever poured out of its bottle. In filling the cells a pipette was used to draw off the solution. Where flaking occurred, the sediment thus remained on the bottom of the bottle. Each cell containing solution was measured relative to a similar cell containing distilled water.

The alkaline solutions are those from which the standard set of spectral transmittancies given in table 1 were obtained. Although both alkaline and neutral solutions were prepared originally for the purpose of establishing standard spectral transmittancy data, the neutral solutions were finally not used for that purpose. However, as the neutral solutions have been studied over a period of 8 years, a summary of the results on these is included in section 8.

3. Methods of Measurement

The solutions were measured on five instruments by three different methods. One instrument operates by a photographic method, primarily for the ultraviolet region, but extending also into the violet and blue; one by a visual method; and three by photoelectric, one of these being for the visible range only.

[3] Standard Sample $K_2Cr_2O_7$, No. 136, may now be obtained from the National Bureau of Standards. At the time these solutions were prepared, the chemicals used all conformed to ACS specification.

3.1. Photographic Method

The photographic data were obtained by means of the Hilger sector photometer with the Fuess quartz spectrograph [11, 12, 13].

The equivalent slit widths for an 0.2-mm slit, which was used throughout all the exposures, are

Wavelength	Slit widths	
$m\mu$	mm	$m\mu$
400	0.2	0.6
310	.2	.25
260	.2	.13
220	.2	.08

On each plate exposures were made of at least two aluminum spark spectra for wavelength calibration purposes. A calibration curve was used to translate scalar values, which were read at the density matchpoints, into wavelengths. Both 1.000- and 4.000-cm cells were used with the Hilger instrument.

3.2. Visual Method

The König–Martens spectrophotometer [13, 14] is a visual instrument. The slit widths used on this instrument are varied, depending upon the wavelength and the spectral characteristics of the sample being measured. With an incandescent source the equivalent slit widths in millimicrons used for two wavelengths and for two settings of the slits are given below:

Wavelength	Slit widths	
$m\mu$	mm	$m\mu$
400	0.5	2.7
500	.2	2.7

The mercury arc, also available for use on this instrument, enables transmittancy measurements to be made that are not subject to possible wavelength or slit-width errors.

Two cell lengths were used with this instrument, namely, 4.000 and 10.000 cm.

3.3. Photoelectric Method

a. Brackett Quartz Double Monochromator and Auxiliary Equipment [15]

The source of illumination used was a special incandescent lamp, with a quartz window, which operated on a 120-volt, 45-ampere battery. The monochromator has three slit systems. The exit slit next to the photoelectric tube was kept at a constant mechanical width for nearly all the measurements, and the other two were varied concurrently. Any stray energy that passes the second slit is effectively eliminated from reaching the exit slit by the use of the second spectrometer provided on this instrument.

The instrument operates with a single wavelength control. Spectral bands transmitted by the slits were comparable in width (mμ) to those obtained with the photographic method. A photoelectric cell of the electron-emission type was used as detector and values of spectral transmittancy were obtained by means of the ratio-of-deflections method with a high-sensitivity galvanometer.

The scale for reading or setting wavelengths on this monochromator is a linear one (not direct reading in millimicrons) and a wavelength calibration curve of the instrument was already available.[6] This curve was based upon scalar settings previously determined for mercury lines down to 237.8 mμ. As the incandescent lamp was the only source of irradiation for the spectrophotometric work, the wavelength calibration was frequently checked at one wavelength (557 mμ) by means of two particular standard glasses whose spectral transmittances are known to be the same at that wavelength. The linear correction determined at this wavelength was then applied to the whole scale.

The lower end of the wavelength calibration curve was extrapolated below 237.8 mμ for these measurements, and the data in this region with the Brackett instrument are therefore of lesser validity.

b. General Electric Recording Spectrophotometer

The General Electric recording spectrophotometer has been described in a series of three papers [16, 17, 18]. The data obtained with this instrument are for the visible range only and extend from 400 to 750 mμ. Checks on the wavelength scale were made in the usual manner by using a calibrated didymium glass. A nominal slit width equivalent to approximately 4 mμ was used throughout the recordings. Cells of 1.000-cm thickness were used for the measurements.

c. Beckman Quartz Spectrophotometer (Model DU)

The Beckman spectrophotometer has been described in a paper by Cary and Beckman [19]. Transmission measurements with a modification of this instrument, which has a constant-temperature enclosure [7] designed and constructed at the National Bureau of Standards, have been described in detail in a paper by Gibson and Balcom [20]. All measurements on the Beckman spectrophotometer were made with a 1.000-cm cell. The cell holder is kept constant at 25° C or other desired temperature by means of water pumped through from a constant-temperature bath.

For wavelength checks the Hg green line (546.1 mμ) was used. When necessary, the whole wavelength scale was adjusted by the slight turning of the internal screw that rotated the collimating mirror. After such check or adjustment, the precise wavelength correction was then applied at each wavelength setting in accordance with the curve illustrated in figure 6 of reference [20].

For transmittancy measurements three sources are available, namely, the incandescent-filament lamp, the hydrogen arc, and the mercury arc, all as supplied by the maker. The incandescent and hydrogen sources were used over the appropriate wavelength ranges, overlapping from 320 to 380 mμ. The slit widths with these sources never exceeded 2 mμ and were usually less than 1 mμ. The mercury arc was also used for transmittancy measurements at certain wavelengths as noted below.

A clear quartz lens similar to that supplied with the instrument was used to effect an approximate collimation of the beam. Over the wavelength range from 330 to 420 mμ with the incandescent source and from 360 to 380 mμ with the hydrogen source, a purple (Corning filter No. 9863) lens was used to reduce stray light as well as to collimate the beam.

4. Standard Spectrophotometric Data

In examining the data obtained during the first two years of the investigation, the type A, or alkaline, solutions were found to give more reproducible results (i. e., less scattering of data on repeated measurements) than the type B, or neutral, solutions. Furthermore, the alkaline solutions were found to give a better range of transmittancies in the extreme ultraviolet than the neutral solutions. Since the alkaline solutions were thus found to fulfill more nearly the requirements of a standard of spectral transmittancy in the ultraviolet, all later work and all the detailed data to be presented refer to the alkaline solution of potassium chromate (0.04 g/liter in 0.05 *N* KOH).

As already noted, the work on the 1940 and 1942 solutions was interrupted in 1943. Sufficient data were obtained, however, that a tentative set of spectral transmittancy values could be evaluated. These values are given [8] in column 2 of table 1, designated as T'_τ. They were read from a curve, of which figure 1 is a tracing. The individual determinations by the five instruments used are plotted and may be identified from the legend. These tentative values thus represent a graphical average of all these earlier data. Measurements were made on the 1940 solutions a few days after their preparation and then again at the end of 2, 4, 7, 8, and 10 months, 2 years 4 months, 2 years 5 months, and 2 years 7 months. The 1942 solutions were measured a few days after their preparation and again in 1, 2, and 6 months.

[6] Acknowledgment is here made to W. F. Roeser and M. S. Van Dusen for making the instrument and its calibration curve available.

[7] In 1942 a few measurements on a Beckman quartz spectrophotometer in the Bureau's Chemistry Division were made on an alkaline solution prepared in 1940. No temperature control was available for these measurements.

[8] These tentative values have also been published in [8; 9, p. 43–44; 10, p. 201].

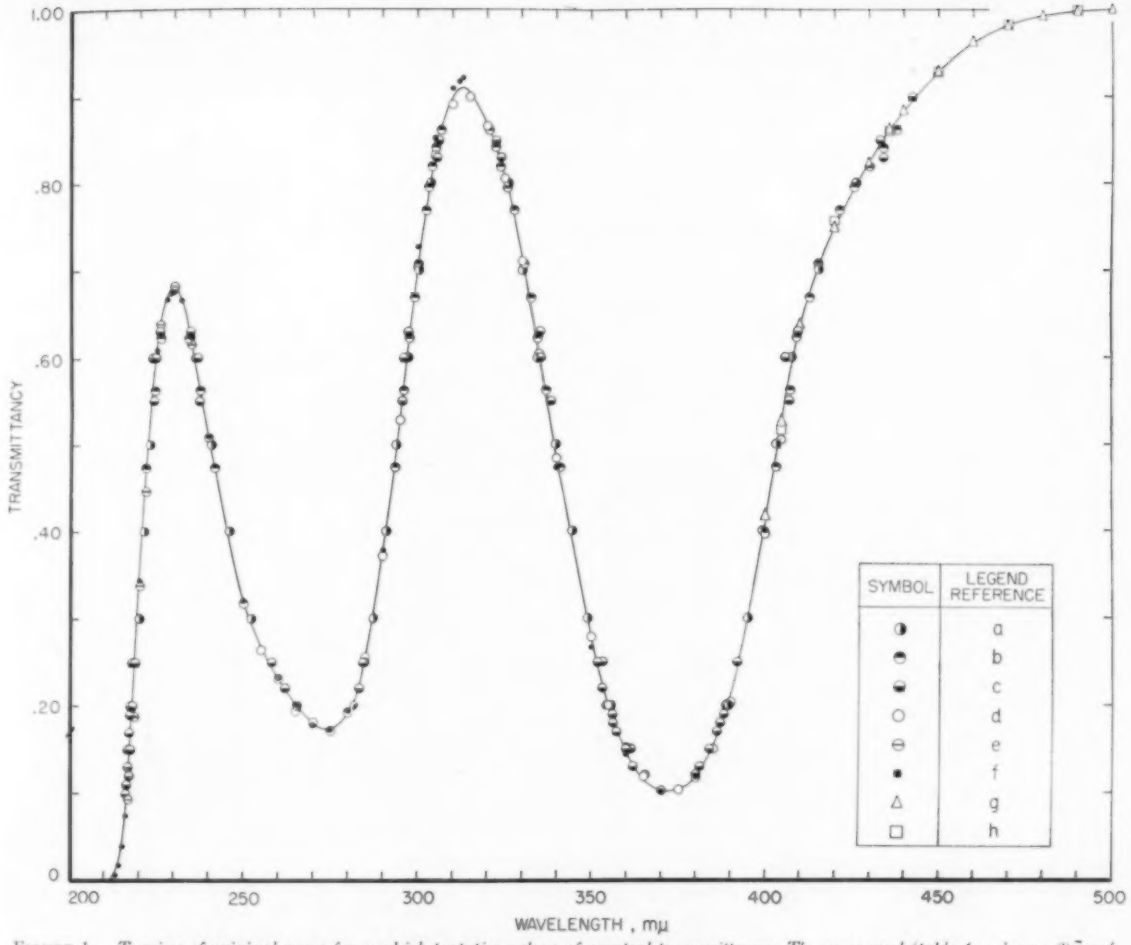

FIGURE 1. *Tracing of original curve from which tentative values of spectral transmittancy, T'_λ, were read (table 1, column 2) and published [8, 9, 10] for potassium chromate solution (0.0400 g/liter of K_2CrO_4 in 0.05 N KOH)*

Distilled water only was used in the solvent cell. These data were obtained in 1940 and 1942, as follows:

	Spectrophotometer	Wavelength range used	Alkaline solution prepared	Cell length	Number of determinations represented
		mμ		*cm*	
a	Hilger sector photometer (photographic).	215 to 450	A_1, 1940 A_2, 1940	1 1	5 to 7
b			A_1, 1940	4	1
c			A_1, 1940 A_2, 1940, 1942	1 1	1 to 3
d	Brackett double monochromator (photoelectric).	240 to 404.7	A_1, 1940, 1942 A_2, 1940, 1942	1 1	2 to 5
e		Adjusted below 240.	A_1, 1942 A_2, 1942	1 1	2
f	Beckman (photoelectric).	213 to 400	A_1, 1940	1	1
g	GE automatic recording (photoelectric).	400 to 750	A_1, 1942 A_2, 1942	1 1	4
h	König-Martens (visual).	404.7 to 600	A_1, 1940 A_2, 1940	4 10	1 to 4

TABLE 1. *Spectrophotometric data for a standard potassium chromate solution (0.0400 g/liter in 0.05 N KOH), unfiltered, at 25° C*

The final values of spectral transmittancy, T_λ, and absorbancy, A_λ, for 1.000 cm determined from this investigation are shown in columns 5 and 9. Derived from these data are values of T_λ for 2.000 cm, molar absorbancy index, a_M, and $\log_{10} a_M$, columns 10, 11, and 12. The tentative values of transmittancy, T'_λ, which have been published [8, 9, 10] were taken from column 2. The solution was measured in every case relative to a similar cell containing distilled water.

Wavelength	Transmittancy, T_λ, for 1.000 cm							Absorbancy, $A_\lambda = -\log_{10} T_\lambda$, for 1 cm	Transmittancy, T_λ, for 2 cm	Molar absorbancy index, a_M ($a_M = A_\lambda/bc$) [b]	$\log_{10} a_M$
	Tentative values of T'_λ [a] based on 1940–42 data (read from fig. 1)	Beckman 1949 data, 25° C		Final values of T_λ (5/24/49)	Deviations from final values						
		Hg source	H and/or incandescent sources		1940–42 data (2) − (5)	1949 Beckman					
						Hg values (3) − (5)	H, and/or incandescent values (4) − (5)				
1	2	3	4	5	6	7	8	9	10	11	12
mμ											
210	0.000	.....	.....	.....	.....	.....	.....	.....	.....	.....	.....
15	.037	.....	0.070	.....	.....	.....	.....	.....	.....	.....	.....
20	.35	.....	.358	0.358	−0.008	.....	0.000	0.446	0.128	2167	3.34
25	.60	.....	.601	.601	−.001	.....	.000	.221	.361	1074	3.03
30	.682	.....	.667	.674	+.008	.....	−.007	.171	.454	832	2.92
35	.617	.....	.615	.616	+.001	.....	−.001	.210	.379	1022	3.01
40	.509	.....	.505	.507	+.002	.....	−.002	.295	.257	1433	3.16
45	.408	.....	.397	.402	+.006	.....	−.005	.396	.162	1922	3.28
50	.319	.....	.319	.319	.000	.....	.000	.496	.102	2410	3.38
53.6	.279	0.278	.280	.279	.000	−0.001	+.001	.554	.078	2693	3.43
55	.258	.....	.258	.258	.000	.....	.000	.572	.072	2778	3.44
60	.232	.....	.234	.233	−.001	.....	+.001	.633	.054	3072	3.49
65	.201	.....	.204	.202	−.001	.....	+.002	.695	.041	3374	3.53
70	.180	.....	.181	.180	.000	.....	+.001	.745	.032	3617	3.56
75	.173	.....	.178	.175	−.002	.....	+.003	.757	.031	3676	3.57
80	.189	.....	.199	.194	−.005	.....	+.005	.712	.038	3459	3.54
85	.254	.....	.261	.257	−.003	.....	+.004	.590	.066	2866	3.46
90	.372	.....	.374	.373	−.001	.....	+.001	.428	.139	2080	3.32
95	.527	.....	.536	.533	−.006	.....	+.003	.273	.284	1327	3.12
98.7	.590	.605	.600	.598	−.008	+.007	+.002	.223	.358	1084	3.04
300	.703	.....	.710	.709	−.006	.....	+.001	.149	.503	726	2.86
02.2	.764	.779	.770	.771	−.007	+.008	−.001	.113	.594	548	2.74
05	.831	.....	.834	.834	−.003	.....	.000	.079	.666	383	2.58
10	.899	.....	.898	.895	+.004	.....	−.007	.048	.801	234	2.37
13.2	.910	.907	.897	.905	+.005	+.002	−.008	.043	.819	211	2.32
15	.904	.....	.893	.900	+.004	.....	−.007	.046	.810	222	2.35
20	.867	.....	.860	.864	+.003	.....	−.004	.064	.746	308	2.49
25	.810	.....	.797	.804	+.006	.....	−.007	.095	.646	460	2.66
30	.715	.....	.706	.710	+.005	.....	−.004	.149	.504	722	2.86
34.2	.622	.620	.619	.620	+.002	.000	−.001	.208	.384	1008	3.00
35	.603	.....	.598	.600	+.003	.....	−.002	.222	.360	1077	3.03
40	.486	.....	.480	.483	+.003	.....	−.003	.316	.233	1535	3.19
45	.379	.....	.367	.373	+.006	.....	−.006	.428	.139	2080	3.32
50	.281	.....	.272	.276	+.005	.....	−.004	.559	.076	2715	3.43
55	.202	.....	.196	.199	+.003	.....	−.003	.701	.040	3405	3.53
60	.148	.....	.148	.148	.000	.....	.000	.830	.022	4030	3.61
65	.115	.114	.118	.116	−.001	−.002	+.002	.936	.013	4544	3.66
70	.102	.....	.104	.103	−.001	.....	+.001	.987	.011	4795	3.68
75	.103	.....	.102	.102	+.001	.....	.000	.991	.010	4815	3.68
80	.118	.....	.116	.117	+.001	.....	−.001	.932	.014	4526	3.66
85	.172	.....	.147	.130	+.002	.....	−.003	.824	.022	4002	3.60
90	.207	.....	.198	.202	+.005	.....	−.004	.695	.041	3374	3.53
95	.301	.....	.287	.294	+.007	.....	−.007	.532	.086	2582	3.41
400	.410	.....	.395	.402	+.008	.....	−.007	.396	.162	1922	3.28
04.7	.521	.515	.508	.515	+.006	.000	−.007	.288	.265	1400	3.15
10	.635	.....	.620	.632	+.003	.....	−.002	.199	.399	968	2.99
20	.748	.....	.754	.751	−.003	.....	+.003	.124	.564	604	2.78
30	.824	.....	.824	.824	.000	.....	.000	.084	.679	408	2.61
35.8	.861	.860	.856	.859	+.002	+.001	−.003	.066	.738	320	2.51
40	.884	.....	.880	.882	+.002	.....	−.002	.054	.778	265	2.42
50	.928	.....	.926	.927	+.001	.....	−.001	.033	.859	160	2.20
60	.961	.....	.959	.960	+.001	.....	−.001	.018	.922	86	1.93
70	.981	.....	.979	.980	+.001	.....	−.001	.009	.960	43	1.63
80	.992	.....	.990	.991	+.001	.....	−.001	.004	.982	19	1.28
90	.998	.....	.996	.997	+.001	.....	−.001	.001	.994	6	.80
500	1.000	.....	.999	1.000	.000	.....	−.001	.000	1.000	.....	.....

[a] These values were read from the original of figure 1 and are consistent with the values published later [8, 9, 10].

[b] $c = 0.0002059\ M$; $b = 1$ cm.

In April 1949 four sets of data were taken on the Beckman spectrophotometer [20], one on each of freshly prepared alkaline (A_1 and A_2) solutions maintained at 25° C, stored both in glass and alkali-resistant ware.

The four sets of data were averaged. Values obtained with the mercury source are listed in column 3 of table 1; values obtained with the hydrogen and/or incandescent sources are listed in column 4.

The final values of T_s shown in column 5 were derived according to the following procedures:

(a) At the mercury wavelengths, a straight average of three sets of data, namely, (1) 1949 Beckman data with mercury line source (column 3); (2) 1949 Beckman data with hydrogen and/or incandescent continuous-spectrum source (column 4); (3) Tentative values based on 1940–42 data, T'_s, (column 2).

(b) At other wavelengths above 220 mμ (with the exception of 295 to 315) a straight average of two sets of data, namely, (1) 1949 Beckman data with hydrogen and/or incandescent source (column 4); (2) Tentative values based on 1940–42 data, T'_s (column 2).

At 295, 300, 305, 310, and 315 mμ slight further adjustments in T_s (not exceeding 0.003) were made to bring the final values into better agreement with the averages obtained at the mercury wavelengths, using procedure (a).

Columns 6, 7, and 8 of table 1 show the deviations of the three sets of data from the final values. It is evident that there may be considerable uncertainty in the third decimal of column 5.

Values of spectral absorbancy, A_s, for a 1.000-cm thickness of solution are given in column 9. These values of A_s were derived from the relation $A_s = -\log_{10} T_s$. To cover the photometric scale below $T_s = 0.10$, values of transmittancy for a 2.000-cm cell were computed and are given in column 10.

Column 11 gives values of the molar-absorbancy index [21] $a_M \equiv A_s/bc$ where c is the concentration expressed in moles per liter, and b is the cell thickness in centimeters. Column 12 gives the values of $\log_{10} a_M$.

5. Comparison of Data with Those of Other Observers

Tabular data on the spectral transmittancy of potassium chromate in 0.05 N potassium hydroxide have been published by von Halban and Siedentopf [22], Rössler [23], Baly, Morton, and Riding [24], and Hogness, Zscheile, and Sidwell [25].

Hogness, Zscheile, and Sidwell used a photoelectric method for their determinations. The potassium chromate was recrystallized four and five times. They show the absorption spectrum for this solution in a figure [25]. The dots through which the curve is drawn in their figure are taken from several series of determinations at 2.5-mμ intervals from 220 to 410 mμ. Values of molar extinction for the maxima and minima and for 366 and 265 mμ were given in tabular form. The experimental conditions under which these tabulated data were obtained are given in table 2.

Figure 2 compares the present data with those already published in tabular form. $\text{Log}_{10} a_M$ is used for this comparison in accord with the practice used in the International Critical Tables [26]. The methods used in the various studies are shown in the caption.

TABLE 2. *Experimental conditions under which certain data of Hogness, Zscheile, and Sidwell [25] were obtained*

Wavelength	Molar-absorbancy index	Spectral region isolated	Cell thickness	Concentration	
mμ	*aM*	*mμ*	*cm*	*g/liter*	*M*
Maxima:					
272.5	3660	0.74	2	0.00860	0.04428×10^{-3}
371.0	4830	1.32	2	.00650	.03347
Minima:					
229.0	752	.72	2	.0400	.2059
312.5	203	1.10	7	.0400	.2059
Mercury lines:					
265.0	3460	.....	2	.00765	.0394
366.0	4720	.....	2	.00575	.0296

From figure 2 it may be seen that in general the agreement in $\log_{10} a_M$ from 220 to 450 mμ found by the five investigators shown is quite close, with the exception of a few points. Below 300 mμ, two values of von Halban (photoelectric method) at 254 and 265 mμ are at variance with the rest. Above 300 mμ, the value of Baly, Morton, and Riding (photographic method) at 313.2 mμ, seems erroneous. Most of the 16 wavelength values of Rössler from 381.5 to 439.0 mμ will be seen to be lower in $\log_{10} a_M$ than those of the others shown. In his paper, Rössler has put these wavelengths in parentheses; apparently these were so indicated because of the relatively low dispersion of the prism in his instrument.

In the present investigation only a single concentration of potassium chromate was used. No attempt was made to carry out a study of conformity to Beer's law, because the one solution in 1- and 2-cm thicknesses covered the photometric range of interest. However, it was known that Hogness, Zscheile, and Sidwell had made a run on exactly the same concentration used by von Halban and found good agreement with their curve [25] obtained from data on optimum concentration. From these data it was concluded that Beer's law held. Results have also been published [27] of Beer's law tests on potassium chromate in 0.05 N KOH at 372 mμ. Various dilutions were used, and the results are given in both tabular and graphical forms. The molecular concentrations used varied from 1.61×10^{-5} to 51.5×10^{-5}. This corresponds to variations in concentration from 0.00313 to 0.1000 g/liter. Determination of this compliance with Beer's law was made as a means of checking the photometric reproducibility of a new spectrophotometer.

6. Effect of Temperature on Spectral Transmittancy

Because it was desirable to know whether or not the potassium chromate solution for use as a calibration standard changed in spectral transmittancy

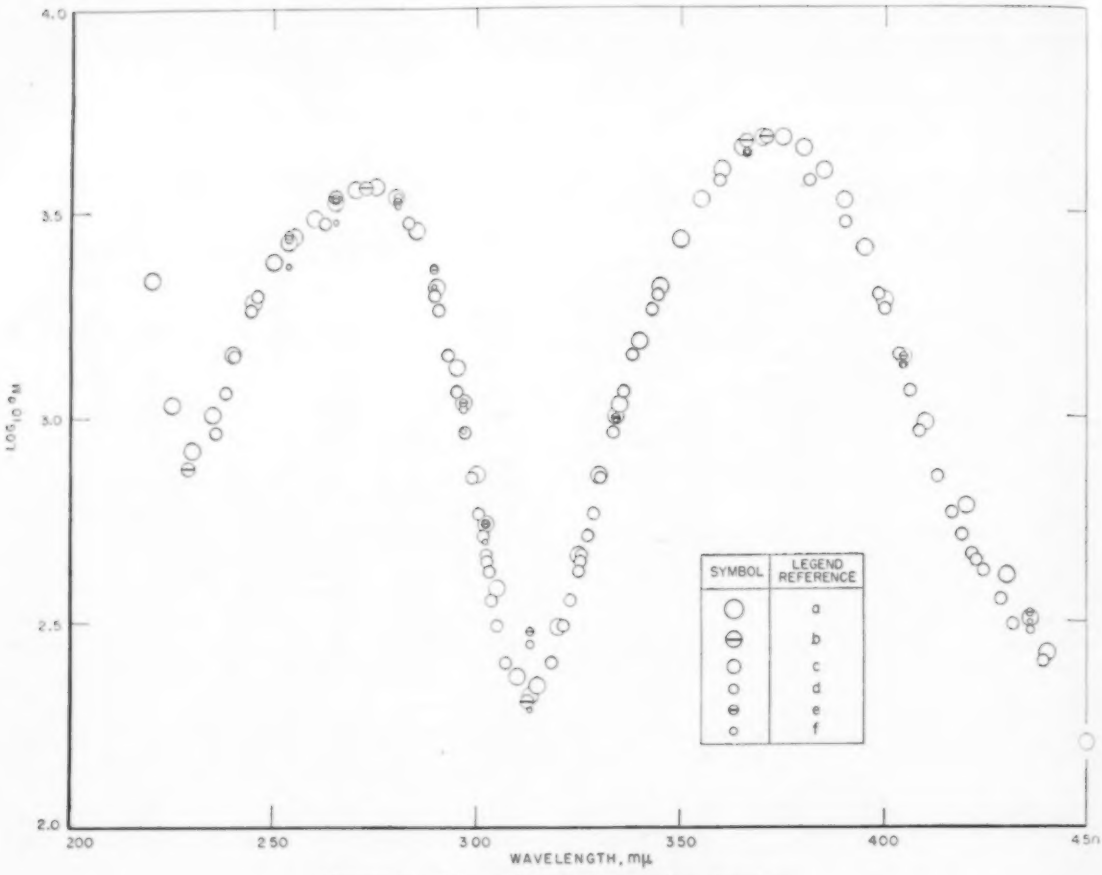

FIGURE 2. *Values of* $\log_{10} a_M$ *for potassium chromate.*

Molar solution in 0.05 *N* KOH. b=1 cm; $a_M = A_s/bc = -\log_{10} T_s/bc$.
a. From NBS final data, column 12 of table 1.
b. Hogness, Zscheile, Sidwell; photoelectric.
c. Rössler; photographic.
d. Baly, Morton, and Riding-Hilger rotating sector; photographic.
e. Baly, Morton, and Riding Judd-Lewis sector; photographic.
f. von Halban; photoelectric.

with change in temperature, several preliminary tests were made in 1948 on the 1942 solutions by means of the Beckman spectrophotometer [20]. The resulting data indicated that the largest effects due to changes in temperature occur below 235 mμ.

A more detailed and complete study of the change in spectral transmittancy with temperature was then made for the 1949 alkaline solutions of both types stored in alkali-resistant bottles. The wavelength range from 215 to 500 mμ was studied for approximately a 25-deg change in temperature. The spectral-transmittancy data were determined for one solution over a definite wavelength range at 25°, 50°, and again at 25° C in a single day. Each change in spectral transmittancy for an approximately 25-deg change in temperature was computed separately for each day's set of measurements. Three sets were averaged and are plotted in large circles in figure 3.

Included in the figure are also points obtained from the measurements made on the 1942 alkaline solutions at various times at each of the temperatures, 25° and 50° C. These data corroborate the data obtained with the 1949 solutions. It may be of interest to point out that the changes in transmittancy with increase in temperature shown in figure 3 are such as to indicate a shift of the absorption bands toward longer wavelengths.

The curve shown in figure 3 was then drawn, from which values of ΔT_s for a change of 25 deg were read. Values of ΔT_s for a change of 10 deg were computed from these curve readings by linear interpolation, and the resulting data are given in table 3. Users of the standard solution should

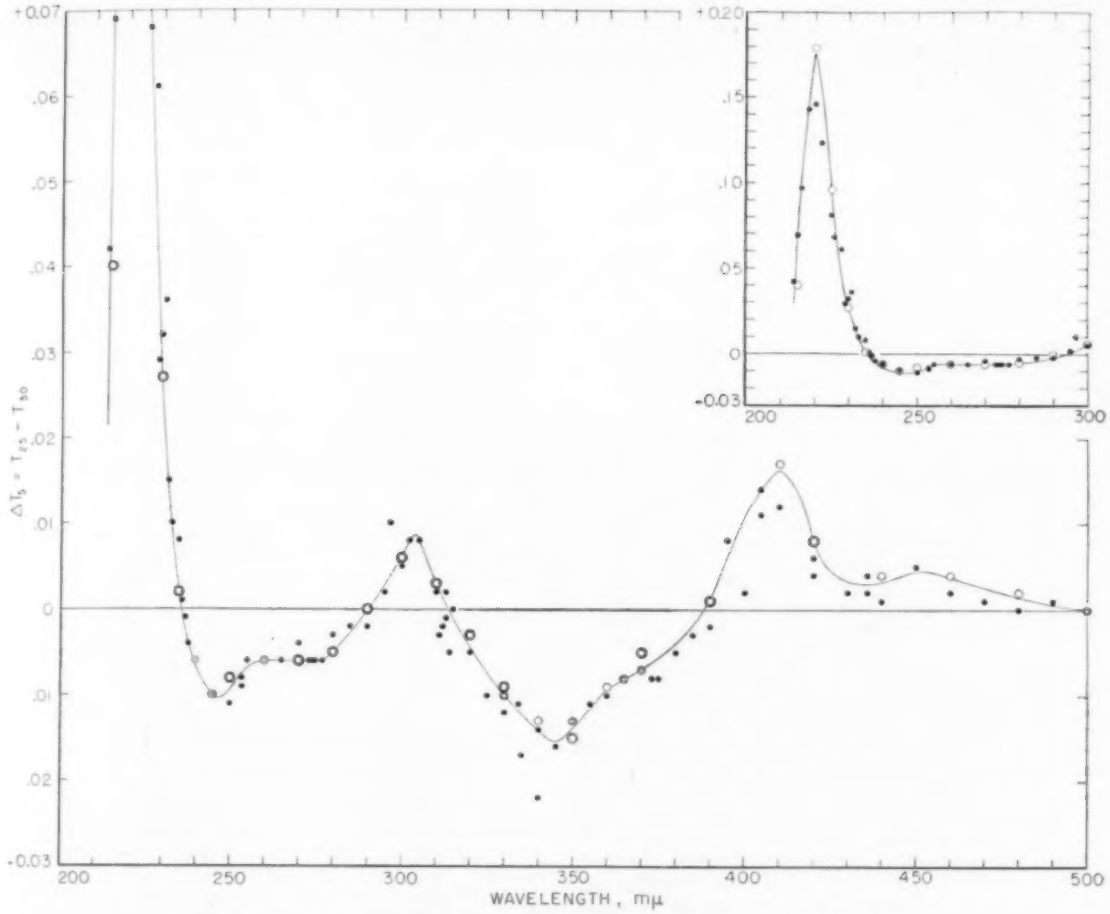

FIGURE 3. *Change in spectral transmittancy for a change in temperature of 25° C.*

In establishing this curve more weight has been given to the data obtained from the 1949 solutions. The values of ΔT_s given in table 3 for a 10° change in temperature were derived from this curve by linear interpolation.

○, $\Delta T_5 (= T_{25} - T_{30})$ for 1949 solutions. (The measurements were all made on the same day.)

●, ΔT_s for 1942 solutions. (The measurements were made in 1948, mostly on different days.)

make use of these corrections proportionately whenever the temperature of the solution deviates importantly from 25° C. Values of ΔA_s in table 3 are derived from the values of ΔT_s by the relation.

$$\Delta A_s = -\log_{10} e \frac{\Delta T_s}{T_{s\,(\mathrm{avg})}}.$$

7. Permanence

Measurements have been made from time to time on these alkaline solutions, and the study has included effects due to the storage of some of the solutions over periods up to 8 years. The 1940 alkaline solution made from K_2CrO_4 in KOH was stored both in an ordinary glass bottle and in a similar bottle lined with ceresin. The 1940 alkaline solution made from $K_2Cr_2O_7$ and the 1942 alkaline solutions made both from chromate and dichromate were stored only in ordinary glass bottles.

Above 260 mμ no definite change in spectral transmittancy was found for the solutions stored in glass. Below 260 mμ the 1940 alkaline solutions showed definite changes at the end of 8 years of storage in glass bottles, the solution made from the dichromate exhibiting the smaller change. The fact that potassium dichromate in stock material exists in a purer state may account for this solution being more stable. However, the 1942 alkaline solutions of both types likewise stored in glass bottles showed little if any change in spectral transmittancy over a period of 6 years.

TABLE 3. *Values of* ΔT_s $(=T_{25}-T_{35}$ *or* $T_{15}-T_{25})$ *for a 10°C change in temperature corresponding to wavelengths listed*

These values are for a cell length of 1.000 cm and are two-fifths of the values read from the curve of figure 3. Values of ΔA_s are derived from the values of ΔT_s.

Wavelength	Values of ΔT_s for 10 deg. C	Values of ΔA_s for 10 deg. C	Wavelength	Values of ΔT_s for 10 deg. C	Values of ΔA_s for 10 deg. C
mμ			mμ		
210	----------	----------	330	.0040	.0024
15	+0.028	−0.22	34.2	.0047	.0033
20	.070	.094			
25	.035	.026	35	.0049	.0035
30	.0100	.0055	40	.0056	.0050
			45	.0032	.0072
35	+.0010	−.0007	50	.0056	.0087
40	−.0026	+.0022	55	.0046	.0099
45	.0040	.0043			
50	.0038	.0051	60	.0037	.0107
53.6	.0030	.0046	65	.0033	.0122
			70	.0028	.0116
55	.0027	.0044	75	.0022	.0093
60	.0024	.0045	80	.0016	.0059
65	.0024	.0051			
70	.0024	.0058	85	−.0007	+.0020
75	.0024	.0059	90	+.0005	−.0011
			95	.0024	.0036
80	.0020	.0045	400	.0043	.0047
85	.0011	.0019	04.7	.0056	.0047
90	−.0001	+.0001			
95	+.0011	−.0009	10	.0085	.0045
96.7	.0016	.0012	20	.0032	.0019
			30	.0013	.0007
300	.0025	.0015	35.8	.0012	.0006
02.2	.0031	.0017	40	.0013	.0006
05	.0032	.0017			
10	.0012	−.0005	50	.0018	.0008
13.2	+.0001	.0000	60	.0015	.0007
			70	.0010	.0004
15	−.0004	+.0002	80	.0005	.0003
20	.0018	.0009	90	+.0002	−.0001
25	.0030	.0016	500	.0000	.0000

For the 1940 alkaline solution made from K_2CrO_4 in KOH and stored in a ceresin-lined bottle, measurements from time to time showed that changes in absorption were occurring. Data obtained at the end of an 8-year period showed that complete absorption had occurred below 370 mμ. Obviously, therefore, an ordinary glass bottle is better for storage of a solution of potassium chromate in KOH than a ceresin-lined bottle. No study of the permanence of the alkaline solutions stored in alkali-resistant bottles has been made.

It must also be concluded from this study that since the data below 260 mμ show possibility of a change in spectral transmittancy after a 6-month period, solutions no older than 6 months should be used for the photometric calibration of a spectrophotometer in this region of the spectrum. On the other hand, for regions above 260 mμ, it seems safe to use alkaline solutions of either type stored in ordinary glass bottles up to a period of 5 years.

8. Neutral Aqueous Solutions of Potassium Chromate

Considerable data were obtained on the B solutions (see section 2) and a summary is presented here.

The spectral-transmittancy curve of neutral solutions of potassium chromate was found by Hantzsch [28] to differ somewhat from the alkaline solution, and the results reported here corroborate this finding. From 400 to 500 mμ the curve for the neutral solution is less steep than that of the alkaline solution with a crossing point at about 440 mμ, above which the transmittancy of the alkaline solution is slightly higher. Between 300 and 330 mμ the neutral solution is slightly lower in transmittancy than the alkaline solution and slightly higher both below and above this range up to 440 mμ. Below 230 mμ this difference is large, the transmittancy at 215 mμ being 0.40 for the neutral solution and 0.07 for the alkaline. The value (0.07) for this wavelength may be found in table 1, column 4. More weight should be given the 1949 Beckman data below 225 mμ, because the measurements were obtained under closely controlled conditions of temperature and while the solutions were still fresh, two important controls for this particular region (sections 6 and 7). However, this particular value may be somewhat in error due to another cause, namely, the possible presence of impurities in the KOH.

Over a period of years the neutral solutions were found to be more permanent than the alkaline solutions. Significant changes from 8-year storage in a glass bottle were confined to the spectral region below 230 mμ; and for storage in a ceresin-lined bottle changes were found only below 260 mμ. A specially pure sample (recrystallized four times) changed still less. The neutral solutions did not cause flaking in the bottles as the alkaline solutions do.

From the standpoint of permanence and convenience in storage the neutral solutions are slightly superior to the alkaline solutions, and had they been found equally reproducible the neutral solutions might be preferable as spectral transmittancy standards instead of the alkaline solutions.

9. Summary

Spectrophotometric studies of neutral and alkaline aqueous solutions of potassium chromate extending over a period of years have shown that the alkaline solution is the better suited for use as a spectral-transmittancy standard in the ultraviolet. The spectral transmittancy of this solution has been determined by five spectrophotometers used according to three different methods, and the final values are given in table 1 from 220 to 500 mμ. The final results are also expressed there in terms of absorbancy, $A_s=-\log_{10}T_s$, for a 1-cm cell; molar absorbancy index, $a_M=A_s/bc$; and $\log_{10}a_M$. Changes of transmittancy with temperature were evaluated, and correction data for deviations from the standard temperature of 25° C are given in table 3.

When stored in ordinary glass bottles, the solution is reasonably stable for 5 or 6 years. For work of the highest precision, however, to avoid unsuspected errors from any cause, it is recommended that solutions not over 6 months old prepared from chemicals of the highest purity be used as transmittancy standards.

10. References

[1] K. S. Gibson, Geraldine K. Walker, and Mabel E. Brown, Filters for testing the reliability of spectrophotometers, J. Opt. Soc. Am. **24**, 58 (1934).

[2] Kasson S. Gibson and Marion A. Belknap, Permanence of glass standards of spectral transmittance, J. Research NBS **44**, 463 (1950) RP2093.

[3] W. W. Coblentz and R. Stair, Data on ultraviolet solar radiation and the solarization of window materials, BS J. Research **3,** 629 (1929) RP113.
[4] W. W. Coblentz and R. Stair, Ultraviolet transmission changes in glass as a function of the wavelength of the radiation stimulus, BS J. Research **13,** 773 (1934) RP744.
[5] Wallace R. Brode, Chemical spectroscopy, 2d ed. (John Wiley & Sons, Inc., 1945).
[6] Photoelectric Spectrometry Group Bulletin No. 4 (J. A. Breckall & Sons, Liverpool, 1951).
[7] Raymond Davis and K. S. Gibson, Filters for the reproduction of sunlight and daylight and the determination of color temperature, Misc. Pub. NBS 114 (1931).
[8] Standards for checking the calibration of spectrophotometers (200 to 1,000 mμ), Letter Circular NBS 929 (1948).
[9] K. S. Gibson, Spectrophotometry (200 to 1,000 millimicrons), Circ. NBS 484 (1949).
[10] Analytical absorption spectroscopy, edited by M. G. Mellon (John Wiley & Sons, Inc., 1950).
[11] K. S. Gibson, H. J. McNicholas, E. P. T. Tyndall, and M. K. Frehafer with the cooperation of W. E. Mathewson, Bureau of Chemistry. The spectral transmissive properties of dyes, I. Seven permitted food dyes in the visible, ultraviolet, and near infrared, Sci. Pap. BS **18,** 121 (1922–23) S440.
[12] H. J. McNicholas, Use of the under-water spark with the Hilger sector photometer in ultraviolet spectrophotometry, BS J. Research **1,** 939 (1928) RP33.
[13] K. S. Gibson, Spectrophotometry at the Bureau of Standards, J. Opt. Soc. Am. **21,** 564 (1931).
[14] H. J. McNicholas, Equipment for routine spectral transmission and reflection measurements, BS J. Research **1,** 793 (1928) RP30.
[15] F. S. Brackett, H. T. Wensel, and J. B. H. Kuper, Quartz double monochromator with single wavelength control, Phys. Rev. **57,** 1059 (1940).
[16] A. C. Hardy, History of the design of the recording spectrophotometer, J. Opt. Soc. Am. **28,** 360 (1938).
[17] J. L. Michaelson, Construction of the General Electric recording spectrophotometer, J. Opt. Soc. Am. **28,** 365 (1938).
[18] K. S. Gibson and H. J. Keegan, Calibration and operation of the General Electric recording spectrophotometer of the National Bureau of Standards, J. Opt. Soc. Am. **28,** 372 (1938).
[19] H. H. Cary and A. O. Beckman, A quartz photoelectric spectrophotometer, J. Opt. Soc. Am. **31,** 682 (1941).
[20] K. S. Gibson and Margaret M. Balcom, Transmission measurements with the Beckman quartz spectrophotometer, J. Research NBS **38,** 601 (1947) RP1798.
[21] Terminology and symbols for use in ultraviolet, visible, and infrared absorptometry, Letter Circular NBS 857 (1947).
[22] H. von Halban and K. Siedentopf, Über die Verwendung von photoelektrischen zellen zur Messung der Lichtabsorption in Lösungen II, Z. physik. Chem. **100,** 208 (1922).
[23] G. Rössler, Bemerkungen zur Technik der photographischen Spectrophotometrie, Ber. chem. Ges. **59,** 2606 (1926).
[24] E. C. C. Baly, R. A. Morton, and R. W. Riding, The measurement of absorptive power, Proc. Roy. Soc. [A] **113,** 709 (1926).
[25] T. R. Hogness, F. P. Zscheile, and A. E. Sidwell, Photoelectric Spectrophotometry—An apparatus for the ultraviolet and visible spectral regions: Its construction, calibration, and application to chemical problems, J. Phys. Chem. **41,** 379 (1937).
[26] International Critical Tables **V,** 330 (McGraw-Hill Book Co., Inc., New York, N. Y., 1929) (see fig. 4).
[27] W. C. Miller, G. Hare, D. C. Strain, K. P. George, M. E. Stickney, and A. O. Beckman, A new spectrophotometer employing a glass Fery prism, J. Opt. Soc. Am. **39,** 377 (1949).
[28] A. Hantzsch, Optische Untersuchungen über die Chromophore farbiger Salze und Säuren, Z. physik. Chem. **72,** 362 (1910).

Washington, April 2, 1952.

Journal of Research of the National Bureau of Standards Vol. 48, No. 6, June 1952 Research Paper 2332

Two Applications of Group Characters to the Solution of Boundary-Value Problems[1]

E. Stiefel[2]

It is shown that the numerical work involved in solving a boundary-value or eigenvalue problem by finite difference methods in a domain with many symmetries can often be reduced by applying the theory of group characters to the group of symmetries of the domain.

In the second part the author considers the problem of solving $\Delta u=0$ in a cube when the prescribed boundary values are invariant under the group of rotations of the cube. In the series representation of the solution in terms of harmonic polynomials only a subset of these polynomials actually occurs, and the theory of group characters facilitates considerably the determination of this subset.

It is very well known that representation of groups may be a useful tool in discussing various eigenvalue problems in quantum mechanics. This is due to the fact that boundary-value problems of Schroedinger's equation are to be solved mostly in the whole space or inside a sphere as fundamental region and therefore the high symmetry of those domains can be used.

It is the purpose of this paper to show that group characters sometimes are appropriate also to simplify the numerical computation of boundary-value or eigenvalue problems in more general-shaped domains, in particular if the problem has been translated into the language of difference calculus. It will be sufficient to explain this discussing simple examples.

Let, for instance, A be any plane region and D a differential operator invariant under Euclidean motions or reflections of the plane. More exactly, if $f(x,y)$ is a function in our plane and M a Euclidean rotation, translation, or reflection, then

$$D(Mf)=M(Df), \tag{1}$$

which is to say that D must commute with any motion M. The Laplace operator Δ and the operator $\Delta\Delta$ of elasticity problems have this property.

In order to solve any given boundary-value problem with respect to the region A and the operator D, we may use the difference technique, introducing a square lattice L in A and replacing f by a lattice function (defined only in the lattice points) and D by a difference operator, which approximates the given differential operator. In the case of a Δ-problem, the corresponding difference operator may be given by figure 1. Relation (1) will be true again in the difference case, provided that by M is understood any motion or reflection transforming the lattice into itself.

Suppose now that the given region A is invariant under a group G of transformations of this type. If A has no symmetry at all, we may use Schwarz's alternating process dividing A into overlapping subregions, each of them having symmetry properties.

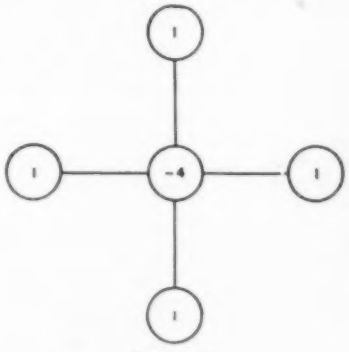

FIGURE 1.

It is our goal to show how the group G can be used in order to simplify the solution of the given boundary-value problem in the region A.

Take, for instance, the square region A of figure 2. The group G is in this case the symmetry group of the square of order 8 having the following similarity classes:

Class	Elements	Number of elements
[1]	Identity	1
[2]	Rotations $\pm 90°$	2
[3]	Rotation 180°	1
[4]	Reflection in horizontal or vertical line	2
[5]	Reflections in diagonal lines	2
	Total	8

(2)

The given boundary-value problem is equivalent to a system of nine linear equations for the values of the wanted function in the nine interior lattice points. Any lattice function f may be visualized as a vector in a nine-dimensional vector space S. Therefore, applying the operations of the table to the lattice functions, we get a linear representation R of the basic group G in S.

[1] This work was performed on a National Bureau of Standards contract with the University of California, Los Angeles, Calif., and was sponsored (in part) by the Office of Naval Research.

[2] University of California, Los Angeles, Calif., and Eidgenossische Technische Hochschule, Zurich, Switzerland.

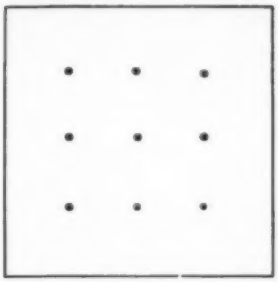

FIGURE 2.

It is not too hard to show that its character χ is given by the following rule: The value $\chi(M)$ of χ for an element M of G is equal to the number of lattice points fixed under the operation M. (Use as coordinate system in S the lattice functions not equal to 0 only in one single lattice point; they are permuted by M.) We want to decompose the representation R into irreducible components:

$$R=c_1R_1+c_2R_2+\ \ldots\ +c_5R_5, \tag{3}$$

Where $R_1, R_2, \ldots, R_5$ are the irreducible representations of G. (There are exactly five because G has five similarity classes). According to the orthogonality theorems of representation theory this has to be done working on the table of characters of G as follows:

Class	[1]	[2]	[3]	[4]	[5]	c
No. of elements	1	2	1	2	2	
χ_1	1	1	1	1	1	3
χ_2	1	1	1	−1	−1	0
χ_3	1	−1	1	1	−1	1
χ_4	1	−1	1	−1	1	1
χ_5	2	0	−2	0	0	2
χ	9	1	1	3	3	

(4)

In the first line we have listed the similarity classes with their numbers of elements and in the following lines the values of the characters of the irreducible representations in those classes. They are recorded in many textbooks of representation theory.[3] The last line is the character χ of our representation R, computed according to the rule previously mentioned. The first number in each line is the degree of the representation (dimension of the vector space transformed by the representation). According to a general formula of character theory the coefficient c_i in (3) is

$$c_i=\tfrac{1}{8}\sum_{(M)}\chi(M)\chi_i(M), \tag{5}$$

with the group element M running through the whole group G. By this we have for instance from our table

$$c_4=\tfrac{1}{8}(9\cdot1-2\cdot1+1\cdot1-2\cdot3+2\cdot3)=1.$$

The multiplicities c_i are listed in the column to the right of the table. Finally, we find

$$R=3R_1+R_3+R_4+2R_5. \tag{6}$$

Therefore, the vector space S splits into subspaces

$$S_1,\quad S_1',\quad S_1'';\quad S_3;\quad S_4;\quad S_5,\quad S_5', \tag{7}$$

each of them being invariant under R and being transformed by the irreducible representation given by its subscript.

Take now a set of subspaces having the same subscript (i. e., being transformed by the same representation) and introduce base vectors in each space of the set. For instance, S_5 and S_5', being both two-dimensional, may be spanned by the base vectors

$$\begin{aligned} S_5:&\quad e_{51},\quad e_{52}\\ S_5':&\quad e_{51}',\quad e_{52}'. \end{aligned} \tag{8}$$

Generally speaking, each set of equally transformed subspaces yields a rectangular arrangement of base vectors by listing the base vectors of each subspace in a line. The length of the rectangle is the degree of the irreducible representation under consideration and its height the multiplicity of this representation as a component of R. It is, of course, possible to choose the base vectors in such a way that each line of the rectangle is transformed exactly in the same way.

It follows then from a well-known generalization [4] of Schur's lemma that each linear operator in S commutable with the transformations of R transforms the vectors of each column in our rectangle among themselves and in each column in the same way. Taking into account the relation (1), we see that the difference operator of the given boundary-value problem has this property. From this follows immediately that the original system of nine linear equations with nine unknowns splits into partial systems. The rectangle (8), for instance, yields two systems of two equations each, having the same coefficient matrices. From the first and the c column of the table (4) we get therefore the following final result. The system of nine equations splits into one system of three simultaneous equations, one single equation, one single equation, and two systems of two simultaneous equations.

If we have to deal with an eigenvalue problem instead of a boundary-value problem, the analogous statement is, that the wanted characteristic polynomial is the product of a factor of third degree, two linear factors and the square of a quadratic factor. In order to carry out the decomposition of the system of nine equations explicitly, it is, of course, necessary

[3] A. Speiser, Die Theorie der Gruppen von endlicher Ordnung, 3d ed., p. 179–180 (Springer, Berlin; and Dover Pub).

[4] B. L. van der Waerden, Die gruppentheoretische Methode in der Quantenmechanik, sect. 13, p. 47–50 (Springer, Berlin, 1932).

to establish the lattice functions, which build the base vectors of the different rectangles (8). The three basic lattice functions corresponding to the first irreducible representation P_1 are simply three linear independent functions invariant under all motions of the square. As another example we give the values of the lattice functions (8) in the nine lattice points.

$$\epsilon_{51}=\begin{matrix}0&0&0\\-1&0&1\\0&0&0\end{matrix},\qquad \epsilon_{52}=\begin{matrix}0&1&0\\0&0&0\\0&-1&0\end{matrix},$$

$$\epsilon'_{51}=\begin{matrix}-1&0&1\\0&0&0\\-1&0&1\end{matrix},\qquad \epsilon'_{52}=\begin{matrix}1&0&1\\0&0&0\\-1&0&-1\end{matrix}. \tag{9}$$

Taking as D the operator of figure 1, we get

$$\begin{aligned} D\epsilon_{51}&=-4\epsilon_{51}+\epsilon'_{51}\\ D\epsilon'_{51}&=\ \ 2\epsilon_{51}-4\epsilon'_{51}. \end{aligned} \tag{10}$$

The functions $\epsilon_{52}, \epsilon'_{52}$ are transformed in the same way.

The eigenvalue problem of the operator D with vanishing boundary values gives the equation

$$Df+\lambda f=0. \tag{11}$$

Let us put $f=a\epsilon_{51}+b\epsilon'_{51}$. Then (10) yields the eigenvalue problem

$$\begin{aligned} (\lambda-4)a+2b&=0\\ a+(\lambda-4)b&=0. \end{aligned} \tag{12}$$

And from this follow the eigenvalues

$$\lambda=4\pm\sqrt{2} \tag{13}$$

of the operator D, each of them having at least the multiplicity 2.

It is not too hard to establish for a lattice in a given region A the rectangles of base vectors when we know the characters and the irreducible representations of the symmetry group of A. It is convenient to choose all those vectors (their total number is equal to the number of lattice points) orthogonal to each other. This is possible because the representation R is orthogonal, and therefore the irreducible subspaces of S are orthogonal.

At the Institute of Applied Mathematics in Zurich (Switzerland) we used the methods of this paper in order to solve the boundary-value problem of Airy's elasticity function inside a dam. As subregions in Schwarz's alternating process, we chose squares of 16 lattice points.

In his book about eigenvalue problems, L. Collatz[5] introduces the notion of "eigenvalues of a graph" and discusses an example, where the graph is built by the segments joining two midpoints of edges of a cube. This problem may also be treated by characters, using the group of all rotations of the cube.

In this section another application of character theory is discussed, related to the methods of S. Bergman and M. Picone for the solution of boundary-value problems. For our purposes those methods may be characterized by the following procedure. At first a complete set of particular solutions of the given partial differential equation is constructed and then the solution of the boundary-value problem is expanded into a series having as terms those particular integrals. Let us take, for instance, Laplace's equation $\Delta u=0$ in three-dimensional space. The particular solutions may be in this case the harmonic polynomials of degree n

$$Y_n^{(m)}(x,y,z)=r^n\cdot e^{m\phi i}\cdot P_n^{(m)}(\cos\ \theta),\qquad n=0,1,2,\ \ldots \tag{14}$$

m running from $(-n)$ to $(+n)$. On the right side, r, θ, ϕ are polar coordinates, $P_n^{(m)}$ is a generalized Legendre polynomial. Suppose now that the fundamental region A of the boundary-value problem is a cube having its center at the origin and suppose furthermore that the given boundary values are invariant under the group G of the 24 rotations of the cube. It is obvious that under those circumstances only harmonic polynomials appear in the Bergman-Picone expansion, which have the same symmetry properties. In other words, we have the problem to establish all harmonic polynomials invariant under the group G of rotations of the cube.[6]

The theory of characters gives general methods in order to solve problems of this type. G has the following similarity classes:

Class	Typical element	Number of elements
[1]	Identity	1
[2]	Rotation $\pm 90°$	6
[3]	Rotation 180° (z-axis)	3
[4]	Rotation 180° (axis: $z=0, x=y$)	6
[5]	Rotation $\pm 120°$ (axis = diagonal)	8
	Total	24

(15)

By any rotation of the cube the $(2n+1)$ harmonic polynomials of a given degree n are transformed linearly among themselves and yield therefore a representation R_n of degree $(2n+1)$ of G. Let M be any rotation of G and $\chi_n(M)$ the character of R_n. The number of linear independent harmonic polynomials of degree n invariant under G is equal to the multiplicity c_n of the unit representation in the decomposition of R_n into irreducible components. (The unit representation of a group maps every

[5] L. Collatz, Eigenwertaufgaben mit technischen Anwendungen, p. 332 (Leipzig, 1949).

[6] This question has been posed and answered by G. Polya and B. Meyer, Sur les symétries des fonctions sphériques de Laplace, Compt. rend. 228, 28-30 (1949); Sur les fonctions sphériques de Laplace de symétrie cristallographique donnée, Compt. rend. 228, (1949).

group element into the one-row matrix=1). This multiplicity is given by the character formula

$$c_n=\frac{1}{24}\sum_{(M)}\chi_n(M), \tag{16}$$

M running through the group. It remains to compute the character $\chi_n(M)$. In order to do this we may restrict ourselves to rotations M around the z-axis. Let μ be the rotation angle. Taking into account (14), it follows that the $(2n+1)$ harmonic polynomials of degree n are transformed by M in the following way:

$$Y_n^{(m)}\to e^{m i\mu}Y_n^{(m)}. \tag{17}$$

The matrix of the transformation is pure diagonal with the trace

$$\chi_n(M)=\sum_{m=-n}^{+n}e^{m i\mu}=\frac{\sin(2n+1)\frac{\mu}{2}}{\sin\frac{\mu}{2}}. \tag{18}$$

From (16) and the table (15) follows now the result:

$$c_n=\frac{1}{24}\left\{(2n+1)+6\,\frac{\sin(2n+1)45^\circ}{\sin 45^\circ}\right.$$
$$\left.+9\sin(2n+1)90^\circ+8\,\frac{\sin(2n+1)60^\circ}{\sin 60^\circ}\right\}. \tag{19}$$

The final result may be expressed in the following terms. Write n in the form of a multiple of 12 and the corresponding remainder

$$n=12\cdot k+r,\qquad 0\le r<12. \tag{20}$$

Then

$$c_n=k+t(r), \tag{21}$$

where $t(r)$ is given by the table

r	0	1	2	3	4	5	6	7	8	9	10	11
$t(r)$	1	0	0	0	1	0	1	0	1	1	1	0

. (22)

The polynomials themselves can be built by choosing any harmonic polynomial of degree n, applying the 24 rotations of the cube and adding up the 24 resulting polynomials.

A more general problem would be to establish the harmonic polynomials being transformed by G according to a given irreducible representation of G. This can be used to simplify the solution of a boundary-value problem in which the given boundary-values have not the symmetry of the cube. The basic idea is, of course, the same as outlined previously in this paper.

Los Angeles, January 29, 1952.

Journal of Research of the National Bureau of Standards Vol. 48, No. 6, June 1952 Research Paper 2313

Heterogeneous Equilibria at the Glass Electrode-Solution Interface

Donald Hubbard and Richard G. Goldman

Heterogeneous equilibria at the glass-solution interface were investigated in connection with the pH response of glasses. The preferential leaching of alkali and other cations from the glass surface by acid aqueous solutions, leaving a silica-rich layer to act as a nonmigratable negatively charged ion, caused an uneven distribution of the migratable ions of the system in accordance with the dictates of the Donnan membrane equilibria and the "equation of products." The uneven distribution of $Ag(NH_3)_2^+$, and Br^- ions for various experimental conditions was readily followed potentiometrically for Corning 015, a series of Na_2O-CaO-SiO_2, and a series of Na_2O-SiO_2 glasses. The Donnan membrane theory is compatible with the various experimentally observed phenomena such as the swelling of the glass surface, repression of swelling by high concentrations of electrolytes, voltage departures in alkaline and hydrofluoric-acid solutions, voltage departures in the "superacid" region, and asymmetry potentials. However, the Donnan membrane considerations do not account for the preferential voltage response of the glass electrode to hydrogen ions with the complete or partial exclusion of other ions.

1. Introduction

Silicate glasses upon immersion in most acid aqueous solutions exhibit a preferential leaching of alkali and other cations from the more durable framework. This remaining silica-rich layer acting as negatively charged nonmigratable ions must necessarily cause an uneven distribution of all migratable ions in the system in accord with the distribution law and Donnan membrane equilibrium [1, 2].[1] Thus, a glass surface, which is generally looked upon as chemically inert and static, turns out to be transient for every solution and seething with activity. However, the framework of the silica-rich layer for many glasses is frequently sufficiently resistant to the attack of a large number of aqueous solutions to establish conditions that are adequately stable to be studied and discussed in terms of equilibria [3, p. 276]. The present investigation was undertaken to ascertain what experimental evidence could be obtained demonstrating the nature of the heterogeneous equilibria at glass-aqueous solution interfaces and to determine what part these equilibra play in the preferential electrical response of many glasses to hydrogen ions with the complete or partial exclusion of the effects of many other ions [3].

2. Theoretical Considerations

Two gases separated by a membrane that is permeable to each will diffuse through this membrane in both directions until at equilibrium both sides of the partition contain mixtures of identical composition. Such a condition also holds true for a membrane separating two solutions of different composition, if the membrane is permeable to both the solute and the solvent. However, for a case in which the membrane is impermeable to one of the ions, these simple conditions no longer prevail. In the case of the leached surface of many silicate glasses there exists an ionogen with one ion, namely, the negatively charged silica-rich layer, which cannot migrate across the glass-solution interface, while all the other ions of the system are free to do so.

For the simple case in which a leached glass surface is placed in an aqueous hydrochloric acid solution, the initial state of the system may be represented as follows: [2]

H^+	H^+
Gel^-	Cl^-
(1)	(2)

As the H^+ and Cl^- ions are free to pass across the interface, but the gel^- ions are not, the equilibrium state may be represented as

H^+	H^+
Gel^-	Cl^-
Cl^-	
(1)	(2)

To visualize the distribution of H^+ and Cl^- ions at equilibrium, it is only necessary to remember that the oppositely charged ions must pass through the interface in pairs, otherwise electrostatic forces will be immediately set up which would prevent further diffusion. Therefore, the rate of migration of these ions across the interface depends upon the frequency with which they chance to arrive in pairs, which in turn is determined by the product of their concentration. Thus at equilibrium, when

[1] Figures in brackets indicate the literature references at the end of this paper.

[2] In the present derivation no attempt will be made to clarify the confused silicate chemistry for glasses of varied composition. One is merely concerned with the facts that the silica-rich layer has a negative charge, adheres to the glass surface, and is permeable to the ions present in the aqueous solution. In the absence of more specific knowledge concerning the valence of the anions of this silica-rich layer, it will merely be represented by a single negative charge. However, any other negative valence ascribed to it will not alter the conclusions.

the transfer of H^+ and Cl^- ions from the outer solution to the silica-rich layer is equal to that from the glass surface to the outer solution, the product of the concentration of these ions must have the same value on either side of the interface.

$$[H^+]_2 \times [Cl^-]_2 = [H^+]_1 \times [Cl^-]_1.$$

The addition of other monomonovalent electrolytes to the system does not destroy the validity of the "equation of products." Further, the addition of polyvalent ions does not greatly complicate the situation. If a polyvalent ion arrives at the interface, it will pass across only when an equivalent number of oppositely charged ions appear there at the same time.

At equilibrium, since silica gel^- as well as H^+ and Cl^- ions are in the silica-rich layer, the hydrogen-ion concentration, $[H^+]_1$, in the gel must be greater than the chloride-ion concentration, $[Cl^-]_1$. The nature of this unequal distribution of ions may well be emphasized and rationalized further. For the outer solution, let $x=[H^+]_2=[Cl^-]_2$, and for the silica-rich layer, let $y=[Cl^-]_1$, and $z=[gel^-]_1$. Hence, $y+z=[H^+]_1$. As the equation of products must be fulfilled, $x^2=y(y+z)$. In this relation the product of equals has been equated to the product of unequals. From inspection it is obvious that the sum of the unequals is greater than the sum of the equals, that is, $2y+z>2x$. The validity of this is readily illustrated by the following simple numerical example chosen at random.

$$x^2=y(y+z) \quad 15\times 15=3(3+72)=225.$$

$$2y+z>2x \quad 3+3+72>15+15, \text{ or } 78>30.$$

From this it becomes evident that the concentration of ions in the silica-rich layer at equilibrium is greater than in the outer solution. This unequal distribution of ions gives rise to an appreciable osmotic pressure across the glass-solution interface. If this excess concentration is represented by e, $2y+z=2x+e$. If z is eliminated by solving simultaneously the equations $2y+z=2x+e$ and $x^2=y(y+z)$, then $x=y+\sqrt{ex}$. This relation shows at a glance that x is greater than y, that is, the concentration of Cl^- ions is greater in the outer solution than in the silica-rich layer. It is evident from this that there should be not only a difference in osmotic pressure, but also a difference in electrical potential, $E=RT/F \log_e x/y$ volts, across the glass-solution interface.

Without continuing further into the derivation of the more complicated thermodynamic aspects of the heterogeneous equilibria to be expected at the glass-solution interface, the above considerations suggest pertinent experiments for partially confirming or wholly disproving the validity of the above conclusions. For example, the osmotic pressure predicted across the glass-solution interface should give rise to persistent forces which would tend to cause swelling of the glass surface, the extent of which would be partially determined by the mechanical strength of the silica framework and its chemical durability. Any such swelling or other surface alterations can be readily followed by means of the interferometer [4, 5].

Another set of experiments which can be readily followed potentiometrically is the uneven distribution of $Ag(NH_3)_2^+$ and Br^- ions between the outer solution and the silica-rich surface of leached glasses.

3. Experimental Procedures

Surface alterations of the glasses brought about by exposure to the various solutions were followed on polished specimens by means of the interferometric procedure previously used in determining the chemical durability of optical and other glasses [4, 5]. The exposures were made at 80° C by partial immersion of rectangular glass specimens having at least one surface sufficiently flat to give interference bands when placed under a fused-silica optical flat. This procedure leaves one portion of the specimen unexposed for use as the reference plane. In all cases, swelling was plotted in the figures as negative attack.

The titration of Ag^+ and Br^- ions was made potentiometrically, using the Ag, AgBr electrode and the glass half-cell as the indicator and reference electrode, respectively. The glass electrode was adopted as the reference electrode in order to eliminate the possibility of contamination of the experimental solutions with chloride ions from the conventional salt bridge of the saturated calomel half-cell. Further, it served as a reliable indicator in the neutralization of excess NH_4OH with sulfuric acid immediately prior to the titration of silver or bromide ions. The use of the glass electrode as the reference cell allows the potentiometric readings to be obtained without transference [6]. However, this latter feature is an unnecessary refinement, and contributes no particular scientific advantage to the present investigation other than operational simplicity. By using the potentiometric procedure it was possible to titrate the solutions in the presence of powdered glass samples and the AgBr precipitated during neutralization, thereby eliminating the use of color indicators and the need for filtration, washing, and evaporation. All potentiometric measurements were made at room temperature, using a Beckman pH meter, model G.

The saturated solution of silver-ammonium bromide, $Ag(NH_3)_2Br$, was prepared by dissolving silver bromide in full-strength aqueous-ammonia solution. Full-strength ammonia was used in every case because of its minimal attack on the silica-rich layer as indicated by previous experiments on voltage departures of the glass electrode [7] and the chemical durability of glasses [5, 8]. By taking advantage of the differences in solubility products of silver iodide, silver bromide, and silver chloride (approximate values 10^{-16}, 8×10^{-13}, and 10^{-10}, respectively), the silver bromide was precipitated and purified by the addition of silver nitrate to a solution containing an excess of potassium bromide. The initial portion of the precipitate was discarded in order to remove any iodide in the potassium bromide, while all

chlorides remained in solution after the addition of the $AgNO_3$ and were eliminated. The silver bromide was washed repeatedly in hot distilled water with vigorous agitation with a centrifugal stirrer to remove K^+, NO_3^-, and excess Br^- ions.

All powdered glass samples were prepared by crushing the experimental glasses in a steel mortar, and that portion was used that fell between the limits of U.S. Standard sieves Nos. 50 and 150.

4. Results and Discussions

4.1. Surface alterations

a. Swelling of Glass Surfaces in Acid Solution

The derivations presented in the section on theoretical considerations pointed out that the concentrations of ions in the silica-rich layer at equilibrium are greater than in the outer solution, and that such unequal distribution must result in an osmotic pressure across the glass-solution interface. This osmotic pressure must in turn tend to cause swelling of the glass surface in all solutions in which the silica-rich layer is formed, and the framework is chemically durable. Table 1 and figure 1 illustrate typical examples of the surface alterations of several glasses upon exposure for 6 hours at 80° C to a series of buffer solutions covering the range from pH2 to pH12. Swelling is exhibited by four of these glasses in the acid buffer solutions in which silicate ions are not readily soluble. However, for the alkaline range in which soluble silicates are formed, the rate of solution of all the glasses exceeds the rate of swelling. Glasses having superior chemical durability, namely, fused silica, Pyrex chemical glassware 774, and a Na_2O-CaO-SiO_2 (18:10:72) glass, showed no detectable swelling in the acid buffers during the period of the test. Such superior glasses are known to show relatively little leaching of alkali by acid solutions [9], and thus the mechanism for initiating the uneven distribution of migratable ions with the attendant swelling is minimized. However, it must not be assumed that these effects are completely absent. Such an assumption would be incorrect, as will be demonstrated by the data presented later on the uneven distribution of migratable ions at the glass-solution interface for chemical Pyrex and fused silica (table 2). Thus, in the present experiments we find surface alterations in the acid solutions ranging from vigorous to not detectable swelling, depending on the nature of the glasses. Such results are at least compatible with the predictions based on Donnan membrane equilibria. Swelling has been found to occur for so many silicate glasses in acid buffers that one is inclined to conclude that swelling always takes place in the earlier stages of attack except for solutions forming soluble silicate or other soluble silicon compounds [5, 8].

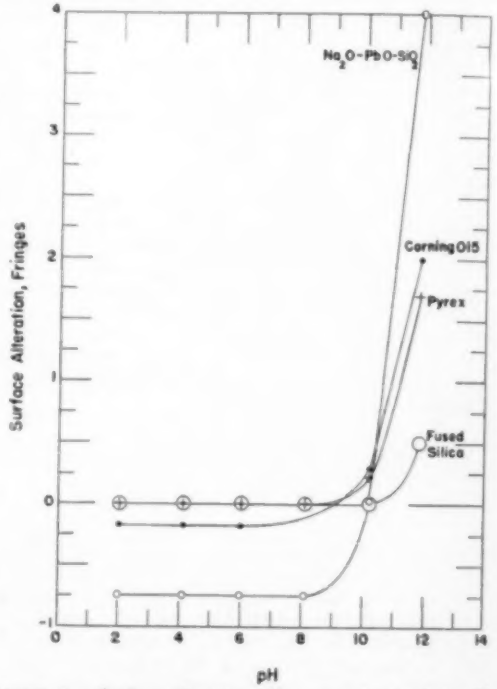

FIGURE 1. *Surface alteration-pH curves for typical silicate glasses for exposures of 6 hours at 80° C.*

TABLE 1. *Typical surface alterations exhibited by various silicate glasses upon exposure for 6 hours at 80° C to Britton Universal buffer mixtures covering the range* pH *2 to* pH *11.8*

Glasses							Surface alteration at pH					
Na_2O	K_2O	PbO	CaO	B_2O_3	P_2O_5	SiO_2	2.0	4.1	6.0	8.1	10.2	11.8
mole %	mole %	mole %	mole %	mole %	mole %	mole %	*Fringes*	*Fringes*	*Fringes*	*Fringes*	*Fringes*	*Fringes*
28	.....	.....	.....	.....	.....	72	36 swell.....	36 swell.....	36 swell.....	36 swell.....	1/10 swell....	120 attack.
18	10	.....	.....	.....	.....	72	36 swell.....	36 swell.....	30 swell.....	30 swell.....	Pitted.....	193 attack.
18	.....	10	.....	.....	.....	72	3/4 swell.....	3/4 swell.....	3/4 swell.....	3/4 swell.....	D attack....	4 attack.
22 [a]	.....	.....	6	.....	.....	72	2/10—swell..	2/10—swell..	2/10—swell..	SC [e]	1/4+attack..	2 attack.
18	.....	.....	10	.....	.....	72	ND [d]	ND	ND	D [f]	1/2 attack..	3 attack.
3.6 [b]	6.2	.....	.....	2.2	13	81	ND	ND	ND	D	1/4—attack..	1 3/4—attack.
(c)	.....	.....	.....	.....	.....	100	ND	ND	ND	ND	ND	1/2—attack.

[a] Corning 015; [b] Pyrex chemical glassware 774; [c] Fused silica; [d] ND, not detectable; [e] SC, surface cut; [f] D, detectable.

TABLE 2. *Excess $Ag(NH_3)_2^+$ ions appearing in the surface, and the surface alterations of soda-lime-silica and soda-silica glasses leached at* pH2 *at 80° C*

Glass			Surface alteration after 6 hr at pH2		Excess $Ag(NH_3)_2^+$
Na_2O	CaO	SiO_2			
%	%	%	*Fringes*		*M-eq/g*
10	20	70	ND		3.1×10^{-4}
15	15	70	ND		5.3
20	10	70	ND		7.2
25	5	70	1/2+swell		42
26	4	70	2 swell		63
27	3	70	6 swell		109
29	1	70	≥0 swell[b]		660
29.5	0.5	70	75 swell[b]		480
29.75	.25	70	120 swell[b]		310
30		70	72 swell		<2
			Minimum exposure	*Excessive exposure*	
32		68	180 swell[b]		<2
30		70	72 swell[b]		<2
29.4		70.6		72 attack[c]	
28		72	36 swell[b]		6
26.7		73.3		22 attack[c]	
26		74	18 swell[b]		982
24		76	12 swell[b]		448
22		78	6—swell[b]		87.2
21.9		78.1		3 1/2+attack[c]	
20		80	2 swell		68
18		82	3/4 swell		43.7
17.4		82.6		1/2+swell	
16		84	1/4+swell		12.5
14		86	2/10 swell		6
13.6		86.4		2/10+swell	
12		88	D[d] swell		2
10.5		89.5		D+ swell	
9		91			2.3
0		100[a]	ND[e]		1.5
Pyrex (774)			ND		1.4

[a] Fused silica.
[b] Values calculated from exposures of 5 minutes or less.
[c] Values calculated from exposures of 15 minutes.
[d] D, detectable.
[e] ND, not detectable.

b. Repression of Swelling of Corning 015 Glass in Acid Solutions

(1) *Effect of Concentration.* In the section on theoretical considerations the relation $x^2=y(y+z)$ expressed the distribution of ions on both sides of the interface. The potential difference across the interface resulting from this uneven distribution was given as $E=RT/F \log_e x/y$ volts. This relation is true even if other ionogens are added to the system, including neutral salts or other electrolytes having polyvalent ions [2]. The addition of any electrolyte must necessarily produce a change in the potential difference by disturbing the equilibrium, yet all ions present when equilibrium is again established are producing the same potential difference regardless of valence. This latter condition may be difficult to visualize, but appears directly in the derivation involving polyvalent ions [2] (see p. 435 on the effect of valence).

If the equation $x^2=y(y+z)$ is solved for y and then substituted in $E=RT/F \log_e x/y$, the relation for the potential between the silica-rich layer and the outer solution becomes

$$E=RT/F \log_e \frac{2x}{-z+\sqrt{4x^2+z^2}}$$

From this it is obvious that upon increasing the value of x while z (the negatively charged silica layer) remains almost constant, E must decrease (along with the osmotic pressure and resulting swelling), approaching zero as a limit, that is,

$$\lim_{x=\infty} E=RT/F \log_e \frac{2x}{4x^2}=0.$$

To test the validity of this reasoning as applied to glasses, Corning 015 electrode glass which exhibited a moderate rate of swelling, table 1 and figure 1, was exposed to various concentrations of organic and mineral acids. In order to emphasize the effects, the exposure time was increased to 48 hours at 80° C. The results are plotted in figure 2. In every case, the rate of swelling was decreased by the higher concentrations and approached zero for the concentrations above 50 percent.[3] According to the theory for swelling as applied to gelatin, the swelling should go through a maximum in passing from very dilute to higher concentrations of electrolytes [2,10]. This same reasoning also holds true for silicate glasses. However, earlier experiment with the swelling of Corning 015 had not revealed such a maximum for a concentration series 10^{-3} N, 10^{-2} N, 10^{-1} N, and N [5].

(2) *Effect of valence upon swelling.* Although the data plotted in figure 2, A, were obtained on solutions prepared only on an approximate percentage basis, they indicate that the acids differ in their capacity to repress the swelling of glass. A more carefully controlled set of experiments was carried out with solutions prepared on a molar basis. The results are plotted in figure 2, B. The values for swelling brought about by the monobasic mineral acid, HCl, and the monobasic organic acid, CH_3COOH, fall essentially on the same curve, whereas the swelling in the case of the dibasic acid, H_2SO_4, is appreciably less. The effect of the tribasic acid, H_3PO_4, follows in a general way the monobasic acids. All of these results can be rationalized, provided it is assumed that the silica-rich layer is not dissolved by any of the acids.

If the heterogeneous equilibrium at a glass-solution interface is a characteristic Donnan membrane equilibrium established by a nondiffusible negative charged gelatinous silica, the repression of swelling of the glass surface brought about by monobasic acids, such as HCl and CH_3COOH, should be essentially the same. On the other hand, strong dibasic acids should repress the swelling more strongly. The present procedure is not sufficiently exact to give a quantitative verification of these predictions, but the results are generally in accord with them. The tribasic acid, H_3PO_4, dissociates as a monobasic acid below pH 4.7 [11] and has been shown in the case of gelatin to influence the membrane potential as well as the osmotic pressure and swelling the same as the monobasic acids [2].

[3] From these observations it is evident that the commercial practice of storing concentrated acids in glass containers is preferable to storing more dilute solutions.

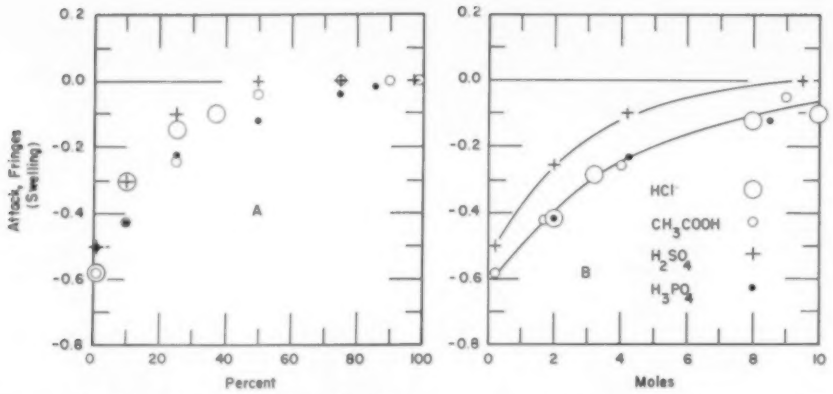

FIGURE 2. *Repression of swelling of Corning 015 glass brought about by increased concentrations of monobasic, dibasic, and tribasic acids.*

Concentrations: A, percent; B, moles; exposure, 48 hours at 80° C.

4.2. Uneven distribution of $Ag(NH_3)_2^+$ and Br^- Ions Between the Silica-Rich Layer of the Glass Surface and the Outer Solution

In the previous sections the uneven distribution of ions at the glass-solution interface has been assumed, but not actually demonstrated. As neither the concentration of ions within the glass surface nor the voltage differential existing across the glass-solution interface is readily obtainable by direct measurement, it was necessary to design experiments that would demonstrate the excess of the migratable positive ions appearing in the swollen glass surface or the excess negative ions appearing in the outer phase. $Ag(NH_3)_2Br$ dissolved in full-strength aqueous NH_3 provided very satisfactory indicator ions for such experiments. Full-strength NH_3 was used because of its low attack upon the silica-rich layer, although the pH is high [5,7].

Glass samples (approximately 10 g) which passed a U. S. Standard 50-mesh sieve and were retained on a 150-mesh screen were leached at pH 2 for 6 hours at 80°C, with occasional stirring. They were then decanted and rinsed twice in full-strength aqueous-ammonia solution, followed by 5 minutes in 50 ml of saturated $Ag(NH_3)_2Br$ solution with intermittent agitation. The glass samples were then separated from the liquid phase by decantation. The glass and liquid phases were acidified with concentrated H_2SO_4 and titrated potentiometrically for excess Ag^+ remaining in the gelatinous silica-rich surface and the excess Br^- ions appearing in the outer solution. For these determinations the solutions were made strongly acid to insure that little change in pH takes place during the titration, and also to bring about ready coagulation of the AgBr precipitated.

a. Na_2O-CaO-SiO_2 Glasses

Potentiometric titrations were made of the $Ag(NH_3)_2^+$ ions appearing in the glass surface in excess of the Br^- ions for a series of Na_2O-CaO-SiO_2 glasses containing 70 percent of SiO_2 and various percentages of Na_2O and CaO. The data are given in table 2 and summarized in figure 3, where the swelling of the glasses at pH2, and the excess $Ag(NH_3)_2^+$ ions appearing at the glass surface are plotted against the composition (percentage of CaO) of the glasses. The results are interesting because of the low titration values obtained on the glasses of superior durability as compared with the glasses of inferior durability. Another interesting feature of these data is the fact that for the two glasses of maximum swelling (29.5 and 29.75 percent of Na_2O, respectively), the excess silver appearing in the glass surface decreased, falling essentially to zero for the end member of the series, 30 percent Na_2O. This apparent anomaly will be discussed and clarified by the data obtained on the Na_2O-SiO_2 glasses (section 4.2, b).

b. Na_2O-SiO_2 Glasses

A similar set of data were obtained for a series of soda-silica glasses, table 2 and figure 4. The excess $Ag(NH_3)_2^+$ ions appearing in the negatively charged silica-rich phase increased for the glass compositions showing increased swelling down to the composition of 74 percent of SiO_2. Below this percentage of silica, the $Ag(NH_3)_2^+$ ions retained at the interface fell sharply toward zero, as in the Na_2O-CaO-SiO_2 series, because the swollen silica-rich surface of the specimens was decreased by solution and by sloughing off of the mechanically weak gel. These data illustrate well the difficulty encountered in obtaining consistent durability data by the interferometer procedure in studying the behavior of very poor glasses in acid solutions. Specimens of these glasses given 15-minute exposures suffered attack as shown in figure 4, whereas exposure of the same glasses for 5 minutes or less resulted in liberal swelling [12, 13].

c. Effect of pH

The data for the excess $Ag(NH_3)_2^+$ appearing at the glass-solution interface after samples of Corning 015 were leached in buffer solutions of different pH

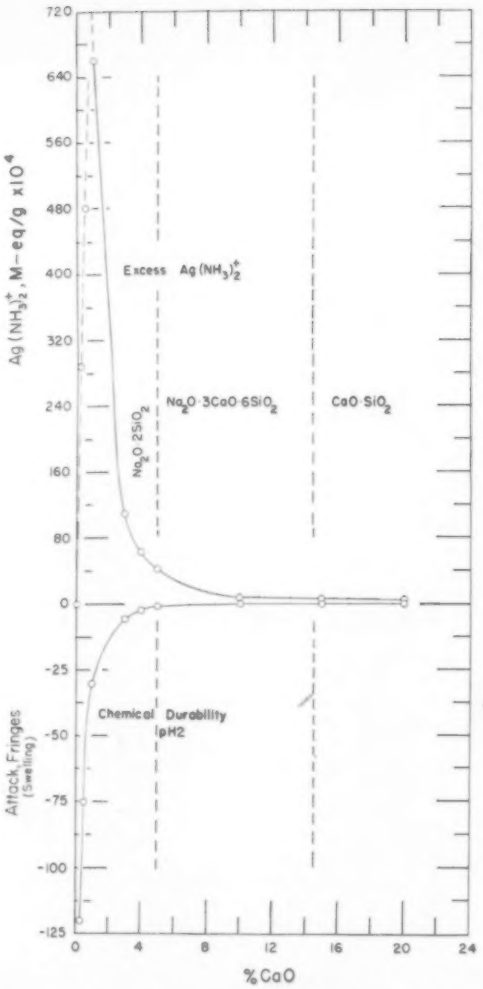

FIGURE 3. *Comparison of the excess* $Ag(NH_3)_2^+$ *ions appearing in the glass surface, with the chemical durability (swelling) of the glass for a series of* Na_2O-CaO-SiO_2 *glasses containing 70 percent of* SiO_2.

Exposure 6 hours at 80° C.

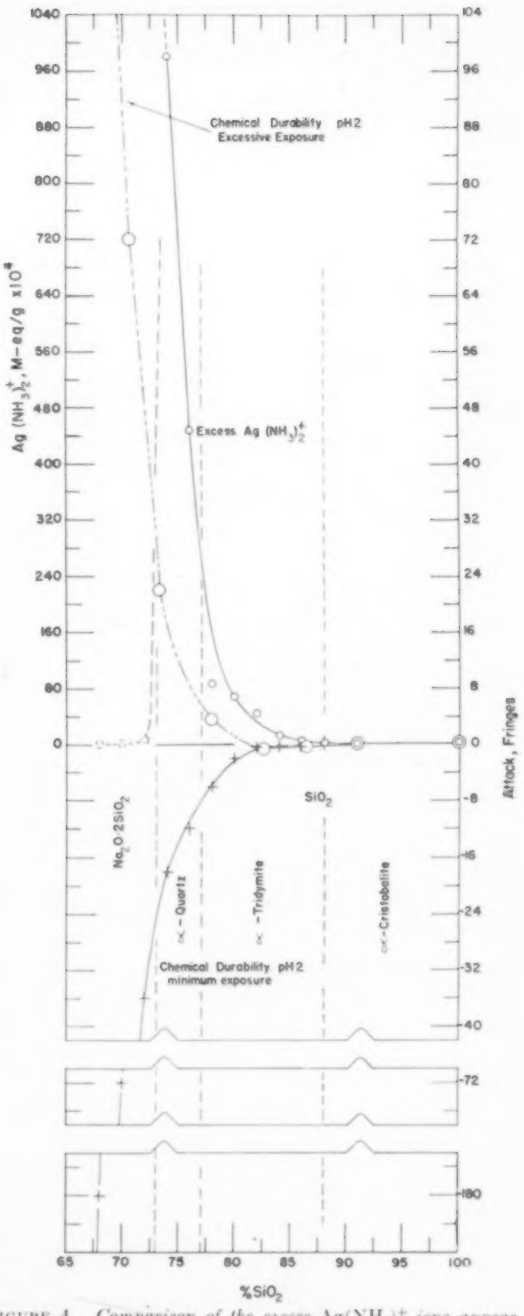

FIGURE 4. *Comparison of the excess* $Ag(NH_3)_2^+$ *ions appearing in the glass surface, with the chemical durability of the glass for a series of* Na_2O-SiO_2 *glasses.*

○, apparent attack for 6 hours at 80° C calculated from observations on specimens given excessive exposure (15 minutes).

+, apparent swelling for 6 hours at 80° C calculated from observations on specimens given minimum exposure (5 minutes or less for the glasses of very poor chemical durability).

are listed in table 3. The resulting curve [4] is compared in figure 5 with the silicic-acid titration curve [14], the chemical-durability [5] and voltage-departure [3, 15] curves of this glass over the same pH range. A set of chemical-durability data that is representative of the "superacid" region is included. It was obtained with sulfuric-acid solutions and reported as log $1/[H_2SO_4]$. From inspection of these curves it is evident that as the negatively charged silica-rich layer is carried away as soluble silicates by alkaline solutions, the magnitude of the uneven distribution

[4] How well the curve represents the correct relative shape is uncertain because at times very large unexpected values for the excess $Ag(NH_3)_2^+$ have been obtained after leaching in solutions of high alkalinity.

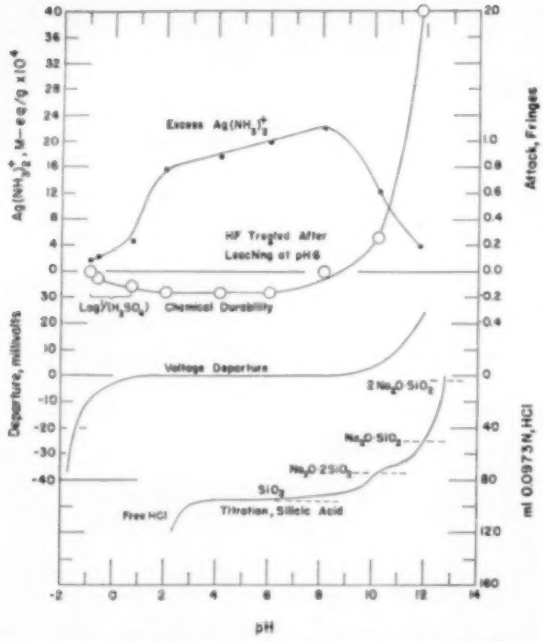

FIGURE 5. *Effect of the* pH *of the buffer solutions on the chemical durability, voltage departure, and the excess* $Ag(NH_3)_2^+$ *ions appearing in the glass-solution interface, compared with a titration curve of sodium silicate* [14].

of migratable ions at the interface decreases. This condition readily rationalizes the controversial, so-called "nonreversibility" of the glass electrode [3, 16, 17, 18]. The removal or partial removal of the silica-rich layer by alkaline solutions must necessarily cause a voltage shift as the nonmigratable member of the interfacial system is changed. The silica-rich surface is not wholly regenerated until the electrode is immersed again in an acid solution.

TABLE 3. *Effect of the* pH *of the leaching solution upon the surface alteration and upon the uneven distribution of migratable ions appearing at the surface of Corning 015 glass*

Solution	Surface alteration	Excess $Ag(NH_3)_2^+$ for specimens	
		As leached	HF-treated after leaching
pH	*Fringes*	*M-eq/g*	*M-eq/g*
2.0	>2/10 swell	15.7×10^{-4}	
4.1	>2/10 swell	17.6	
6.0	>2/10 swell	20	4.3×10^{-4}
8.1	SC[a]	22.1	
10.2	1/4+attack	12.3	
11.8	2 attack	4.0	
log $1/M\ H_2SO_4$			
0.7	1/10 swell	4.7	
−.6	D[b] swell	2.1	
−.95	ND[c]	1.7	

[a] SC, surface cut; [b] D, detectable; [c] ND, not detectable.

In the low pH range, the correspondence of the repression of swelling and the uneven distribution of migratable ions in H_2SO_4 solutions (table 4 and fig. 6) with the voltage departures reported for the "superacid" region, is entirely logical. However, there are several other considerations that must not be overlooked. First, it must be borne in mind that the decrease in the water activity of the solutions at the increased concentrations also parallels the performance of the glass electrode and strongly supports the theory that the glass-electrode functions as a "water electrode" [3, 19, 20]. This theory is also strongly supported by the general correspondence of the hygroscopicity of experimental glasses with their electrode function (pH response) [13, 21].

However, as pointed out in the present investigation, there should be a lowering of the interfacial voltage with increased acid concentration in accord with the equation

$$\lim_{x=\infty} E = RT/F \log_e \frac{2x}{-z+\sqrt{4x^2+z^2}} = 0.$$

This voltage shift should theoretically be independent of any water activity interpretation, but obviously for aqueous solutions it would be accompanied by a decrease in the water activity of the solutions, and the two theories would have this same feature in common. Yet the source of the voltage departure in the first theory would be internal, whereas in the

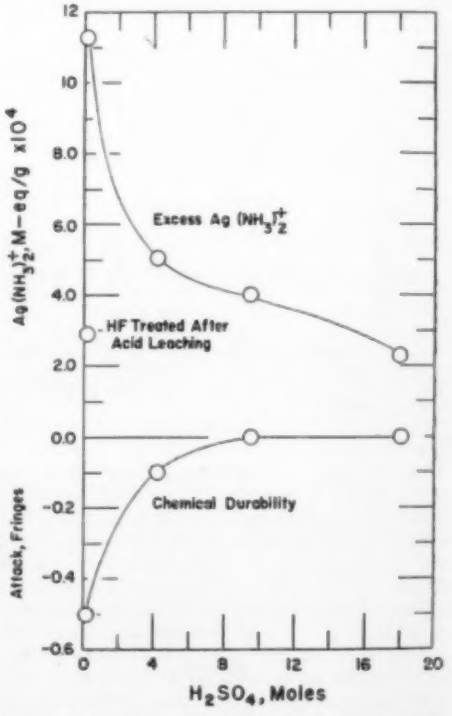

FIGURE 6. *Surface alterations (swelling) of Corning 015 glass in the "superacid" region and the accompanying uneven distribution of migratable ions.*

second, the postulated cause of the voltage departure would be at the interface.

TABLE 4. *Typical surface alterations (swelling) exhibited by Corning 015 glass upon exposure for 48 hours at 80° C to various concentrations of aqueous H_2SO_4, and the uneven distribution of migratable ions appearing in the glass surface*

H_2SO_4 solutions	Surface alterations	Excess $Ag(NH_3)_2^+$ for specimens	
		As leached	HF-treated after leaching
M	*Fringes*	*M-eq/g*	*M-eq/g*
0.2	0.5 swell	11.3×10^{-4}	2.9×10^{-4}
4.2	1/10 swell	5.1	.....
9.5	Not detectable	4.0	.....
18.1	do	2.3	.....

A further consideration, the repression of swelling with the accompanying decrease in the formation of nonmigratable ions and the attendant displacement of the heterogeneous equilibria at the glass-solution interface, is essentially a byproduct of the conditions postulated by the equation.

In selecting a theory that adequately accounts for the voltage departures of the glass electrode in the "superacid" region there is a liberal list from which to choose, namely, (1) Dehydration of the electrode glass [3, 8, 18], (2) alteration of the physical and chemical nature of the surface of the electrode [5, 8], (3) operation of the glass as a "water electrode" [3, 19, 20, 22], and (4) alteration of the interfacial voltage in accord with the above equation [1, 2]. If any one of them is correct, any disagreement as to which it is can merely center about agreement on which member of the list is the cause and which ones are the effects. Probably, as is so prevalent throughout nature, any ultimate explanation will be faced with an anomaly or contradiction.

4.3. Surface Equilibria and Glass Electrode Voltage

Although Donnan membrane phenomena occupy such a dramatic role in the glass-solution interface equilibria, they apparently can play little or no part in the preferential response of the glass electrode to the hydrogen-ion activity of aqueous solutions and the partial or complete exclusion of the effects of the other ions in the system [23]. This conclusion can be reached by an inspection of the basic equations of the equilibrium state.

The equation for the voltage appearing across the glass-solution interface due to the uneven distribution of a migratable monovalent ion is $E=RT/F \log_e x/y$ volts. If an ionogen yielding an ion of any other valency, M^{n+} is added to this system, the voltage contributed by this ion at equilibrium will be

$$E=RT/nF \log_e \frac{[M^{n+}]_{\text{solution}}{}^{5}}{[M^{n+}]_{\text{glass surface}}{}^{5}}.$$

From the equation of products $[M^{n+}]_g \times [Cl^-]_g^n = [M^{n+}]_{sol} \times [Cl^-]_{sol}^n$ and $[H^+]_g^n \times [Cl^-]_g^n = [H^+]_{sol}^n \times [Cl^-]_{sol}^n$, from which it follows that

$$\frac{[M^{n+}]_{sol}}{[M^{n+}]_g} = \frac{[H^+]_{sol}^n}{[H^+]_g^n} = \frac{x^n}{y^n}.$$

Therefore, $E=RT/nF \log_e x^n/y^n = RT/F \log_e x/y$.

It is evident from this derivation that at equilibrium all ions in the system, regardless of their valence, are contributing identical voltages across the glass solution interface. Thus, as far as this particular type of heterogeneous equilibria is concerned, the glass electrode should respond equally well as an indicator of any ion in the aqueous solution [24, 22], provided all other positive ions were held constant except the one under consideration. As this latter conclusion is so conspicuously contrary to the generally observed voltage performance of the glass electrode as used, it is obviously necessary to look elsewhere for an explanation of the selective voltage response of the glass electrode to hydrogen-ion activity. This does not imply that the voltage across the glass-solution interface due to the uneven distribution of the migratable ions is negligible or that it plays no part in the observed voltage of the glass electrode.

In reality, this interfacial voltage seems to be of considerable magnitude. For example, consider the large voltage shift (so-called "soda error") that appears when the silica-rich surface is partially or completely removed by alkaline solutions [3, 5, 19, 20] that form soluble silicates. From similar evidence obtained on the voltage shift in hydrofluoric-acid solutions, it appears that the interfacial voltage caused by the presence of the gelatinous silica-rich layer must often be greater than 250 mv, figure 7. These data were obtained with a well-conditioned glass electrode of Corning 015 compared against the hydrogen electrode [3, p. 124; 25]. The observed voltage departure cannot be attributed to hydrogen ions, because both electrodes when unattacked respond equally well to hydrogen-ion activity. Furthermore, the voltage shift cannot be attributed to an equilibrative response of either electrode to fluoride ions, because in neutral solutions no such response to fluoride ions is observed [3, p. 131]. The complete or partial removal of the silica-rich layer with its interfacial distribution of migratable ions is apparently the main contributing variable.

The surface equilibria also play an important role in the origin of the asymmetry potential of the glass electrode. The inner and outer surface of a glass-electrode bulb of the Cremer-Haber type [25, 26] are known to be very different, as shown by their capacity to sorb dyes [17]. With different heterogeneous equilibria and accompanying voltages of different magnitudes on the two surfaces an asymmetry potential for the glass electrode is inevitable. Further, upon taking appropriate steps to make the two surfaces identical, the asymmetry potential

[5] Hereafter abbreviated "sol" and "g".

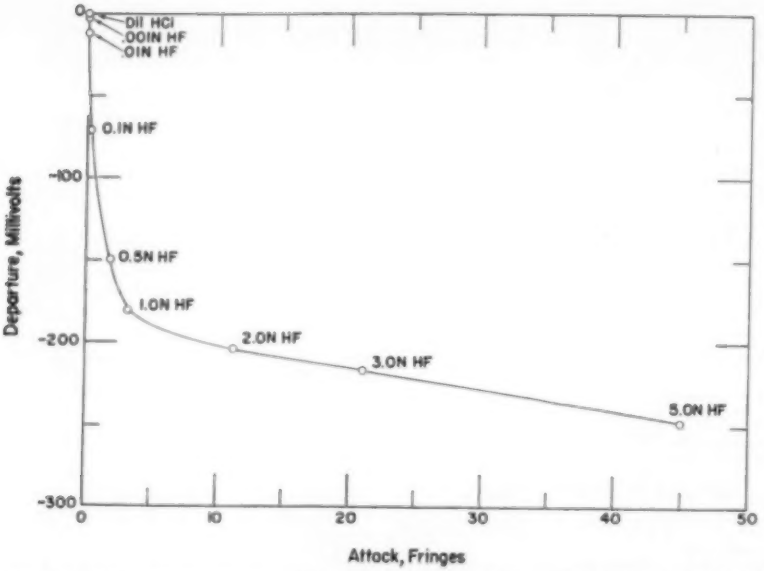

FIGURE 7. *Voltage departure of the glass electrode brought about by the partial removal of the silica-rich surface.*

Any voltage response to the hydrogen ions and fluoride ions is eliminated by the experimental techniques.

should theoretically disappear and actually does [27, 28].

5. Conclusions

Application of the Donnan membrane equations and the "Equation of Products" to the heterogeneous equilibria at the glass-electrode–solution interface accounts qualitatively for the observed uneven distribution of $Ag(NH_3)_2^-$ and Br^- ions between the glass surface and the ambient solution, the swelling of the glass surface in solutions of low and intermediate concentrations, the repression of swelling by high concentrations of electrolytes, voltage departures in alkaline and hydrofluoric-acid solutions, voltage departures in the "superacid" region, and asymmetry potentials. However, the Donnan membrane considerations do not account for the preferential voltage response of the glass electrode to the hydrogen ions.

6. References

[1] F. G. Donnan, The theory of membrane equilibrium in the presence of a non-dialyzable electrolyte, Z. Elektrochem. **17,** 572 (1911).

[2] John Arthur Wilson, Application of the thermodynamics of heterogeneous equilibria to the theory of colloidal phenomena, Colloidal Behavior, **I,** Robert Herman Bogue (McGraw-Hill Book Co., Inc., New York, N. Y.).

[3] M. Dole, Glass electrode (John Wiley & Sons, Inc., New York, N. Y.); Theory of the glass electrode, J. Am. Chem. Soc. **53,** 4260 (1931).

[4] E. Berger, Grundsätzliches über die chemische Angreifbarkeit von Gläsern I., Glastech Ber. **14,** 351 (1936).

[5] Donald Hubbard, Edgar H. Hamilton, and Alfred N. Finn, Effect of the solubility of glass on the behavior of the glass electrode, J. Research NBS **22,** 339 (1939) RP1187.

[6] Roger G. Bates and S. F. Acree, pH of aqueous mixtures of potassium dihydrogen phosphate and disodium hydrogen phosphate at 0° to 60° C, J. Research NBS **34,** 373 (1945) RP1648.

[7] S. E. Hill, The validity of the glass electrode in ammonium chloride buffers, J. Gen. Physiol. **12,** 813 (1929).

[8] Donald Hubbard and Gerald F. Rynders, Voltage anomalies of the glass electrode and the chemical durability of the glass, J. Research NBS **39,** 561 (1947) RP1848.

[9] D. E. Sharp, et al., Report of the committee on the chemical durability of glass, Bul. Am. Ceram. Soc. **14,** 181 (1935).

[10] H. R. Procter, The equilibrium of dilute hydrochloric acid and gelatin, J. Chem. Soc. **105,** 313 (1914).

[11] W. Mansfield Clark, The determination of hydrogen ions, (Williams & Wilkins Co., Baltimore, Md.).

[12] Gerald F. Rynders, Oscar H. Grauer, and Donald Hubbard, Electrode function (pH response) of the soda-silica glasses, J. Research NBS **41,** 273 (1948) RP1923.

[13] Donald Hubbard, Mason H. Black, Sylvanus F. Holley, and Gerald F. Rynders, Electrode function (pH response), hygroscopicity and chemical durability of soda-potash-silica glasses, J. Research NBS **46,** 168 (1951) RP2189.

[14] H. T. S. Britton, Hydrogen ions, D. Van Nostrand Co., Inc., New York, N. Y.; J. Chem. Soc. **425** (1927).

[15] D. A. MacInnes and D. Belcher, Further studies on the glass electrode, J. Am. Chem. Soc. **53,** 3315 (1931).

[16] H. F. Launer, Determination of the pH values of papers, J. Research NBS **22,** 553 (1939) RP1205.

[17] Edgar H. Hamilton and Donald Hubbard, Effect of the chemical durability of glass on the asymmetry potential and reversibility of the glass electrode, J. Research NBS **27,** 27 (1941) RP1400.

[18] M. Dole, Recent advances in the theory of the glass electrode for pH determinations, ASTM Symposium on pH Measurement (June 24–28, 1946).

[19] M. Dole, The relation between the activity of the water and the potentials of the glass electrode, J. Am. Chem. Soc. **54,** 2120 (1932).

[20] M. Dole, The theory of the glass electrode. II. The glass as a water electrode, J. Am. Chem. Soc. **54,** 3095 (1932).
[21] Donald Hubbard, Given W. Cleek, and Gerald F. Rynders, Electrode function (pH response), hygroscopicity and chemical durability of Na_2O-CaO-SiO_2 glasses, J. Research NBS **44,** 247 (1950) RP2076.
[22] Theodore Shedlovsky, Electromotive force from proton exchange reactions, Nat. Acad. Sci., Annual Meeting 1951; Symposium on Electrochemical Constants, National Bureau of Standards, Sept. 1951 (publication pending).
[23] Ludwig Kratz, Wirkungsweise und Theorie der Glaselektrode, Glastech. Ber. **23,** 35 (1950).
[24] B. Lengyel and E. Blum, The behavior of the glass electrode in connection with the chemical composition, Trans. Faraday Soc. **30,** 461 (1934).
[25] F. Haber and Z. Klemensiewicz, On electrical interfacial potentials, Z. physik, Chem., **67,** 385 (1909).
[26] M. Cremer, On the causes of the electromotive properties of tissue and a discussion of polyphase electric cells, Z. Biol. **47,** 562 (1906).
[27] W. Brauer, The cause of asymmetric potentials of the glass electrode, Z. Electrochem. **47,** 638 (1941).
[28] Henry H. Carey and Warren P. Baxter, Glass electrode and method, U. S. Patent 2,366,489.

WASHINGTON, February 12, 1952.

Preparation of D-Mannitol-C^{14} and Its Conversion to D-Fructose-1-(and 6)-C^{14} by Acetobacter Suboxydans[1]

Horace S. Isbell and J. V. Karabinos

Methods are described for the production of D-mannitol-1-C^{14} and D-fructose-1-(and 6)-C^{14}. These materials are powerful new tools for research in biology and chemistry. D-Mannitol-1-C^{14} was prepared in 80-percent yield from D-mannono-γ-lactone. D-Fructose-1-(and 6)-C^{14} was produced in 54-percent yield by growth of Acetobacter suboxydans on a D-Mannitol-1-C^{14} substrate.

1. Introduction

The Bureau recently undertook a program for the development of methods for the production of a variety of position-labeled sugars [1].[2] The preparation of D-glucose-1-C^{14} and D-mannose-1-C^{14} in high yield was described in a previous report [2]. This paper deals with the production of D-mannitol-1-C^{14} and its conversion to D-fructose-1-(and 6)-C^{14} by oxidation with Acetobacter suboxydans.[3] Prior to the present investigation, randomly labeled fructose had been prepared by photosynthesis [3], but position-labeled fructose had not been reported. It was known that D-mannitol could be obtained by reduction of D-mannose, and that it could be converted to D-fructose by oxidation with Acetobacter suboxydans [4]. D-Mannitol differs from D-mannose in that the ends of the molecule are alike. For this reason a 1-labeled mannitol (I) can be considered as either 1- or 6-labeled, and any unsymmetrical derivative prepared from this substance would be 1,6-labeled, provided the carbon chain remains intact. Thus, by oxidation of D-mannitol-1-C^{14} one would obtain D-fructose-1-(and 6)-C^{14} (II).

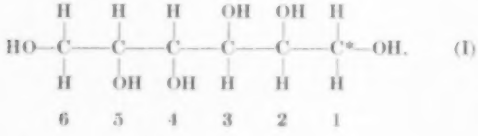

(I)

D-Mannitol-1-C^{14}

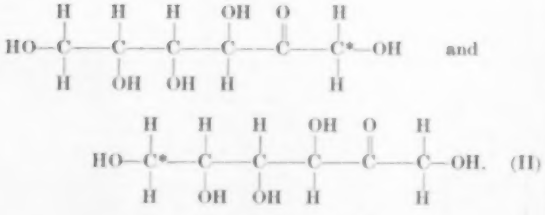

and

(II)

D-fructose-1-(and 6)-C^{14}

As both D-mannitol-1-C^{14} and D-fructose-1-(and 6)-C^{14} would provide powerful tools for the elucidation of many problems in biology and chemistry, the preparation of these compounds was undertaken.

2. Discussion of the Processes

The production of D-mannitol-1-C^{14} includes: (1) preparation of D-mannono-γ-lactone-1-C^{14} by the method already described [2], (2) conversion of the lactone to D-mannose-1-C^{14} by sodium amalgam reduction, and (3) catalytic reduction of the sugar with hydrogen. Each step in the process was studied in detail, and procedures were developed to obtain D-mannitol-1-C^{14} from D-mannono-γ-lactone-1-C^{14} in an over-all radiochemical yield of about 80 percent.

The production of D-fructose-1-(and 6)-C^{14} involves oxidation of D-mannitol-1-C^{14} with Acetobacter suboxydans. It has been established [5] that Acetobacter suboxydans preferentially oxidizes the

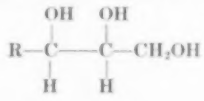

group to the

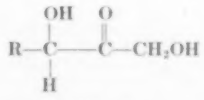

group. In agreement with this property, D-fructose-1-(and 6)-C^{14} is obtained by oxidation of D-mannitol with Acetobacter suboxydans.[4] As pointed out in section 1, the ends of the molecule are alike. For this reason, oxidation could proceed equally well from either end of the molecule, and, in the event that oxidation took place at both ends, a diketo derivative would be formed. Thus, prolonged action of Acetobacter suboxydans on mannitol should yield the diketo derivative

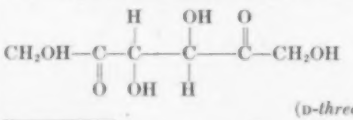

(D-*threo*-5-oxo-2-ketohexose).

[1] The work described in this paper was sponsored by the Atomic Energy Commission.

[2] Figures in brackets indicate the literature references at the end of the paper.

[3] A proof by chemical degradation for the 1- and 6-structure ascribed to the fructose formed will be presented in a later report.

[4] See footnote 3.

To ascertain whether the oxidation did, in fact, proceed beyond the fructose stage, a series of mannitol Acetobacter suboxydans cultures were set up and, as given in table 1, the course of the reaction was followed by determinations of fructose and total copper-reducing substance. The fructose concentration was determined from the polarization at two temperatures [6]. Total reducing substance was determined by the modified Scales method [7]. Curve 1 of figure 1 gives the yield of D-fructose determined from the difference in optical rotation at two temperatures. Curve 2 gives the copper-reducing power of the solution expressed as the percentage of the reducing power of a solution containing the amount of D-fructose molecularly equivalent to the mannitol originally present. The copper-reducing value represents all reducing substances present and is expressed arbitrarily on the fructose scale. The yield of D-fructose reached a maximum in about 2 days, and then decreased for about 6 days when active growth of the organism had slowed down. In every sample, after the first day the copper-reducing value exceeded that of the D-fructose determined from the polarization at two temperatures. Hence, the solution contained a constituent having copper-reducing power other than D-fructose. Presumably, this substance was the anticipated diketo compound or a substance derived therefrom. The results clearly show that it is necessary to control the reaction time to obtain maximum yields of D-fructose. The experiment of figure 1 was conducted with a surface-volume ratio of 1.28. In agreement with the work of Fulmer, Dunning, and Underkofler, a somewhat higher yield of fructose was obtained with a higher surface-volume ratio. In the preparation of D-fructose-1-(and 6-)C^{14} on a tracer level, a surface-volume ratio of 1.59 was used, and a radiochemical yield of 54 percent was obtained.

3. Experimental Procedures

3.1. D-Mannono-γ-lactone-1-C^{14}

This substance was prepared in 67-percent yield by the sodium-bicarbonate–carbon-dioxide method previously described [2].

3.2. Conversion of D-Mannono-γ-lactone-1-C^{14} to D-Mannitol-1-C^{14}

One millimole of D-mannono-γ-lactone-1-C^{14} having an activity of 10 μc was dissolved in 20 ml of water; 1.5 g of benzoic acid was added, and the mixture was stirred in an ice bath until cold. Sodium amalgam pellets (4.6 g, containing 5 percent of sodium) were added and stirring was continued. After 2 hours the mercury was removed, and another addition of 1.2 g of benzoic acid and 4.6 g of amalgam was made. Stirring was continued at 0° to 5° C for 2 hours, after which the mercury was removed, and 1.26 g of oxalic acid was added. Then the mixture was extracted with chloroform to remove the benzoic acid. The sodium oxalate in the aqueous solution was precipitated by the addition of approximately 2 volumes of methanol and 2 of ethanol. The insoluble salts were separated by filtration and washed with methanol. The resultant alcoholic liquor was concentrated under reduced pressure to about 5 ml and was diluted again with 2 volumes of methanol and 2 of ethanol. The resultant precipitate was separated and washed with methanol. The alcoholic liquor was evaporated to approximately 2 ml and was then transferred with 3 ml of water to the tube of a high-pressure hydrogenator containing 0.1 g of calcium carbonate and 0.5 g of Raney nickel catalyst. The mixture was hydrogenated for 2 hours at 125° C and 1,000 lb/in^2. Then the mixture was cooled to room temperature, filtered, and passed through a column (1.4 by 25 cm) containing equal portions of Amberlite IR 100-H and Duolite A4. The effluent and wash liquor were combined and lyophilized. The residue was dissolved in the minimum quantity of hot methanol. After the addition of an equal volume of isopropanol, and seeding, the solution was set aside for crystallization of D-mannitol. In the course of 3 days 117 mg of D-mannitol-1-C^{14}(6.4 μc) was obtained. It melted at 165° C, in substantial agreement with the accepted value of 166° to 168° C. "Carrier" D-mannitol (100 mg) was dissolved in the mother liquor and, after crystallization, 98 mg of D-mannitol-1-C^{14} was obtained with a radioactive content of 1.6 μc. The total radioactive recovery was 80 percent.

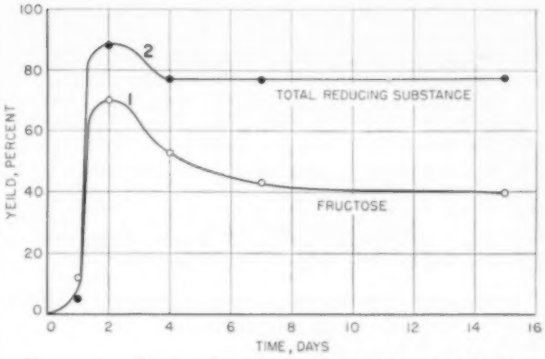

FIGURE 1. *Fructose formed from mannitol by Acetobacter suboxydans.*

3.3. Preliminary Study of the Oxidation of D-Mannitol to D-Fructose with Acetobacter Suboxydans

Aliquots (25 ml) of an aqueous solution containing 9.1 g of D-mannitol, 2.5 g of yeast extract, and 1.5 g of potassium dihydrogen phosphate in 500 ml were placed in 125-ml Erlenmeyer flasks and sterilized for 15 minutes at a steam pressure of 15 lb. Each flask was then inoculated with five drops of a previously prepared inoculum of Acetobacter suboxydans and allowed to stand at 30° C in an incubator. The inoculum was prepared by growth, at 30° C for 45 hours, of a fresh culture of Acetobacter suboxydans on a solution containing 2 g of mannitol, 0.2 g of yeast extract, and 40 ml of water.

At regular intervals following the inoculation, one of the flasks was removed from the incubator. The liquid was transferred to a 25-ml volumetric flask and diluted to volume. One-half gram of neutral lead acetate trihydrate was then added. The mixture was transferred to a centrifuge tube, and the precipitate was removed by centrifugation. To the clear solution was added 0.25 g of potassium oxalate monohydrate, and the resulting precipitate was again removed by centrifugation. The clear solution was then used directly for measurements of optical rotation and copper-reducing power.

TABLE 1. *Acetobacter suboxydans oxidation of mannitol*

(Surface-volume ratio, 1.28)

Incubation time	Polarization at two temperatures				Fructose yield		Reducing sugar yield	
Days	*°C*	*°S*	*°C*	*°S*	*g/100ml*	*Percent*	*g/100ml*	*Percent*
1.0	20	−0.47	57.3	−0.20	0.21	11.7	0.09	5.0
2.0	20	−6.52	63.6	−4.67	1.17	65.0	1.58	87.8
4.0	20	−5.54	64.5	−4.01	0.95	52.8	1.39	77.2
7.0	20	−5.10	63.2	−3.87	.77	42.8	1.39	77.2
15.0	20	−4.86	56.0	−3.92	.71	39.4	1.40	77.8
28.0	20	−4.50	63.0	−3.45	.66	36.7	1.46	81.1

The optical rotations given in table 1 were made at two temperatures with a Bates saccharimeter and a 2-dm tube. The rotations at the higher temperatures were corrected [6] for expansion by use of the coefficient 0.00044 for each degree rise in temperature. The difference between the corrected rotation and that at 20°, divided by the temperature difference and by 0.03441, equals the number of grams of D-fructose per 100 ml of solution. Complete conversion to D-fructose of the mannitol originally in the solution would have given 1.8 g of D-fructose per 100 ml.

Copper-reducing values, also given in table 1, were determined on the solutions by the modified Scales method [7] standardized against D-fructose. The values so obtained represent all substances that reduce the alkaline copper reagent.

3.4. Conversion of D-Mannitol-1-C^{14} to D-Fructose-1-(and 6)-C^{14}

One millimole (182 mg) of D-mannitol-1-C^{14}, with a radioactive content of 8.8 μc/millimole, was dissolved in 10 ml of aqueous solution containing 50 mg of yeast extract and 30 mg of potassium dihydrogen phosphate in a 50-ml Erlenmeyer flask (surface/volume=1.59 cm^2/ml). The mixture was allowed to incubate at 30° C with three drops of a previously prepared inoculum of Acetobacter suboxydans to the point of maximum rotation and reducing power (45 hours). To this solution was then added 1 ml of a 20-percent solution of zinc sulfate and an equivalent quantity (previously determined with bromothymol blue indicator) of a saturated solution of barium hydroxide. After removal of the precipitate by centrifugation, the solution and washings were passed slowly through a (1.2 by 22 cm) column containing a mixture of Amberlite IR 100–H and Duolite A4. The effluent and aqueous wash liquor were concentrated by lyophilization to an amorphous residue weighing 145 mg. This residue was dissolved in several drops of methanol, isopropanol was added to the point of incipient turbidity, and the mixture was seeded with D-fructose. Crystallization was allowed to proceed for several days, after which 56 mg of crystalline product was obtained. The specific rotation ($[\alpha]_D^{20}=-82°$) as well as the radioactivity (0.0428 μc/mg) of the material was about 10 percent too low. Hence, the yield of C^{14}-labeled fructose was actually 49 mg (27%) instead of 56 mg. An additional quantity of labeled fructose was separated by the use of 200 mg of carrier D-fructose. An aqueous solution of the carrier was added to the mother liquor, and the solution was evaporated to substantial dryness. The residue was taken up in 1 ml of methanol, and crystallization was induced by the addition of 2 ml of isopropanol and seeding with crystalline fructose. The crystals that separated weighed 210 mg and had an activity of 0.0114 μc/mg. The crop of fructose undiluted with carrier contained 2.40 μc, and the carrier-diluted sugar contained 2.39 μc; thus the radiochemical yield was 4.79 μc, or 54.4 percent.[5]

The authors express their appreciation to Nancy B. Holt and to Abraham Schwebel of the Bureau, who conducted the analytical work, and to Laura C. Stewart of the National Institutes of Health, who supplied a culture of Acetobacter suboxydans and made suggestions concerning its use.

4. References

[1] H. S. Isbell, J. V. Karabinos, H. L. Frush, and A. Schwebel, Synthesis of C^{14}-labeled sugars, abstracts of papers, XII International Congress of Pure and Applied Chemistry, p. 113 (New York, September 10 to 13, 1951).

[2] H. S. Isbell, J. V. Karabinos, H. L. Frush, N. B. Holt, and A. Schwebel, J. Research NBS **48,** 163 (1952) RP2301.

[3] S. Rubin, W. Z. Hassid, and M. D. Kamen, J. Am. Chem. Soc. **61,** 661 (1939); E. W. Putnam, W. Z. Hassid, G. Krothov, and H. A. Barker, J. Biol. Chem. **175,** 785 (1948).

[4] E. I. Fulmer, J. W. Dunning, and L. A. Underkofler, Iowa State Coll. J. Sci. **13,** 279 (1939).

[5] R. M. Hann, E. B. Tilden, and C. S. Hudson, J. Am. Chem. Soc. **60,** 1201 (1938).

[6] F. J. Bates and associates, Polarimetry, saccharimetry, and the sugars, NBS Circular 440, p. 217 (1942).

[7] H. S. Isbell, W. W. Pigman, and H. L. Frush, J. Research NBS **24,** 241 (1940) RP1282.

WASHINGTON, March 3, 1952.

[5] A limited quantity of D-fructose-1-(and 6)-C^{14} with an activity of 0.5 μc/mg made by this process, is now available from this Bureau at a cost of $1.00 per microcurie.

Journal of Research of the National Bureau of Standards Vol. 48, No. 6, June 1952 Research Paper 2335

Analysis of Goniophotometric Reflection Curves

Isadore Nimeroff

Surface appearance, apart from texture, is defined by the goniophotometric curve giving the angular distribution of the reflected light, but a summary of current goniophotometric techniques shows that essential parts of these fundamental data have been neglected. An established method of statistics is applied to the problem of goniophotometric-curve analysis and interpretation whereby such data are reduced to dispersion, skewness, and kurtosis indexes. The kurtosis index is shown to correlate better with subjective estimates of the distinctness of the reflected images than the conventional measure, 60° specular gloss. The kurtosis index is applied to one problem in the selection of optimum glossmeter geometry.

1. Introduction

In pursuit of a method for specifying glossiness, or luster, of surfaces many theorists, researchers, and engineers, physical and psychophysical, have devoted thought and time to theorizing and experimenting. Techniques for measurement have been devised, ranging from observation with a single set to observations involving many sets of illuminating and viewing conditions. The former of these techniques is an oversimplified solution to the problem; the latter is too costly and time consuming to perform for every surface under consideration. Such a complete set of data was published by Thaler [1] [1] for a series of magnesium oxide surfaces. A compromise between these extremes is required. Such a compromise involves obtaining goniophotometric curves near the angle of specular reflection in the plane of measurement for one unidirectional incidence angle.[2]

2. Goniophotometers

The earliest known goniophotometer is the one devised by Bouguer [2] in attempting to corroborate Lambert's law [3] by experimental evidence. Since then many goniophotometers have been developed and described. The problem of how to analyze and interpret the curves obtained on goniophotometers still remains. This paper proposes using an established statistical method to analyze monoplane goniophotometric reflection curves, yielding numerics that correlate with specular gloss and estimates of distinctness-of-image gloss.

Many workers in the field of glossimetry have realized that the only way to specify completely the optical properties of reflecting surfaces is by analyzing goniophotometric curves of the reflected light. In the interest of economy one goniophotometric reflection curve for one angle of incidence and one plane of view may provide an adequate account of what happens to the flux reflected by a surface. This flux distribution can be measured visually or photoelectrically. The most detailed description of a visual goniophotometer is given by McNicholas [4]. His instrument had provision for diffuse and unidirectional illumination and multiplane view. He used his goniophotometer to obtain distribution curves for diffusing media.

Wetlaufer and Scott [5] described a photoelectric goniophotometer with rectangular source and receiver apertures summing to 50′ by 5.5°, but the relative sizes of these apertures were not given. They obtained goniophotometric data near the angle of specular reflection with 45° incidence for 13 materials exhibiting reflection ranging from nearly completely specular to nearly completely diffuse, and drew conclusions about the relative merits of large and small incidence angles in the measurement of specular gloss. Only one incidence angle was used, and no analysis of the goniophotometric data was made.

In a paper on 60° specular-gloss measurement [6] Hammond and Nimeroff described the optics of a photoelectronic monoplane goniophotometer having high resolution, 0.3° circular source, and 0.6° circular receiver apertures. With this instrument fractional reflectance curves were obtained for a series of specimens obviously differing in appearance, yet having approximately the same 60° specular-gloss readings according to the ASTM Method [7].[3] The curves indicated that these specimens had radically different fractional-reflectance distributions. If the information contained in these curves could be adequately expressed as a single number, a better index of gloss characteristics would be obtained than is possible from the simple measurement of specular gloss.

3. The Concept of Moments

A method for the description of these fractional-reflectance curves may be found in the field of statistics, where the technique of characterizing various types of frequency distributions is of fundamental importance. In statistics the measures of dispersion, skewness, and peakedness have been found to facilitate comparisons between distributions. These measures are computed by the use of moments. A brief résumé of the concept of moments follows.

With observed frequencies, $f_1, f_2, \ldots, f_n$, corresponding to variables, $x_1, x_2, \ldots, x_n$, and with the sum of the frequencies, $f_1+f_2+\ldots+f_n$ equal

[1] Figures in brackets indicate the literature references at the end of this paper.

[2] Photometric definitions and terms used here are contained in a paper by Hammond and Nimeroff [6].

[3] Wherever 60° specular gloss is mentioned this method is implied.

to $\sum_1^n f_i$, we define the kth moment,

$$\mu_k \equiv \frac{\sum_1^n f_i x_i^k}{\sum_1^n f_i} = \frac{\sum_1^n f_i x_i^k}{N}, \tag{1}$$

where $N = \sum_1^n f_i$. In other words, the kth moment is the arithmetic mean of the kth powers of the variate, x_i. When the axis of moments is taken about the centroid of mean, $\bar{x}$, or the variable x_i then,

$$\pi_k = \frac{\sum_1^n f_i (x_i - \bar{x})^k}{N} \tag{2}$$

is the kth monent about the centroid, or mean.

4. Curve Analysis

Harrison [8] suggests that polar-intensity distribution curves should be analyzed to obtain the desired information about surface appearance. He suggests also that these polar curves should not be considered as composed of ellipses, circles, and straight lines, because the specular components (lines) cannot be separated physically from the diffuse components (circles). Barkas [9] suggests a method for theoretically separating these two components for fairly matte surfaces by substituting an equivalent surface for a physical surface. The Barkas treatment has not yet been applied to semiglossy and glossy surfaces.

Pokrowski [10] found that by summing the diffuse reflection and the specular-reflection components one could obtain for a given angle of illumination the distribution of reflected flux for all directions. The computation of these components is made on the assumption that diffuse reflection obeys Lambert's law and that the specular reflection obeys Fresnel's law [11] for an equal distribution of mirror facets oriented at all possible angles. Chinmayanandam [12] derived an exponential expression to account theoretically for the reflection from optically rough surfaces by assuming that the angles between the reflecting elements and the gross plane are randomly distributed according to the probability law.

Typical goniophotometric curves observed for materials ranging from matte to high gloss are shown in figure 1. Clues as to how to analyze these data are difficult to obtain from a polar graph. However, if rectangular coordinates are used for the data in figure 1 and fractional reflectance, F, is plotted on a logarithmic scale as the ordinate against angular departures from the specular angle, d, on a linear scale as abscissa (see fig. 2) their resemblance to normal frequency distributions about the arithmetic mean becomes apparent.

In the analysis of frequency distributions, mathematical statistics (see, for example, Reitz [13] and Croxton and Cowden [14]) has shown that three indexes are important. These three indexes are

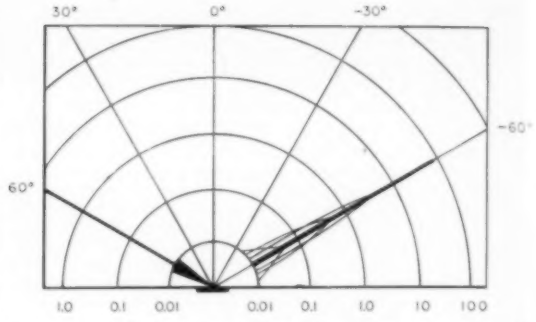

FIGURE 1. *Typical goniophotometric curves on log-polar coordinates.*

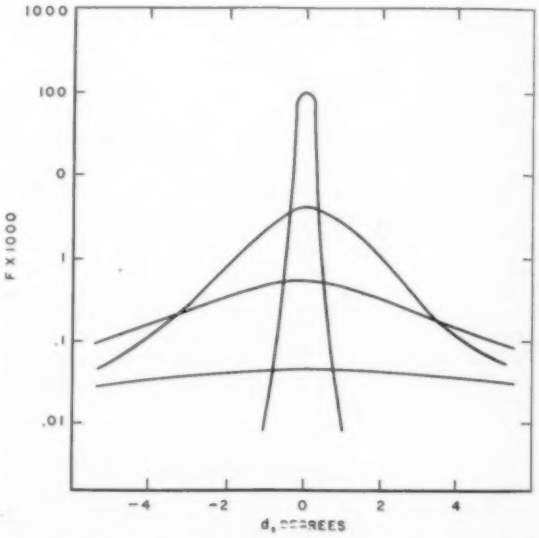

FIGURE 2. *Typical goniophotometric curves on log-linear coordinates.*

Same data as figure 1.

dispersion index, σ; skewness index, α_3; and kurtosis index, α_4. For the purposes of this paper, they are defined as follows:

$$\sigma \equiv (\pi_2)^{\frac{1}{2}} \tag{3}$$

$$\alpha_3 \equiv \frac{\pi_3}{(\pi_2)^{\frac{3}{2}}} = \frac{\pi_3}{\sigma^3} \tag{4}$$

$$\alpha_4 \equiv \frac{\pi_4}{(\pi_2)^2} = \frac{\pi_4}{\sigma^4} \tag{5}$$

The first index, σ, gives an indication of the spread of the distribution, the second, α_3, gives an indication of the dissymmetry of the distribution about the mean, and the third, α_4, gives an indication of the peakedness of the distribution. This last index is of primary importance in goniophotometric curve analysis for, as will be shown later, its correlation

with estimates of distinctness-of-reflected-image gloss is almost perfect.

A method was devised by Pelton [15] in which he obtains a series of measurements of photometric brightness, B_θ, by tilting a specimen about an axis in the photometric plane. Thus he obtained a type of goniophotometric distribution curve with simultaneously varying incidence and viewing angles. This curve suggested to him an analogy to the frequency distribution curve according to the law of probability. He then computed the dispersion index, σ, (usually called standard deviation) using the relation,

$$\sigma=\sqrt{\frac{\Sigma_\theta B_\theta \theta^2}{\Sigma_\theta B_\theta}}, \tag{6}$$

where θ is the angle of tilt of the specimen. This equation is analogous to taking the square root of eq (1), for which $k=2$. As the standard deviation has an inverse relation to the sharpness of his curves, Pelton took $1/\sigma$ as a measure of what he called "peakiness."

4.1. Computation Short Cuts

To shorten the computation we define deviates, d_i, from an assumed mean, x'. Then moments

$$\nu_k=\frac{\sum_1^n f_i(d_i)^k}{N} \tag{7}$$

about x' are related to π_k about the mean by the general expression obtained from the expansion of the binomial in eq (2),

$$\pi_k=\sum_0^k {}_t\binom{k}{t}(-\nu_1)^t(\nu_{k-t}), \tag{8}$$

where

$$\binom{k}{t}=\frac{k!}{t!(k-t)!},$$

t being an integer having values, $0\le t\le k$.

The first five moments about the mean (π_0, π_1, π_2, π_3, and π_4) are in table 1. Dispersion, skewness, and kurtosis indexes may then be defined in terms of these moments.

TABLE 1. *Definition of indexes*

k	π_k
0	1
1	0
2	$\nu_2-\nu_1^2$
3	$\nu_3-3\nu_1\nu_2+2\nu_1^3$
4	$\nu_4-4\nu_1\nu_3+6\nu_1^2\nu_2\times3\nu_1^4$

To facilitate the computation of the three indexes the data were taken at the angle of specular reflection and at 1° intervals for 5° on either side of the specular angle. To show the ease of computation an example is shown in table 2 for a plaque of white ceramic tile illuminated at 60°, specular gloss of about 90. The computation is further simplified, because we can readily take

$$f_i d_i^k=d_i f_i d_i^{k-1}, \tag{9}$$

where d_i is the departure from the specular angle (assumed mean), and f_i is the goniophotometrically obtained fractional reflectance (distribution frequency).

TABLE 2. *Computation of indexes*

Angle (deg)	d_i	f_i	$f_i d_i$	$f_i d_i^2$	$f_i d_i^3$	$f_i d_i^4$
55	−5	0.009	−0.045	0.225	−1.125	5.625
56	−4	.014	−.056	.224	−0.896	3.584
57	−3	.033	−.099	.297	−.891	2.673
58	−2	.15	−.30	.60	−1.20	2.40
59	−1	1.45	−1.45	1.45	−1.45	1.45
60	0	7.94	0.00	0.00	0.00	0.00
61	1	2.04	2.04	2.04	2.04	2.04
62	2	0.26	0.52	1.04	2.08	4.16
63	3	.053	.159	0.477	1.431	4.293
64	4	.019	.076	.304	1.216	4.864
65	5	.010	.050	.250	1.250	6.250
	Σ	11.978	+0.895	6.907	+2.455	37.339

$$\nu_1=\frac{\Sigma f_i d_i}{N}=+\frac{0.895}{11.978}=0.0747$$

$$\nu_2=\frac{\Sigma f_i d_i^2}{N}=\frac{6.907}{11.978}=0.577$$

$$\nu_3=\frac{\Sigma f_i d_i^3}{N}=+\frac{2.455}{11.978}=0.205$$

$$\nu_4=\frac{\Sigma f_i d_i^4}{N}=\frac{37.339}{11.978}=3.117$$

$$\pi_2=\nu_2-\nu_1^2 \qquad =0.571$$

$$\pi_3=\nu_3-3\nu_1\nu_2+2\nu_1^3 \qquad =0.76$$

$$\pi_4=\nu_4-4\nu_1\nu_3+6\nu_1^2\nu_2-3\nu_1^4 \qquad =3.072$$

$$\sigma=(\pi_2)^{1/2} \qquad =0.756$$

$$\alpha_3=\pi_3/(\pi_2)^{3/2} \qquad =0.176$$

$$\alpha_4=\pi_4/(\pi_2)^2 \qquad =9.42$$

4.2. Characteristics of the Indexes

If a distribution is symmetrical, the skewness index, α_3, has a value of zero. There is no upper limit to the magnitude of α_3. Mathematically stated,

$$0\le|\alpha_3|\le\infty.$$

Values for α_3 as great as ±2 indicate marked skewness, however.

The kurtosis index, α_4, has a value of 3 for the normal curve, $y=ae^{-x^2/2\sigma^2}$. For curves more peaked than the normal curve, α_4 is greater than 3, whereas for curves flatter than the normal curve, α_4 is less than 3. There is no upper limit for α_4. For a flat curve, that is for f_i constant, the value of α_4, designated α_4', is determined from the number of observations on which computations are made. From the definitions of α_4, π_4, and π_2 we see that

$$\alpha_4'=\frac{\pi_4}{(\pi_2)^2}=\frac{\sum_1^n f_i d_i^4/N}{\left(\sum_1^n f_i d_i^2/N\right)^2}=n\frac{\sum_1^n d_i^4}{\left(\sum_1^n d_i^2\right)^2} \tag{10}$$

where $n=N/f_i$=number of angle settings. The general case for 1° intervals is shown as follows: We have

$$\left.\begin{aligned}\sum_1^n{}_i d_i^2 &= 2\sum_1^M{}_i X_i^2\\ \sum_1^n{}_i d_i^4 &= 2\sum_1^M{}_i X_i^4\end{aligned}\right\}, \tag{11}$$

where X_i represents positive numbers ranging from 1 to M, since observations are made at positive and negative angles. Then, $n=2M+1$ since n includes $d_i=0°$. The sums of the first two even powers of the first M natural numbers may be computed from the following equations:

$$\left.\begin{aligned}&\sum_1^M{}_i X_i^2=\left(\frac{2M+1}{3}\right)\left(\frac{M(M+1)}{2}\right)\\ &\text{and}\\ &\sum_1^M{}_i X_i^4=\left(\frac{3M^2+3M-1}{5}\right)\left(\frac{2M+1}{3}\right)\left(\frac{M(M+1)}{2}\right)\end{aligned}\right\} \tag{12}$$

Thus

$$\alpha_4'=\frac{2(2M+1)\left(\frac{3M^2+3M-1}{5}\right)\left(\frac{2M+1}{3}\right)\left(\frac{M(M+1)}{2}\right)}{4\left(\frac{2M+1}{3}\right)\left(\frac{M(M+1)}{2}\right)\left(\frac{2M+1}{3}\right)\left(\frac{M(M+1)}{2}\right)}=\frac{9}{5}-\frac{3}{5M(M+1)}.$$

The upper limiting value, $L_{\alpha_4'}$, of the kurtosis index for a complete diffusor as M increases without bound is

$$L_{\substack{\alpha_4'\\ M\to\infty}}=9/5=1.8.$$

The lower limit occurs when $M=1$, that is when observations are taken at the specular angle and at $\pm 1°$. In this case $\alpha_4'=1.8-0.3=1.5$. Thus we may state, mathematically:

$$1.5\leq\alpha_4'\leq 1.8.$$

For the number of the intervals used in this analysis, that is five intervals on either side of the specular angle, $n=11$, $M=5$. Thus for a completely diffusing surface, that is, one having constant f_i

$$\alpha_4'=1.80-\frac{3}{25(6)}=1.78.$$

Should we wish to define a scale of peakedness for which a perfect diffuser is assigned the value zero, then we may subtract α_4' from α_4, and call the resulting difference the peakedness index, P.

Thus

$$P\equiv\alpha_4-\alpha_4'. \tag{13}$$

If the ordinates of one distribution are a constant factor of the corresponding ordinates of another distribution, then the indexes σ, α_3, and α_4 for one distribution will equal the corresponding indexes for the other. To distinguish one curve from the other, one point on each curve needs to be specified. A convenient point is the value of the fractional reflectance at the specular angle.

The dispersion index, σ, is at its lower limit for completely specular reflection, and is large for completely diffuse reflection. The lower limit is zero, because $d_i=0°$ at the specular angle. The value for completely diffuse reflection is determined as follows:

For completely diffuse reflection, f_i=constant,

$$\sigma=\left(\frac{\sum_1^n{}_i d_i^2}{n}\right)^{\frac{1}{2}}.$$

But from eq 11

$$\sigma=\left(\frac{2\sum_1^M{}_i X_i}{n}\right)^{\frac{1}{2}}.$$

Here also $n=2M+1$, and from eq 12

$$\sigma=\left(\frac{M(M+1)}{3}\right)^{\frac{1}{2}}. \tag{14}$$

For the number of the intervals used in this analysis, $M=5$. Thus when f_i is constant, $\sigma=3.16$.

The characteristics for the indexes, α_4 and σ, lead to conclusions about their utility in describing surface appearance. Consider the ranges of these two indexes for the number of observations used in this analysis. Mathematically stated, from flat to peaked curves, the ranges are $1.78\leq\alpha_4\leq\infty$ and $3.16\geq\sigma\geq 0$.

When a reflection curve is flat, α_4 has a small value in its range, while σ has a large value in its range. Conversely, when a curve describes a completely specular reflection, α_4 is at its upper limit, and σ is at its lower limit. Thus α_4 may indicate glossiness directly, and σ may indicate glossiness inversely.

5. Application to Glossimetry

The practice of glossimetry is now quite well established and generally yields satisfactory discriminations, but must be recognized as an abridged goniophotometric technique. Just as in the problems of colorimetry, the standardization of abridged methods of measurement is necessary to enable one to obtain on a common basis rapid comparisons during production of a specific material. The gen-

eral method of analyzing goniophotometric distribution curves described in this paper may be the means of arriving at some instrumental geometry and recommended procedures for making objective evaluations of the surface appearance attribute ascribable to gloss.

Subjective observations on the specular gloss of specimens are usually made without use of angle-measuring devices. Therefore, as the skewness index is a measure of dissymmetry of a distribution, no attempt is made to correlate this index with the surface-appearance attribute ascribable to gloss.

The first problem confronting this analysis is, do the indexes α_4 and σ correlate with surface appearance, specular gloss, and distinctness-of-image gloss, as well as or better than the existing glossimetry techniques? If the correlations prove satisfactory, the next problem is how to interpret this analysis so that instrument geometry for abridged methods may be selected wisely. Three important geometric variables of a glossmeter are (1) angle of incidence, (2) receiver aperture size, (3) the ratio of the angular size of the source to the receiver aperture.

5.1. Correlation with Distinctness of Reflected Images

One of the attributes of surface appearance is the distinctness with which images are reflected. This attribute is influenced by at least two properties of specimens. One of the properties is the smoothness of the surface, the other is the diffuse reflection of the specimen. Lack of smoothness tends to distort the reflected images, and diffuse reflection controls the contrast between highlight and shadow.

Heretofore no satisfactory method has been devised to measure objectively distinctness-of-image gloss. Hunter [16] in 1936 described a photographic technique for recording distinctness of reflected images. However, no quantitative analysis was indicated in his paper.

a. Experimental Conditions

As there is need for a quantitative index of distinctness of reflected images, the kurtosis index was tested for correlation with distinctness of image estimates. For this experiment estimates were made by six observers, ranging in familiarity with the problems from thoroughly experienced to completely naive.

The 22 specimens used were of the following materials: Polished black glass, sand-blasted black glass, acid-etched black glass, polished white Vitrolite, depolished white Vitrolite, and white ceramic tile. These specimens were placed on a black cloth-covered table. The table was placed near a window so that the specimens were illuminated by north-sky light. The estimates made by the observers were on the distinctness of the images of the crossbars of the window. Observers were permitted to turn, tilt, or raise the specimens during the evaluations. The observers arranged the specimens in the order of estimated decreasing distinctness of the reflected images. The resulting data are shown in table 3, together with the ranking obtained by the kurtosis index, dispersion index, and 60° specular-gloss values of the specimens.

b. Rank Correlation

Correlation indexes were computed on the basis of Spearman's rank correlation coefficient, ρ. This correlation coefficient has been found quite useful in correlating ordered or ranked data. The equation for computing ρ is

$$\rho = 1 - \frac{6\Sigma D^2}{N(N^2-1)}, \tag{15}$$

where D is the rank difference, and N is the number of items.

This equation indicates by its sign whether the correlation is direct (+) or inverse (−). Whenever there is a tie in rank, the positions are split among the different items in the tie.

TABLE 3. *Rank order according to distinctness of image estimates, peakedness, 60° gloss, and dispersion*

Specimen [1]	Observers						Decreasing peakedness	Decreasing 60° gloss	Increasing dispersion
	MMB	DBJ	HKH	GWH	IN	HS			
B94	1	1	1	1	1	1	1	2	1
V90	7	6	6	7	7	7	2	3	2
S1	2	2	2	2	2	2	3	5	5
S2	3	3	3	3	3	3	4	7.5	3.5
G102	8	8	8	8	8	8	5	1	3.5
S3	4	4	4	4	4	4	6	10	6
S4	5	5	5	5	5	5	7	13	7
S5	6	7	7	6	6	6	8	16.5	8
G87	10	10	10	11	10	9	9	4	9
A1	9	9	9	9	9	11	10	6	10
G80	13	12	12	13	12	10	11	7.5	11
A2	11	11	11	11	10	12	12	9	12
G70	15	14	15	15	15	15	13	11	13
A3	12	13	13	12	13	13	14	12	14
G60	17	15	16	16	16	16	15	14	15
G50	16	17	17	17	17	17	16	15	16
A4	14	16	14	14	14	14	17	16.5	17
G40	18	18	18	18	18	18	18	18	18
G30	19	19	19	19	19	19	19	19	19
G20	20	20	20	20	20	20	20	20	20
G10	21	21	21	21	21	21	21	21	21
V1	22	22	22	22	22	22	22	22	22

[1] G, white ceramic; V, white Vitrolite; B, black glass, polished; A, black glass acid etched; S, black glass, sand-blasted.

The data indicate that confusion exists among the estimates where the specimens have nearly the same distinctness of image, but one is black and the other white. Therefore, computation of ρ was made for the entire group and for the group of black and the group of white specimens.

The correlation indexes obtained by the six observers for the three correlation conditions are shown in table 4. These results indicate that correlation of image distinctness with α_4 is better than with σ and is far better than with 60° specular gloss. When the specimens are separated into two groups according to reflectance, then correlation with α_4 is nearly perfect. We may conclude that the diffuse reflectance of a specimen is an important factor in distinctness-of-image estimates.

TABLE 4. *Summary of correlation coefficients*

Observer	Rank correlation coefficient								
	Black and white			Black only			White only		
	α_4	σ	60° gloss	α_4	σ	60° gloss	α_4	σ	60° gloss
DBJ	0.975	0.965	0.795	1.000	0.988	0.664	1.000	1.000	0.993
HKH	.968	.958	.786	1.000	.988	.664	1.000	1.000	.993
IN	.962	.951	.771	1.000	.988	.664	1.000	1.000	.993
HS	.963	.952	.773	1.000	.988	.664	1.000	1.000	.993
MMB	.957	.952	.765	1.000	.988	.664	1.000	1.000	.986
GWH	.955	.948	.760	1.000	.988	.664	1.000	1.000	.993
Mean	0.963	0.954	0.775	1.000	0.988	0.664	1.000	1.000	0.992

5.2. Correlation With 60° Specular Gloss

One of the satisfactory glossimetry techniques is the 60° specular gloss method. If the indexes obtained by analysis of goniophotometric curves correlate with 60° specular gloss and also yield more information, then this analysis is an improvement over the abridged method. To see if correlation exists between kurtosis and 60° specular gloss, we plot α_4 on a logarithmic scale against 60° specular-gloss readings for the 22 specimens listed in table 3 and determine if a smooth curve will fit the resulting points. Figure 3 is a plot of the data showing division into two distinct groups, shown by solid lines, depending on the appearance of the reflected image. Those specimens forming sharp images shaded by varying haze fall into one group. Those specimens forming no sharp images, but having varying specular gloss, fall in the other group. This examination for correlation indicates not only that direct correlation exists, but also that separation into distinct groups in accord with visual appearance is accomplished by the goniophotometric curve analysis, whereas the glossmeter readings alone do not suggest the existence of these two groups.

Correlation of dispersion, σ, with 60° specular gloss is shown in figure 4. This figure shows the division of the specimens into the same two groups. The correlation for σ is inverse, that is, where σ is large, gloss is low, and conversely.

We must conclude from the above data that this analysis not only correlates with existing glossimetry techniques but yields additional information about surface appearance.

5.3. Selection of Instrumental Geometry

This analysis has been shown to have advantages over abridged methods in surface-appearance evaluation. Abridged methods of measurement, using

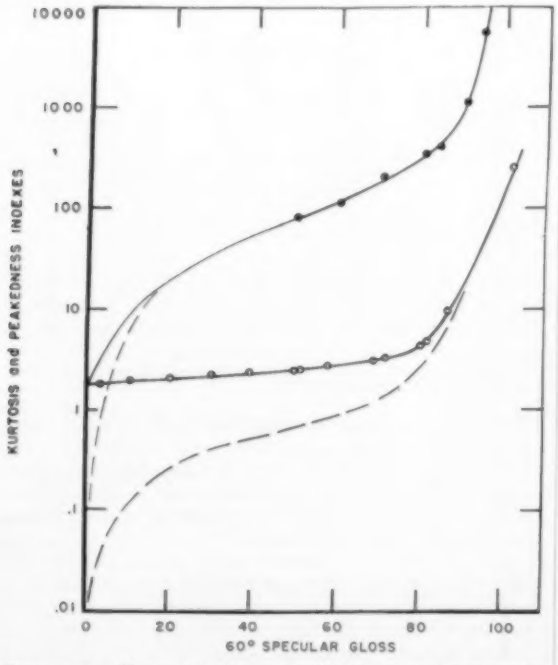

FIGURE 3. *Kurtosis index, α_4 (solid lines), and peakedness index, P (dashed lines), plotted against 60° specular gloss.*

These indexes differ by a constant amount, 1.78, which, for the indexes above 10, is unimportant, so that points for kurtosis index alone are shown above 10. Note the division of the specimens into two groups: specimens forming sharp images, ●; specimens forming no sharp images, ○.

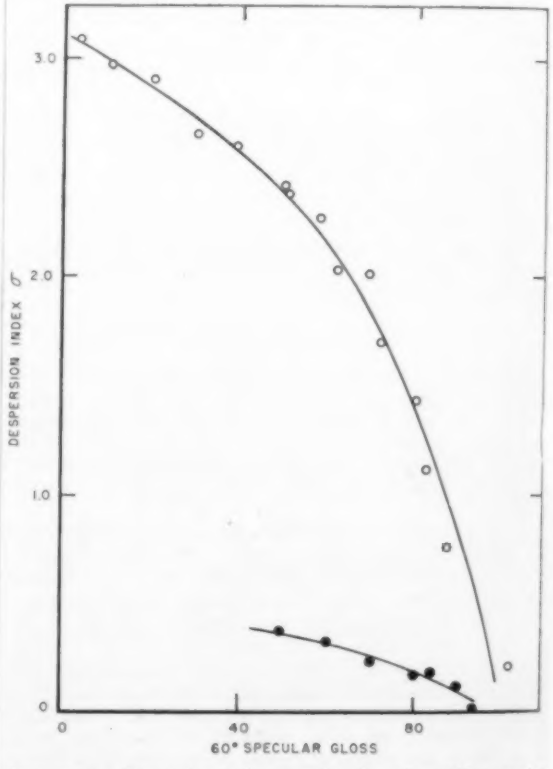

FIGURE 4. *Dispersion index, σ, plotted against 60° specular gloss.*

Specimens forming sharp images, ●; specimens forming no sharp images, ○

glossmeters, are required to obtain information economically during the production of materials. Glossmeters, as well as goniophotometers, should have geometry to yield optimum discrimination between specimens. Assuming that the receiver is adequately sensitive, the resolution and the incidence angle may be chosen to yield this optimum discrimination.

To determine the optimum geometric conditions for goniophotometry and glossimetry a series of goniophotometric curves should be obtained with various materials for incidence angles ranging from perpendicular to grazing. Then the information from the goniophotometric curves needs to be correlated with visual estimates of gloss. The data for two specimens, A (acid-etched black glass) and S (sand-blasted black glass), having 60° specular-gloss values of about 80, will serve to illustrate the procedure for finding optimum geometry (see fig. 5).

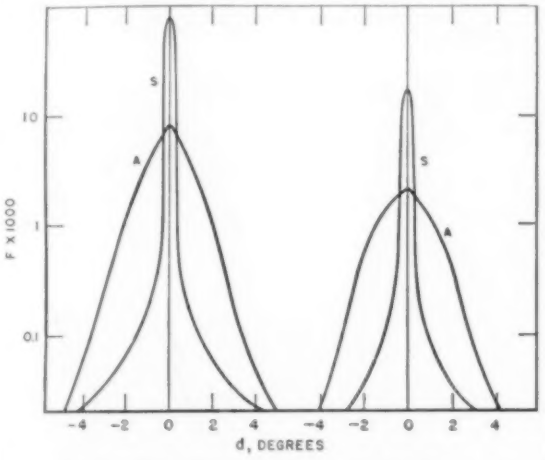

FIGURE 5. *Comparison of 60° with 20° incidence angles.*

60° incidence on left; 20° incidence on right; sand-blasted black glass, S; acid-etched black glass, A.

a. Choice of Incidence Angle

Let us consider first how the peakedness index, P, may be used in the problem of choice of incidence angle.

Greatest discrimination between specimens is indicated where the difference between peakedness indexes is greatest. In the illustration, for 20° incidence, the difference between P_S (index for specimen S) and P_A (index for specimen A) is $P_S-P_A=153-1.6=151.4$. For 60° incidence this difference is $P_S-P_A=379-2.8=376.2$. Thus for greater discrimination between S and A, 60° incidence is superior to 20° incidence for goniophotometric measurements.

This reasoning may be applied to glossmeter measurements. The receiver aperture of a glossmeter includes flux reflected near the specular angle. Thus for optimum discrimination between specimens S and A, glossmeter measurements should be made at 60° rather than at 20° incidence, provided that the flux accepted for measurement is sufficiently close to the specular angle. To answer the question, what is meant by "sufficiently close", we must consider the problem of choice of receiver aperture size.

b. Choice of Receiver Aperture Size

Let us now consider how the goniophotometric curves may be used in the problem of choice of receiver aperture size.

The goniophotometric curves provide sufficient information for the choice of receiver aperture size needed for discriminations. For goniophotometric measurements the receiver aperture needs to be sufficiently small to trace adequately the geometric distribution of the fractional reflectances. Glossmeters, on the other hand, integrate the flux entering the receiver entrance window at the specular angle. The glossmeter must distinguish between different specimens by integrating between the limits of the receiver entrance window the areas under the respective goniophotometric curves. The limits of integration may be evaluated from either of the following relationships:

$$\int_{-a}^{a} F_1\delta d-\int_{-a}^{a} F_2\delta d=K, \tag{16}$$

or

$$\int_{-a}^{a} F_1\delta d=K\int_{-a}^{a} F_2\delta d, \tag{17}$$

where a is the limit of integration, F_1 and F_2 are fractional reflectances of two specimens, d is the departure from the specular angle, and K is an experimentally determined constant. Equation (16) states that the difference between the integrated areas is constant. Equation (17) states that the ratio of the integrated areas is constant. The constant K should be evaluated for specimens of similar materials from visual estimates of either gloss differences or gloss ratios. No attempt should be made to evaluate K for radically dissimilar specimen types.

6. Conclusions

Since the surface appearance attribute ascribable to gloss may be evaluated most advantageously by monoplane goniophotometric curves, a technique for analyzing these curves needs to be adopted. The variables of classical statistics, dispersion, skewness, and kurtosis, have been studied in this connection, and it is found that the kurtosis index in particular summarizes in a meaningful way the information given by the goniophotometric curve. Correlation between 60° specular gloss and kurtosis index is fairly good, and indicates that the two measure similar properties of surfaces such as those studied. Furthermore, correlation between distinctness of image and kurtosis index is a decided improvement over correlation between distinctness of image and 60° specular gloss. Kurtosis index is therefore proposed for adoption as a standard technique for re-

ducing goniophotometric data to meaningful numbers. This index has been applied successfully for choosing instrumental geometry for abridged goniophotometry, that is, glossimetry.

7. References

[1] F. Thaler, Die diffuse Reflexion des Lichtes an matten Oberflachen, Ann. Physik [4] **11,** 996 (1903).

[2] P. Bouguer, Optice de diversis luminis gradibus dimentien dis. Opus posthumum in lucem editum a D. de la Caille et in latinum conversum a Joachimo Richtenberg, J. S. Joannis Thomae Trattner. Book 2, section 3, art. 3 (1762).

[3] J. H. Lambert, Photometria sive de mensura gradibus luminis, colorum, et umbrae, Augsburg (1760).

[4] H. J. McNicholas, Equipment for measuring the reflective and transmissive properties of diffusing media, J. Research NBS **13,** 211, (1934) RP704.

[5] L. A. Wetlaufer and W. E. Scott, The measurement of gloss, Ind. Eng. Chem., Anal. Ed. **12,** 647 (1940).

[6] H. K. Hammond, III, and I. Nimeroff, Measurement of sixty-degree specular gloss, J. Research NBS **44,** 585 (1950) RP2105.

[7] ASTM tentative method of test for 60° specular gloss of paint finishes, D 523, Book of ASTM Standards, Part 4 (1949).

[8] V. G. W. Harrison, Definition and measurement of gl[illegible], p. 106 (Patra, Cambridge, England, 1945).

[9] W. W. Barkas, Analysis of light scattered from a surf[illegible] of low gloss into its specular and diffuse componen[illegible], Proc. Phys. Soc. (London) **51,** 274 (1939).

[10] G. I. Pokrowski, Zur Theorie der Diffusen Licht[illegible]flexion, Z. Physik. Part I, **30,** p. 66 (1924), Part II, **35,** p. 34 (1925), Part III, **35,** p. 390 (1926), Part IV, **36,** p. 472 (1926).

[11] A. Fresnel, Calcul des teintes que polarization developpe dans lames cristallisees, Ann. chim. phys. **17,** 194, 312 (1821).

[12] T. K. Chinmayanandam, On the specular reflection from rough surfaces, Phys. Rev. (London) [II], **13,** 96 (1919).

[13] H. L. Reitz, Mathematical Statistics (The Open Court Publishing Co., LaSalle, Ill., 1927).

[14] F. E. Croxton and D. J. Cowden, Applied general statistics (Prentice Hall, New York, N. Y., 1946).

[15] M. P. Pelton, The luster of textile fabrics and a method of measurement, Trans. Opt. Soc. (London) **31,** 184 (1930).

[16] R. S. Hunter, Gloss investigations using reflected images of a target pattern, J. Research NBS **16,** 357 (1936) RP879.

Washington, February 29, 1952.

INDEX TO VOLUME

A

Page

Absorption spectra of methanol, ethanol, and n-propanol, RP2314 ... 281
Acetobacter suboxydan, action on D-mannitol, RP2334 ... 438
Acetylene, deutero, mass spectra, RP2304 ... 188
Acid-base reactions in benzene, RP2326 ... 381
Acquista, Nicolo, Earle K. Plyler, Infrared absorption spectra of five halomethanes, RP2290 ... 92
Adsorbent, commercial solid, RP2319 ... 325
Alcohols, three, infrared spectra, RP2314 ... 281
Alloys, aluminum, thermal expansion, RP2308 ... 209
Alfred, Charles M., Chart for the TE_{11} mode piston attenuator, RP2293 ... 109
Aluminum and some aluminum alloys, thermal expansion, RP2308 ... 209
Ammeters, testing, RP2296 ... 121
Atomic energy levels of gallium, indium, and thallium, RP2320 ... 334
Attenuator, chart for the TE_{11} mode piston, RP2293 ... 109
Audio frequencies, measurement of current and voltage at, RP2296 ... 121
Austenite, chromium-nickel, solubility of carbon in, RP2281 ... 40

B

Barium D-gluconate from cyanohydrin, synthesis, RP2301 ... 163
Bases, comparative strengths in benzene, RP2326 ... 381
Bentonite, surface changes, RP2319 ... 325
Benzene, deutero, mass spectra, RP2304 ... 188
Benzene, strengths of bases in, RP2326 ... 381
Berghoiz, Walter A., Determination of metallic beryllium and beryllium carbide in beryllium metal, RP2306 ... 201
Beryllium metal, determination of metallic beryllium and beryllium carbide in, RP2306 ... 201
Binding energies for different types of electrons, RP2285 ... 61
Boundary-value problems, numerical computation, RP2332 ... 424
Bristle, pigmentation in, RP2315 ... 287
Bromophthalein magenta, reaction with bases in benzene, RP2326 ... 381
Butadiene and styrene, heats of polymerization, RP2313 ... 275

C

Capuano, Ruth, Herbert E. Salzer, Ruth Zucker, Table of the zeros and weight factors of the first twenty Hermite polynomials, RP2294 ... 111
Carbohydrates, radioactive, position-labeled, RP2301 ... 163
Carbon, determination in beryllium metal, RP2306 ... 201
Carbon dioxide, gaseous heat capacity, RP2303 ... 179
Carbon disulfide and carbon dioxide, infrared spectrum, RP2327 ... 392
Carbon-14-labeled, D-mannitol, and D-fructose, preparation, RP2334 ... 438
Carbon, solubility in chromium-nickel austenite, RP2281 ... 40
Carwile, Nesbit L., Glenn W. Geil, Effect of strain-temperature history on the flow and fracture of ingot iron at low temperatures, RP2329 ... 399
—, —, *Thomas G. Digges*, Influence of nitrogen on the notch toughness of heat-treated 0.3-percent-carbon steels at low temperatures, RP2305 ... 193
Cauchy-Riemann equations, RP2328 ... 395
Ceramics, pure oxides, RP2316 ... 298
Cesium-137, measurement, RP2298 ... 147
Chromium-nickel austenite, solubility of carbon in, RP2281 ... 40
Chromium orthophosphate, crystal forms of, RP2300 ... 159
Clay, adsorbents and catalysts: acid treatment, RP2319 ... 325
Cobalt-60, measurement, RP2298 ... 147
Coe, J. R., Jr., J. F. Swindells, T. B. Godfrey, Absolute viscosity of water at 20° C, RP2279 ... 1
Copolymerization and polymerization, heats of, of butadiene, and styrene, RP2313 ... 275
Corrosion stress, film-rupture mechanism of, RP2291 ... 99
Crystal forms of cromium orthophosphate, RP2300 ... 159
Crystal growing, RP2299 ... 152
Crystal growth, mica, RP2323 ... 360
Cyanohydrin synthesis, improvements in, RP2301 ... 163

D

Daniels, Raymond D., Jr., Arnold Wexler, Pressure-humidity apparatus, RP2312 ... 289
Davis, Marion Maclean, Hannah B. Hetzer, Comparative strengths of four organic bases in benzene, RP2326 ... 381
Dean, Helen, Fred L. Mohler, Vernon H. Dibeler, Laura Williamson, Mass spectra of deuteroacetylenes, monodeuterobenzene, and deuteronaphthalenes, RP2304 ... 188
Deitz, Victor R., Juan de Dios Lopez-Gonzalez, Surface changes in an original and an activated bentonite, RP2319 ... 325
Deutero, acetylenes, benzene, and naphthalenes, mass spectra, RP2304 ... 188
Dibeler, Vernon H., Fred L. Mohler, Laura Williamson, Helen Dean, Mass spectra of deuteroacetylenes, monodeuterobenzene, and deuteronaphthalenes, RP2304 ... 188
Diethylbarbituric acid, ionization constant, RP2289 ... 84
Digges, Thomas G., Glenn W. Geil., Nesbit L Carwile, Influence of nitrogen on the notch toughness of heat-treated 0.3-percent-carbon steels at low temperatures, RP2305 ... 193
—, *William D. Jenkins*, Effect of temperature on the tensile properties of high-purity nickel, RP2317 ... 313
Di-o-tolylguanidine, reaction with bromophthalein magenta in benzene, RP2326 ... 381
Dissociation constant of diethylbarbituric acid, RP2289 ... 84
Dosimetry, electron, RP2295 ... 117

E

Eigenvalue problems, numerical computation of:
RP2286 ... 68
RP2332 ... 424
Electrical instruments, testing of, RP2296 ... 121
Electrical properties of leather, effect of moisture and temperature, RP2322 ... 349
Electrode-, glass, solution interface, heterogeneous equilibria, RP2333 ... 428
Electrode, silver-chloride, in solutions of diethylbarbituric acid, RP2289 ... 84
Electron dosimetry, RP2295 ... 117
Electrons, binding energies of different types, RP2285 ... 61
Energies, binding, for electrons of different types, RP2285 ... 61
Error, truncation, in solution of Laplace's equation, RP2321 ... 345
Ethylenimine, heats of combustion and formation, RP2307 ... 206
Expansion, thermal, aluminum and aluminum alloys, RP2308 ... 209

F

Fillmore, C. L., S. M. Lang, L. H. Maxwell, The system beryllia-alumina-titania: Phase relations and general physical properties of three-component porcelains, RP2316 ... 298
Film dosimetry of electrons, RP2295 ... 117
Film-rupture mechanism of stress corrosion of some metals and alloys, RP2291 ... 99
Fleeman, J., F. S. Frantz, Jr., Film dosimetry of electrons in the energy range 0.5 to 1.4 million electron volts, RP2295 ... 117
Fortet, R., On some functionals of Laplacian processes, RP2280 ... 32
—, On the estimation of an eigenvalue by an additive functional of a stochastic process, with special reference to the Kac-Donsker methods, RP2286 ... 68
Frantz, F. S., Jr., J. Fleeman, Film dosimetry of electrons in the energy range 0.5 to 1.4 million electron volts, RP2295 ... 117
D-Fructose-1-(and 6)-C^{14}, preparation, RP2334 ... 438
Frush, H. L., H. S. Isbell, J. V. Karabinos, N. B. Holt, A. Schwebel, Synthesis of D-glucose-1-C^{14} and D-mannose-1-C^{14}, RP2301 ... 163
Fuels, reference, synthesis and properties, RP2287 ... 76
Functionals of Laplacian processes, RP2280 ... 32

G

Gailar, Norman M., Earle K. Plyler, Thomas A. Wiggins, Some accurately measured infrared wavelengths for calibration of grating spectrometers, RP2309 ... 221
—, —, The $3\gamma_3$ bands of carbon disulfide and carbon dioxide, RP2327 ... 392
Gailkowski, T. T., H. S. Isbell, J. V. Karabinos, H. L. Frush, N. B. Holt, A. Schwebel, Synthesis of D-glucose-1-C^{14} and D-mannose-1-C^{14}, RP2301 ... 163
Gallium, arc spectrum, RP2320 ... 334
Gamma radiation from a cesium and a cobalt source, measurement, RP2298 ... 147
Geil, Glenn W., Nesbit L. Carwile, Thomas G. Digges, Influence of nitrogen on the notch toughness of heat-treated 0.3-percent-carbon steels at low temperatures, RP2305 ... 193
—, —, Effect of strain-temperature history on the flow and fracture of ingot iron at low temperatures, RP2329 ... 399
Glass-electrode-solution interface, heterogeneous equilibria, RP2333 ... 428
Glasses, nonhygroscopic, pH function, RP2324 ... 370
D-Glucose-1-C^{14}, preparation, RP2301 ... 163
Godfrey, T. B., J. F. Swindells, J. R. Coe, Jr., Absolute viscosity of water at 20° C., RP2279 ... 1
Goldman, Richard G., Donald Hubbard, Heterogeneous equilibria at the glass-electrode, solution interface, RP2333 ... 428
—, —, pH response of nonhygroscopic glasses, RP2324 ... 370
Goniophotometry, analysis of curves, RP2335 ... 441
Group theory in computation of eigenvalue problems, RP2332 ... 424
Grove, G. R., Measurement of cesium-137 and cobalt-60 gamma radiation with a pressure ionization chamber, RP2298 ... 147

H

Halomethanes, infrared spectra, RP2290 ... 92
Haupt, G. W., An alkaline solution of potassium chromate as a transmittancy standard in the ultraviolet, RP2331 ... 414
Heat capacity of gaseous carbon dioxide, RP2303 ... 179
Heats of combustion and formation of ethylenimine, RP2307 ... 206
Heats of polymerization and copolymerization of butadiene and styrene, RP2313 ... 275
Heptane, properties and synthesis, RP2287 ... 76
Hermach, Francis L., Thermal converters as ac-dc transfer standards for current and voltage measurements at audio frequencies, RP2296 ... 121
Hermite polynomials, table of the zeros and weight factors of, RP2294 ... 111
Heterogeneous equilibria at the glass-electrode-solution interface, RP2333 ... 428
Hetzer, Hannah B., Marion Maclean Davis, Comparative strengths of four organic bases in benzene, RP2326 ... 381
Hidnert, Peter, H. S. Krider, Thermal expansion of aluminum and some aluminum alloys, RP2308 ... 209
Holt, N. B., H. S. Isbell, J. V. Karabinos, H. L. Frush, A. Schwebel, Synthesis of D-glucose-1-C^{14} and D-mannose-1-C^{14}, RP2301 ... 163

Page

Horsehair, pigmentation in, RP2315 287
Hubbard, Donald, Richard G. Goldman, Heterogeneous equilibria at the glass-electrode-solution interface, RP2333 428
—, —, pH response of nonhygroscopic glasses, RP2324 370
Humidity, relative, apparatus for control of, RP2312 269
Hydrocarbons, heptane, 2,2,4-trimethylpentane and intermediates, RP2287 76
Hydrogen-ion response of nonhygroscopic glasses, RP2324 370

I

Indicator reactions in benzene, RP2326 381
Indium, arc spectrum, RP2320 334
Infrared absorption of carbon dioxide and carbon disulfide, RP2327 392
Infrared absorption spectra of substituted methanes, RP2290 92
Infrared bands of water vapor, RP2325 377
Infrared spectra of methanol, ethanol, and n-propanol, RP2314 281
Infrared standards for calibrating grating spectrometers, RP2309 221
Ionization constant of diethylbarbituric acid, RP2289 84
Irish, Carolyn R., Samuel J. Rosenberg, Solubility of carbon in 18-percent-chromium–10-percent-nickel austenite, RP2281 40
Iron, ingot, effect of strain and temperature on flow and fracture, RP2329 399
Isbell, H. S., J. V. Karabinos, H. L. Frush, N. B. Holt, A. Schwebel, Synthesis of D-glucose-1-C^{14} and D-mannose-1-C^{14}, RP2301 163
—, —, Preparation of D-mannitol-C^{14} and its conversion to D-fructose-1-(and 6)-C^{14} acetobacter suboxydans, RP2334 438
Iterants, some general theorems on, RP2288 82
Iterative methods,[1] RP2330 407

J

Jenkins, William D., Thomas G. Digges, Effect of temperature on the tensile properties of high-purity nickel, RP2317 313
Jessup, Ralph S., Raymond A. Nelson, Heats of combustion and formation of liquid ethylenimine, RP2307 206
—, —, *Donald E. Roberts*, Heats of copolymerization of butadiene and styrene from measurements of heats of combustion, RP2313 273

K

Kac-Donsker method on estimation of eigenvalues, RP2286 68
Karabinos, J. V., Horace S. Isbell, Preparation of D-mannitol-C^{14} and its conversion to D-fructose-1-(and 6)-C^{14} by acetobacter suboxydans, RP2334 438
—, —, *H. L. Frush, N. B. Holt, A. Schwebel*, Synthesis of D-glucose-1-C^{14} and D-mannose-1-C^{14}, RP2301 163
—, *R. A. Paulson, W. H. Smith*, Thiophosphation of 2-methyl-2-nitro-1-propanol and the preparation of monothiophosphoric acid, RP2318 322
Kiess, C. C., Wavelengths of rotational lines in the water-vapor bands of 0.93 and 1.13 microns, RP2325 377
Kirk, Floyd S., George G. Manov, Kathryn E. Schuette, Ionization constant of 5-5′-diethylbarbituric acid from 0° to 60° C, RP2289 84
Krider, H. S., Peter Hidnert, Thermal expansion of aluminum and some aluminum alloys, RP2308 209

L

Lang, S. M., C. L. Fillmore, L. H. Maxwell, The system beryllia-alumina-titania: Phase relations and general physical properties of three-component porcelains, RP2316 298
Laplace's equation, truncation error in the solution of, RP2321 345
Laplacian processes, functionals of, RP2280 32
Leather, electrical properties, effect of moisture and temperature, RP2322 349
Liebkein, Julius, Properties of certain statistics involving the closest pair in a sample of three observations, RP2311 255
Linear equations, gradient methods in the solution of systems of, RP2330 407
Logan, Hugh L., Film-rupture mechanism of stress corrosion, RP2291 90
Lopez-Gonzales, Juan de Dios, Victor R. Deitz, Surface changes in an original and an activated bentonite, RP2319 325
Lubkin, Samuel, A method of summing infinite series, RP2310 228
Lukacs, Eugene, Otto Szasz, Some nonnegative trigonometric polynomials connected with a problem in probability, RP2297 139

M

D-Mannitol-1-C^{14}, preparation of and conversion to D-fructose, RP2334 438
D-Mannose-1-C^{14}, preparation, RP2301 163
Manometers, sensitive mercury-level detecting unit, RP2283 54
Manov, George G., Kathryn E. Schuette, Floyd S. Kirk, Ionization constant of 5-5′-diethylbarbituric acid from 0° to 60° C, RP2289 84
Masi, Joseph F., Benjamin Petkof, Heat capacity of gaseous carbon dioxide RP2303 179
Mathematical tables, RP2294 111
Matrices, Hermitian, RP2288 82
Matrix, bounds of characteristic roots of:
RP2284 89
RP2292 106
Mass spectra of deuteroacetylenes, monodeuterobenzene, and deuteronaphthalenes, RP2304 188
Maxwell, L. H., S. M. Lang, C. L. Fillmore, The system beryllia-alumina-titania: Phase relations and general physical properties of three-component porcelains, RP2316 298
McMurdie, Howard F., Barbara M. Sullivan, Crystal forms of chromium orthophosphate, RP2300 139
Meggers, William F., Robert J. Murphy, Arc spectra of gallium, indium, and thallium, RP2320 334
Melting points, determination, RP2299 152
Mercury-level detecting unit for manometers, RP2283 54
Metal, beryllium, determination of metallic beryllium and beryllium carbide in, RP2306 201
Metals and alloys, stress corrosion of some, RP2291 90
Methanes, fluorinated, infrared spectra, RP2290 92
2-Methyl-2-nitro-1-propanol, thiophosphation of, RP2318 322
Mica, synthesis of, RP2323 360
Mohler, Fred L., Vernon H. Dibeler, Laura Williamson, Helen Dean, Mass spectra of deuteroacetylenes, monodeuterobenzene, and deuteronaphthalenes, RP2304 188
Moisture and temperature, effect on electrical properties of leather, RP2322 349
Molecular structure of carbon disulfide and carbon dioxide, RP2327 392
Monothiophosphoric acid, preparation, RP2318 322
Moore, Charlotte E., Henry Norris Russell, Binding energies for electrons of different types, RP2285 61
Murphy, Robert J., William F. Meggers, Arc spectra of gallium, indium, and thallium, RP2320 334

N

Naphthalene, deutero-mass spectra of, RP2304 188
Nelson, Raymond A., Ralph S. Jessup, Heats of combustion and formation of liquid ethylenimine, RP2307 206
—, —, *Donald E. Roberts*, Heats of copolymerization of butadiene and styrene from measurements of heats of combustion, RP2313 273
Newman, Sanford B., Pigmentation in bristle and horsehair, RP2315 287
Nickel, high-purity, effect of temperature on tensile properties, RP2317 313
Nimeroff, Isadore, Analysis of goniophotometric reflection curves, RP2335 441
Nitrogen adsorption at liquid-nitrogen temperature, RP2319 325
Nitrogen, influence on steels, RP2305 190
Notch-toughness of steels, influence of nitrogen on, RP2305 190

O

Ordway, Fred, Techniques for growing and mounting small single crystals of refractory compounds, RP2299 152
Orthophosphate, cromium, crystal forms of, RP2300 139
Oxide porcelains of BeO-Al_2O_3-TiO_2, RP2316 298

P

Paulson, R. A., J. V. Karabinos, W. H. Smith, Thiophosphation of 2-methyl-2-nitro-1-propanol and the preparation of monothiophosphoric acid, RP2318 322
Pentane, 2,2,4-trimethyl, properties and synthesis, RP2287 76
Peterson, Raymond P., Uniformly best constant risk and minimax point estimates, RP2282 49
Petkof, Benjamin, Joseph F. Masi, Heat capacity of gaseous carbon dioxide, RP2303 179
Phase equilibria of the system beryllia-alumina-titania, RP2316 298
Pigmentation, in bristle and horsehair, RP2315 287
Pike, Robert G., Alvin Van Valkenburg, Synthesis of mica, RP2323 360
Piston attenuator chart, RP2293 109
Plyler, Earle K., Infrared spectra of methanol, ethanol, and n-propanol, RP2314 281
—, *Nicolo Acquista*, Infrared absorption spectra of five halomethanes, RP2290 92
—, *Norman M. Gailar*, The $3\gamma_3$ bands of carbon disulfide and carbon dioxide, RP2327 392
—, —, *Thomas A. Wiggins*, Some accurately measured infrared wavelengths for calibration of grating spectrometers, RP2309 221
Point estimates, uniformly best risk and minimax, RP2282 49
Polarographic diffusion currents, effect of suppressors on, RP2302 172
Polymerization and copolymerization heats of, of butadiene and styrene, RP2313 273
Pomerantz, Philip, Synthesis and physical properties of n-heptane and 2,2,4-trimethylpentane, RP2287 76
Porcelains, pure oxides, properties and phase equilibria, RP2316 298
Portland cement compounds, preparation of crystals, RP2299 152
Potassium chromate as standard of spectral transmittancy, RP2331 414
Pressure-humidity apparatus, RP2312 269
Probability, some trigonometric polynomials connected with, RP2297 139

R

Radiation, gamma, from a cesium and a cobalt source measurement, RP2298 147
Reflection curves, goniophotometric, analysis, RP2335 441
Refractories, pure oxides, RP2316 298
Refractory compounds, growing and mounting small crystals of, RP2299 152
Roberts, Donald E., Raymond A. Nelson, Ralph S. Jessup, Heats of copolymerization of butadiene and styrene from measurements of heats of combustion, RP2313 273
Roots, bounds of characteristic, of a matrix:
RP2284 89
RP2292 106
Rosenberg, Samuel J., Carolyn R. Irish, Solubility of carbon in 18-percent-chromium–10-percent-nickel austenite, RP2281 40
Rotation lines in water vapor, wavelengths of, RP2325 377
Russell, Henry Norris, Charlotte E. Moore, Binding energies for electrons of different types, RP2285 61

S

Salzer, Herbert E., Ruth Zucker, Ruth Capuano, Table of the zeros and weight factors of the first twenty Hermite polynomials, RP2294 111
Sample of three observations, closest pair in, RP2311 255
Scandium and yttrium, binding energies, RP2285 61
Schuette, Kathryn E., George G. Manov, Floyd S. Kirk, Ionization constant of 5-5′-diethylbarbituric acid from 0° to 60° C, RP2289 84
Schwebel, A., H. S. Isbell, J. V. Karabinos, H. L. Frush, N. B. Holt, Synthesis of D-glucose-1-C^{14} and D-mannose-1-C^{14}, RP2301 163
Series, infinite, method of summing, RP2310 228
Smith, Roberta E., John Keenan Taylor, Effect of maxima suppressors on polarographic diffusion currents, RP2302 172
Smith, W. H., J. V. Karabinos, R. A. Paulson, Thiophosphation of 2-methyl-2-nitro-1-propanol and the preparation of monothiophosphoric acid, RP2318 322
Spectra of gallium, indium, and thallium, RP2320 334
Spectra, infrared, of carbon disulfide and carbon dioxide, RP2327 392
Spectra, infrared of fluorinated methanes, RP2290 92
Spectra, infrared, of three alcohols, RP2314 281
Spectra, mass, of deuteroacetylenes, monodeuterobenzene, and deuteronaphthalenes, RP2304 188

Page

Spectral transmittancy of potassium chromate, RP2331 414
Spectrometers, calibration, RP2309 221
Spectrophotometric standard for the ultraviolet, RP2331 414
Spectroscopy, infrared, RP2309 221
Standard, spectrophotometric, potassium chromate as, RP2331 414
Standards, infrared for calibrating grating spectrometers, RP2309 221
Steels, influence of nitrogen, RP2305 193
Stein, Martin L., Gradient methods in the solution of systems of linear equations, RP2330 407
Stein, P., A note on bounds of multiple characteristic roots of a matrix, RP2284 59
—, A note on the bounds of the real parts of the characteristic roots of a matrix, RP2292 106
—, Some general theorems on iterants, RP2288 82
Stiefel, E., On Cauchy-Riemann equations in higher dimensions, RP2328 395
—, Two applications of group characters to the solution of boundary-value problems, RP2332 424
Stochastic process in estimating eigen values, RP2286 68
Strain-temperature, effect on flow and fracture of ingot iron at low temperatures, RP2329 399
stress corrosion of brasses; 248T aluminum alloy; low-carbon steel; stainless steel; AZ31 magnesium alloy, RP2291 99
Styrene and butadiene, heats of copolymerization, RP2313 275
Sugars, C^{14}-labeled, synthesis, RP2301 163
Sugars, carbon-14-labeled-, D-mannitol, and D-fructose, preparation, RP2334 438
Sullivan, Barbara M., Howard F. McMurdie, Crystal forms of chromium orthophosphate, RP2300 159
Surface appearance analysis, RP2335 441
Surface area of adsorbents, RP2319 325
Swindells, J. F., J. R. Coe, Jr., T. B. Godfrey, Absolute viscosity of water at 20° C, RP2279 1
Synthesis of mica, RP2323 360
Synthesis of position-labeled carbohydrates, RP2301 163
Szasz, Otto, Eugene Lukacs, Some nonnegative trigonometric polynomials connected with a problem in probability, RP2297 139

T

Taylor, John Keenan, Roberta E. Smith, Effect of maxima suppressors on polarographic diffusion currents, RP2302 172
Temperature and moisture, effect on electrical properties of leather, RP2322 349
Temperature, effect on tensile properties of high-purity nickel, RP2317 313
Temperature-strain, effect on flow and fracture of ingot iron, RP2329 399
Tensile properties of high-purity nickel, effect of temperature, RP2317 313
Tetrabromophenolphthalein ethyl ester, reaction with bases in benzene, RP2326 381
Thallium, arc spectrum, RP2320 334

Page

Thermal converters for current and voltage measurements, RP2296 121
Thermal expansion of aluminum and aluminum alloys, RP2308 209
Transmittancy, spectral, of potassium chromate, RP2331 414

U

Ultraviolet standard of spectral transmittancy, RP2331 414
Uniformly best constant risk and minimax point estimates, RP2282 49

V

Van Valkenburg, Alvin, Robert G. Pike, Synthesis of mica, RP2323 360
Viscosity, absolute, of water, RP2279 1
Voltage measurements at audio frequencies, RP2296 121
Voltmeters, testing, RP2296 121

W

Wasow, Wolfgang, On the truncation error in the solution of Laplace's equation by finite differences, RP2321 345
Water, absolute viscosity, RP2279 1
Water-vapor bands, wavelengths of rotational lines in, RP2325 377
Wave guide, below cutoff, chart for TE_{11} mode, RP2293 109
Wavelengths of water-vapor band lines, RP2325 377
Weir, Charles E., Influence of temperature and moisture on the electrical properties of leather, RP2322 349
Wexler, Arnold, Raymond D. Daniels, Jr., Pressure-humidity apparatus, RP2312 269
Whitewares, pure oxides, RP2316 298
Wiggins, Thomas A., Earle K. Plyler, Norman M. Gailar, Some accurately measured infrared wavelengths for calibration of grating spectrometers, RP2309 221
Williams, W. E., Jr., Sensitive mercury-level detecting unit for manometers, RP2283 54
Williamson, Laura, Fred L. Mohler, Vernon H. Dibeler, Helen Dean, Mass spectra of deuteroacetylenes, monodeuterobenzene, and deuteronaphthalenes, RP2304 188

X

X-ray diffraction, preparation of specimens, RP2299 152

Z

Zucker, Ruth, Herbert E. Salzer, Ruth Capuano, Table of the zeros and weight factors of the first twenty Hermite polynomials, RP2294 111

Engineering
Library
RR

Journal of Research

of the

National Bureau of Standards

U3
A

JUNE 1952

VOLUME 48 NUMBER 6

U. S. DEPARTMENT OF COMMERCE
Charles Sawyer, Secretary
NATIONAL BUREAU OF STANDARDS
A. V. Astin, Director

JUNE 195
VOLUME • 4
NUMBER

JOURNAL OF RESEARCH

of the

NATIONAL BUREAU OF STANDARDS

PERIODICALS OF THE NATIONAL BUREAU OF STANDARDS

As the principal agency of the Federal Government for fundamental research in physics, chemistry, mathematics, and engineering, the National Bureau of Standards conducts projects in fifteen fields: electricity, optics and metrology, heat and power, atomic and radiation physics, chemistry, mechanics, organic and fibrous materials, metallurgy, mineral products, building technology, applied mathematics, electronics, ordnance development, radio propagation, and missile development. The Bureau has custody of the national standards of measurement and conducts research leading to the improvement of scientific and engineering standards and of techniques and methods of measurement. Testing methods and instruments are developed; physical constants and properties of materials are determined; and technical processes are investigated.

JOURNAL OF RESEARCH

Internationally known as a leading scientific periodical, the Journal presents research papers by authorities in the specialized fields of physics, mathematics, chemistry, and engineering. Complete details of the work are presented, including laboratory data, experimental procedures, and theoretical and mathematical analyses. Each of the monthly issues averages 85 two-column pages; illustrated. Annual subscription: domestic, $5.50; foreign, $6.75.

TECHNICAL NEWS BULLETIN

Summaries of current research at the National Bureau of Standards are published each month in the Technical News Bulletin. The articles are brief, with emphasis on the results of research, chosen on the basis of their scientific or technologic importance. Lists of all Bureau publications during the preceding month are given, including Research Papers, Handbooks, Applied Mathematics Series, Building Materials and Structures Reports, and Circulars. Each issue contains 12 or more two-column pages; illustrated. Annual subscription: domestic, $1.00; foreign, $1.35.

BASIC RADIO PROPAGATION PREDICTIONS

The Predictions provide the information necessary for calculating the best frequencies for communication between any two points in the world at any time during the given month. The data are important to all users of long-range radio communications and navigation, including broadcasting, airline, steamship, and wireless services, as well as to investigators of radio propagation and ionosphere. Each issue, covering a period of one month, is released three months in advance and contains 16 large pages, including pertinent charts, drawings, and tables. Annual subscription: domestic, $1.00; foreign, $1.25.

Order all publications from the Superintendent of Documents
U. S. Government Printing Office, Washington 25, D. C.

The printing of this publication has been approved by the Director of the Bureau of the Budget, April 6, 1950

Journal of Research of the National Bureau of Standards Vol. 48, No. 6 June 1952

Contents

	Page
Effect of strain-temperature history on the flow and fracture of ingot iron at low temperatures. Glenn W. Geil and Nesbit L. Carwile. RP2329	399
Gradient methods in the solution of systems of linear equations. Marvin L. Stein. RP2330	407
An alkaline solution of potassium chromate as a transmittancy standard in the ultraviolet. Geraldine W. Haupt. RP2331	414
Two applications of group characters to the solution of boundary-value problems. E. Stiefel. RP2332	424
Heterogeneous equilibria at the glass electrode-solution interface. Donald Hubbard and Richard G. Goldman. RP2333	428
Preparation of D-mannitol-C^{14} and its conversion to D-fructose-1-(and 6)-C^{14} by acetobacter suboxydans. Horace S. Isbell and J. V. Karabinos. RP2334	438
Analysis of goniophotometric reflection curves. Isadore Nimeroff. RP2335	441
Index to volume 48 (January to June 1952, Research Papers RP2279 to RP2335).	449

The above Research Papers may be obtained from the Superintendent of Documents, Government Printing Office, Washington 25, D. C., as follows: RP2329 10¢; RP2330 10¢; RP2331 10¢; RP2332 5¢; RP2333 10¢; RP2334 5¢; RP2335 10¢.

For sale by the Superintendent of Documents, U. S. Government Printing Office, Washington 25, D. C. • Price 50 cents
$5.50 per year on subscription; $6.75 foreign.

UNITED STATES GOVERNMENT PRINTING OFFICE, WASHINGTON : 1952